Optimization of a train of bunches for plasma wakefield acceleration

Inaugural-Dissertation

zur Erlangung des Doktorgrades
der Mathematisch-Naturwissenschaftlichen Fakultät
der Heinrich-Heine-Universität Düsseldorf

vorgelegt von

Roberto Martorelli

aus Rome, Italy

Düsseldorf, May 10$^{\text{th}}$, 2016

aus dem Institut für Theoretische Physik I
der Heinrich-Heine-Universität Düsseldorf

Gedruckt mit der Genehmigung der
Mathematisch-Naturwissenschaftlichen Fakultät der
Heinrich-Heine-Universität Düsseldorf

Referent: Prof. Dr. A. Pukhov
Korreferent: Prof. Dr. G. Pretzler
Tag der mündlichen Prüfung:

Statement of Autorship

I decleare under oath that I have compiled my dissertation independently and withouth any undue assistance by third parties under consideration of the "Principles for the Safeguarding of Good Scientific Practice at Heinrich Heine Universität Düsseldorf".

Roberto Martorelli
Düsseldorf, May 10th, 2016

Abstract

Particle accelerators are a fundamental instrument for the understanding of fundamental mechanism in nature. The need of always higher energies for the particle beams requires a huge increase of the sizes of the accelerators using the actual technology. Moreover the highest energies are achieved nowadays by circular colliders, not perfectly suitable for acceleration of electrons and positrons due to the radiation losses. In order to overcome this problem a new branch of physics studying alternative technique for particle acceleration has been developed.

Among the various alternatives a promising one is the plasma wakefield acceleration (PWFA), in which a driver bunch interacts with a cold background plasma, exciting a plasma wave. The electric field of the plasma wave is then used for the acceleration of a second bunch. Such a mechanism allows to reach fields strength far beyond currently available, limited by the dielectric strength of the material. Among the different driver configurations, a promising one is the use of a modulated beam, namely a train of bunches, that provides a coherent interference among the electric fields generated by the single bunches. Such mechanism is subjected to a renewed interest in view of the forthcoming AWAKE experiment at CERN in which the long proton beam produced at the SPS facility is used as a driver. This possibility is achieved thanks to the onset of the self-modulation instability that modulates the long beam in a train of approximately 100 bunches. In order to accelerate the witness bunch to high energies is necessary on the other hand an efficient exchange of energy from the driver to the accelerated bunch, as well as a long duration of the driver so that can propagates for kilometers.

This thesis deals with this two last aspects. The aim of this work is to provide an optimization for the modulated driver in order to improve specific features of the PWFA. This work shows the possibility to achieve an improved efficiency for the energy transfer by properly controlling the shape of the single bunches composing the driver, as well as the distance between the bunches. Moreover the work shows as a fine tuning of the periodicity of the bunches allows the production of a more stable driver, especially considering the instability arising from the emittance-driven head erosion.

Zusammenfassung

Teilchenbeschleuniger sind ein wichtiges Instrument zum Verständnis fundamentaler Vorgänge in der Natur. Im Rahmen der aktuell zur Verfügung stehenden Technologie müssen immer größere Beschleuniger gebaut werden, um die wachsenden Anforderung an immer höherer Strahlenergien zu erfüllen. Die höchsten Energien pro Teilchen werden in Zirkularbeschleunigern erreicht, wobei ein hoher Energieverlust durch Synchrotronstrahlung (insbes. bei der Beschleunigung von Elektronen und Positronen) entsteht. Um dieses Problem zu umgehen, befasst sich ein Teilgebiet der Physik mit der Erforschung alternativer Beschleunigungsmethoden.

Eine der vielversprechendsten Methode ist die Beschleunigung in Plasma [plasma wakefield acceleration (PWFA)]. Hier wechselwirkt ein Treiber mit kaltem Hintergrundplasma, wodurch eine Plasmawelle angeregt wird. Das elektrische Feld innerhalb der Plasmawelle wird anschließend genutzt, um einen gefangenen Teilchenstrahl zu beschleunigen. Die bei dieser Methode auftretenden Feldstärken sind um viele Größenordnungen höher, als in herkömmlichen Beschleunigern, da sie nicht durch einen möglichen Materialzusammenbruch begrenzt sind. Eine vielversprechende Methode, Plasmawellen anzuregen, ist die Benutzung eines modulierten , hoch energetischen Teilchenstrahls als Treiber. Hierbei überlagern sich die elektrischen Felder einer Reihe von kleineren Strahlen kohärent zu einem großen. Dieser Mechanismus ist besonders interessant, da in naher Zukunft das AWAKE Experiment am CERN durchgeführt werden soll. Hierbei wird ein langer Protonenstrahl, der in der SPS-Einrichtung vorbeschleunigt wurde, als ein Treiber genutzt. Die Zerlegung in einzelne kleinere Strahlpakete (ca. 100 Stück) geschieht anschließend durch die Selbstmodulationsinstabilität. Damit ein in der Plasmawelle gefangener Teilchenstrahl auf hohe Energien beschleunigt werden kann, ist ein effizienter Energieaustausch zwischen Treiber und Strahl, sowie eine lange Lebenszeit des Treibers notwendig.

Diese Arbeit behandelt die letzten beiden Aspekte der Teilchenbeschleunigung in Plasma. Das Ziel der Arbeit ist es, die Modulation des Treibers zu optimieren und damit spezifische Eigenschaften der PWFA zu verbessern. Um die Effizienz des Energietransfers zu verbessern, wird eine Methode vorgestellt, die es erlaubt, die Form und den Abstand der einzelnen Strahlpakete im gesamten Protonenstrahl zu kontrollieren. Darüber hinaus zeigt diese Arbeit, wie die Feinabstimmung der Periodizität der Teilstrahlen die Lebenszeit des Treibers verlängern kann. Hierbei wird insbesondere auf die durch die Emittanz am Kopf des Treibers induzierte Instabilität eingegangen.

Contents

Abstract ii

Zusammenfassung iii

List of Figures vi

1 Introduction 1

2 Particle accelerator 6

3 Basic plasma physics 11
3.1 Plasma dynamics . . . 11
3.1.1 Kinetic theory . . . 11
3.1.2 Fluid theory . . . 12
3.2 Fundamental quantities . . . 13
3.2.1 Plasma frequency . . . 13
3.2.2 Debye length . . . 15

4 Plasma wakefield 16
4.1 Linear theory of PWFA . . . 18
4.1.1 Quasi-static approximation . . . 18
4.1.2 1-dimensional theory . . . 19
4.1.3 2-dimensional theory . . . 21
4.2 Scale ordering in a plasma wakefield . . . 24
4.3 Properties of plasma wakefield . . . 25
4.3.1 Transformer ratio . . . 25
4.3.2 Beam loading and energy spread . . . 27

5 Beam dynamics 30
5.1 Emittance pressure . . . 30
5.2 Envelope model . . . 32

6 Transformer ratio enhancement 34
6.1 Transformer ratio of a train of flat-top bunches . . . 34
6.2 Transformer ratio of a train of Gaussian bunches . . . 39
6.3 Weighted Transformer Ratio . . . 41
6.4 Optimization of the Transformer Ratio . . . 43

7 Stability of a modulated beam **49**
7.1 Beam envelope model in a plasma wakefield 50
7.2 Equilibrium configuration 52
7.2.1 Equilibrium configuration for flat-top bunches 52
7.2.2 Equilibrium configurations for Gaussian bunches 59
7.3 Emittance-driven evolution of the modulated beam 60
7.3.1 Evolution for longitudinal flat-top bunches 61
7.3.2 Evolution for longitudinal Gaussian bunches 65
7.4 Optimization of a train of Gaussian bunches 69

8 Conclusion **78**

A Derivation of the 2-dimensional wakefield equations **81**

B Particle in Cell and Quasi-static VLPL **88**

C Derivation of the beam envelope model **91**

References **99**

Acknowledgments **105**

List of Figures

1 Future particle accelerators 2
2 Linac scheme 7
3 Cyclotron scheme 8
4 Synchrotron scheme 9
5 Livingston plot 10
6 Livingston plot for plasma based accelerator 17
7 Scheme for PWFA 18
8 1-dim PWFA 20
9 Sketch of 2-dim PWFA 22
10 Sections of 2-dim PWFA 23
11 Full 2-dim PWFA 24
12 R vs FWHM for a single Gaussian bunch 27
13 Beam loading and energy spread 28
14 Sketch of emittance 31
15 Field from a train of bunches with periodicity λ_p 37
16 Field from a train of two bunches with different densities . . . 38
17 Field from a train of flat-top and Gaussian bunches 40
18 Weighted field and R_W 42
19 Optimal R_W and bunch parameters (rigid train of bunches) . . 44
20 Optimal R_W and bunch parameters (fully optimized) 45
21 Map of R_W vs two parameters 46
22 Drift of the pinching point 54
23 Normalized transverse force 55
24 Equilibrium radii (flat-top bunches) 57
25 Equilibrium configurations (flat-top bunches) 58
26 Equilibrium configuration (Gaussian bunches) 60
27 Trapping potential (flat-top bunches) 61
28 Equilibrium drift (flat-top bunches) 62
29 Single bunch drift (flat-top bunches) 63
30 Equilibrium drift scheme (flat-top bunch) 64
31 Equilibrium drift (Gaussian bunches) 66
32 Equilibrium drift scheme (Gaussian bunch) 67
33 Single bunch drift (Gaussian bunches) 68
34 Trapping potential (Gaussian bunches) 70
35 Normalized particle trapped 71
36 Matching bunch positions 72
37 Normalized particle trapped and accelerating field 73
38 Optimized periodicity 74
39 Bunch densities from PIC simulations 75

40 Accelerating field from PIC simulations 76
41 Accelerating field for the rigid and optimized configuration . . 77
42 Contour of integration 85
43 Phase-space sampling for Vlasov and PIC codes 89
44 Scheme for quasi-static PIC 91

1 Introduction

One of the most ambitious achievement in physics in the last decades involved the acceleration of particles.

The confirmation of the Standard Model has widely relied on the use of particle accelerator. Some of the discoveries performed using particle accelerators are:

- Observation of the antiproton in 1955 at the Bevatron [1];
- Observation of the J/Ψ meson and confirmation of the existence of the quark charm in 1974 at the Stanford Linear Accelerator Center (SLAC) [2] and at the Brookhaven National Laboratories (BNL) [3];
- Observation of the τ particle at SLAC in 1975 [4];
- Observation of the gluon at the Deutsches Elektronen-Synchrotron(DESY) in 1979 [5];
- Observation of the W and Z bosons at European Organization for Nuclear Research (CERN) in 1983 [6, 7];
- Observation of an Higgs boson-like particle at CERN in 2012 [8–10].

The use of particle accelerators goes beyond the application in experimental particle physics [11].

Condensed matter experiments relies as well in the synchrotron radiation produced by bending particles accelerated to relativistic energies (usually electrons due to their small masses). From Tantalus, developed at the Synchrotron Radiation Center (SRC) in 1968 [12], to the more recent SOLEIL facility whose first operation dated back to 2006 [13], synchrotron radiation has been always widely used for spectroscopy.

Not less important are the applications of particle accelerators to medicine. An example is the hadron therapy for cancer treatment, where accelerated particles, usually protons, are shot on tumor tissues [14]. Today such technique is widespread all over the world, with plans for the development of new facilities [15, 16].

Such a wide application of particle accelerators, as well the promising results that provide, pushes the construction of new facilities to achieve the desired energies and beam features to be used in these applications.

Such development on the other hand is a challenge by itself due to the high cost and huge increase in the facilities dimension in order to reach the desired characteristics.

Plans are made for next generation of hadron colliders, such as those performed by the Future Circular Collider (FCC) studies [17,18]. A proposal is to build a new accelerator ring using the existing LHC facility as a pre-accelerator as shown in Fig.1a.

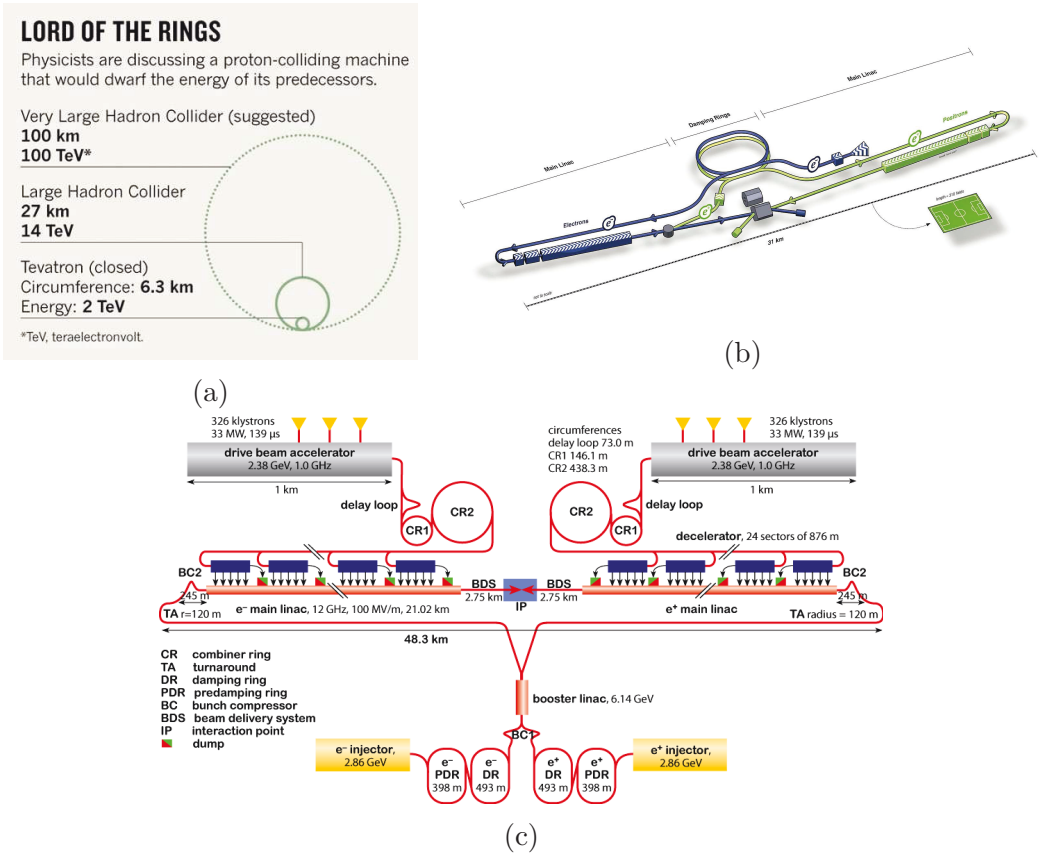

Figure 1: Suggested scheme for future particle accelerators: a)Future Circular Collider (suggested name Very Large Hadron Collider(VLHC). Picture taken from Ref. [17]); b) the International Linear Collider (ILC) (Picture taken from Ref. [19]); c) the Compact Linear Collider (CLIC) (Picture taken from Ref. [20])

Together with problems related to the cost of the new facilities, remains the challenge to accelerate electrons and positrons to high energies, a goal difficult to achieve in circular accelerators due to radiation losses.

The current optimal facilities for the electron/positron colliders are still the linear accelerators (linac). Plans are ongoing as well for the development of new machines aimed to reach the TeV threshold for the energy in the center of mass also for such colliders.

The International Linear Collider (ILC) [19] uses the already established concept of the linear collider simply extending its size (Fig.1b). The Compact Linear Collider (CLIC) [20] plans instead to use an accelerated beam as generator for the electric fields required to accelerate a second beam as can be seen in Fig.1c.

The greater size of the facilities, together with the increment in the cost, opened to the study of alternative ways to accelerate particles to such energies. One of the promising alternatives for electrons/positrons acceleration are the Plasma WakeField Accelerators (PWFA), where the particles are accelerated by the electric field generated by a plasma perturbation.

The concept was first suggested by Tajima and Dawson [21] reaching nowadays impressive results [22, 23].

In such accelerating scheme a "driver", either a laser pulse or a particle beam, is used to generated a Langmuir wave by perturbing a plasma. A "witness" bunch, of electrons or positrons, is then injected on the trail of the driver to be accelerated by the electric field of the plasma wave.

Such concept provides an accelerating gradient up to 100 GeV/m much higher than those achieved by standard radio frequency(rf) accelerator.

Although great results have been achieved in such a framework, there are still great challenges to be faced before a possible widespread application as actual accelerators.

The main problem for laser driven PWFA is represented by the short accelerating length that can be achieved. This is usually defined by the smallest among the Rayleigh length, the dephasing length and the pump depletion length.

The Rayleigh length is the length at which the laser is diffracted. A laser not focused drives a weaker wave, reducing so the efficiency of the acceleration. The dephasing length is the length for which the witness bunch overcome the wave, being no more in the accelerating phase. Lastly, the pump depletion length is the length for which the laser loses its power.

Due to these difficulties in laser driven PWFA, studies are performed also for particle driven PWFA.

The main advantage of such configuration is the longer dephasing length and the high energies of the driver, corresponding to a longer propagation distance before it loses all its energy. These two features guarantees the possibility to accelerate the witness bunch eventually for kilometers.

Another promising feature of such technique is the possibility to use existing accelerating facilities for producing the drivers of the wakefield. One important project in this direction is the AWAKE [24,25] in which the proton bunch produced at the Super Proton Synchrotron (SPS) at CERN is used as

driver for the wakefield.

In such experiment the long proton bunch is modulated through the self-modulation instability [26] in a train of approximately 100 bunches that coherently excite the wave.

In spite of the promising performances expected by such experiment, and more in general experiments involving a train of bunches, there are still problems that need to be faced.

In this work we address explicitly two of such problems, namely the efficiency of energy transfer from the driver to the witness bunch and the stability of the driver.

The parameter used to study the efficiency of the energy transfer is the transformer ratio, defined as the ratio between the energy gained by the witness bunch over the energy deposited by the driver in the plasma. For linear theories and symmetric drivers such parameter is limited to 2. Nevertheless, using a train of bunches, it is possible to enhance such limit, improving the performances of the configuration.

In the present work we study the transformer ratio for a train of Gaussian bunches, extending the previously known results obtained for a train of flat-top bunches. We find that the scaling holding for the flat-top bunches parameters that provides an increasing transformer ratio, does not hold for Gaussian bunches. Therefore we perform a scan on the parameters of the train of Gaussian bunches in order to obtain the maximum achievable transformer ratio for this particular configuration.

The other important issue is the stability of the driver. The driving beam, especially a long one as in the AWAKE experiment, is subject as well to the wakefield excited. This leads to a fast deterioration of the driver and consequently to a smaller acceleration distance.

In this work we study the transverse equilibrium for a modulated beam with both flat-top and Gaussian density profile, optimizing the configurations in order to obtain a stable driver.

In particular we look for the effects of the emittance-driven expansion of the head of the beam on the stability of the whole configuration, observing a backward shift of the equilibrium structure due to this effect. We try therefore to mitigate such instability by reshaping the train of bunches modifying the periodicity of the structure. This provides a more stable configuration as well a more intense accelerating field respect to a periodicity of λ_p.

In the first chapter we provide a brief description of the actual techniques for particle acceleration involving rf accelerators. In the second chapter an introduction to plasma physics is provided. In the third chapter we explain the basic concepts of the PWFA in the 1-dimensional and 2-dimensional case,

explaining the existing models and describing the main features of this concept. In the fourth chapter we provide a model for describing the transverse dynamic of the beam. In the fifth chapter we start analyzing the efficiency of energy transfer from the driver to the witness bunch in the case of a train of bunches, extending the results to Gaussian bunches. We provide an optimization of the configuration in order to maximize the efficiency. In the sixth chapter the stability of the driver is studied, providing first an analysis of the equilibrium configuration achieved by a modulated beam and then studying the effects of the head expansion driven by the emittance on the stability of the whole beam. In the last chapter we summarize the results and provide some conclusion and prospective.

2 Particle accelerator

Particle physics has been and still is one of the research areas that has been most developed in the last decades. Starting from the first experiment on the nature of the atom performed by Rutherford [27, 28], until the discovery of the Higgs boson [8–10], this topic has always seen an increasing interest.

The further development of applications of accelerated particles in out of fundamental physics research, such as medical applications [29], has brought additional stimulus to the topic.

The need of high energetic particles for the various range of applications was achieved through the development of particle accelerators of always greater performances.

The acceleration of particles is simply achieved by applying an electric field. The longer the distance the particle is accelerated, the higher the energy that can be achieved. The direct application of an electrostatic field is limited by the dielectric strength of the material and does not allow to reach the high energies required.

To overcome this problem the idea to perform the acceleration in more than one single stage was developed, with the voltage of the different stages well below the dielectric strength. This idea involves the use of radio-frequency (rf) fields, and is the cornerstone of most of the particle accelerators in use nowadays.

One of this kind of accelerators, and also the first one developed using rf fields, is the linear accelerator (linac) (Fig.2). In the linac, the particle travels straight through a sequence of accelerating section separated by isolated structure.

The length of the drift cavities is increasing with the number of the cavity. This way the time needed to the accelerated particles to pass through the single cavities is always the same and correspond to the frequency of the rf field.

The downside of this approach is the increasing size of the accelerator due to the always longer drift cavities necessary. The Stanford Linear Accelerator Center (SLAC), one of the most important linac nowadays, is able to accelerate electrons and positrons up to 50 GeV in 3 Km.

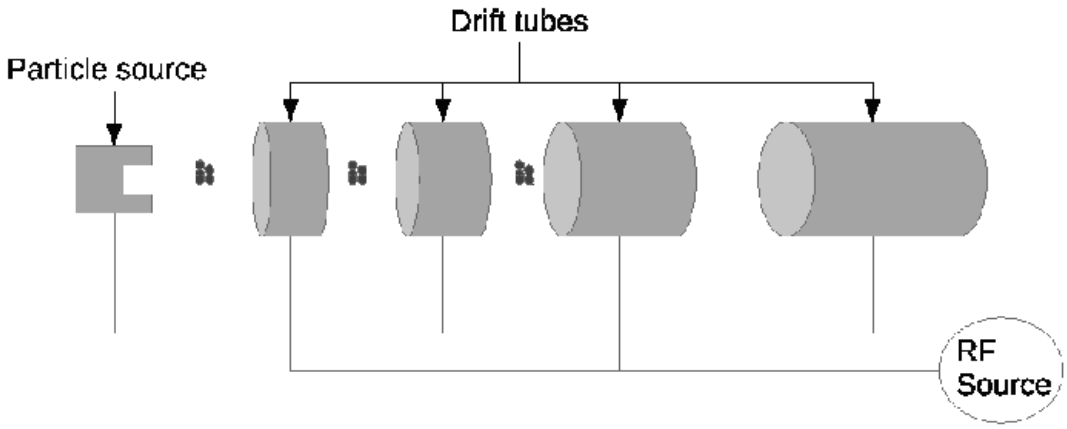

Figure 2: Basic scheme of a linear accelerator. A radio frequency electric field accelerates an injected bunch of particles in the section between the drift tubes.

One way to reduce the size of the accelerator was introduced with the concept of the cyclotron (Fig.3).

In the cyclotron an external magnetic field is applied in the drift section of the accelerator. The Lorenz force arising from the presence of the magnetic field bends the trajectories of the particles inducing a circular motion with cyclotron frequency $\omega_c = qB/m$. After half of the circle the particles are out of the drift cavity. By properly setting the frequency of the rf field to $f = 2\pi/\omega_c$, the particles will be once again in the accelerating phase. The mechanism will continue up to the point in which the gyroradius is greater than the area in which the magnetic field is apply. The accelerated particles will then drift straight with constant velocity.

The main problem of the cyclotron emerges when particles approach relativistic regime. Becomes in this case the influence of the Lorentz factor on the mass of the particle $m = m_0\gamma$ with $\gamma = (1 - v^2/c^2)^{-\frac{1}{2}}$. It is clear how in this case the cyclotron frequency is not constant anymore but dependence by the particle velocity.

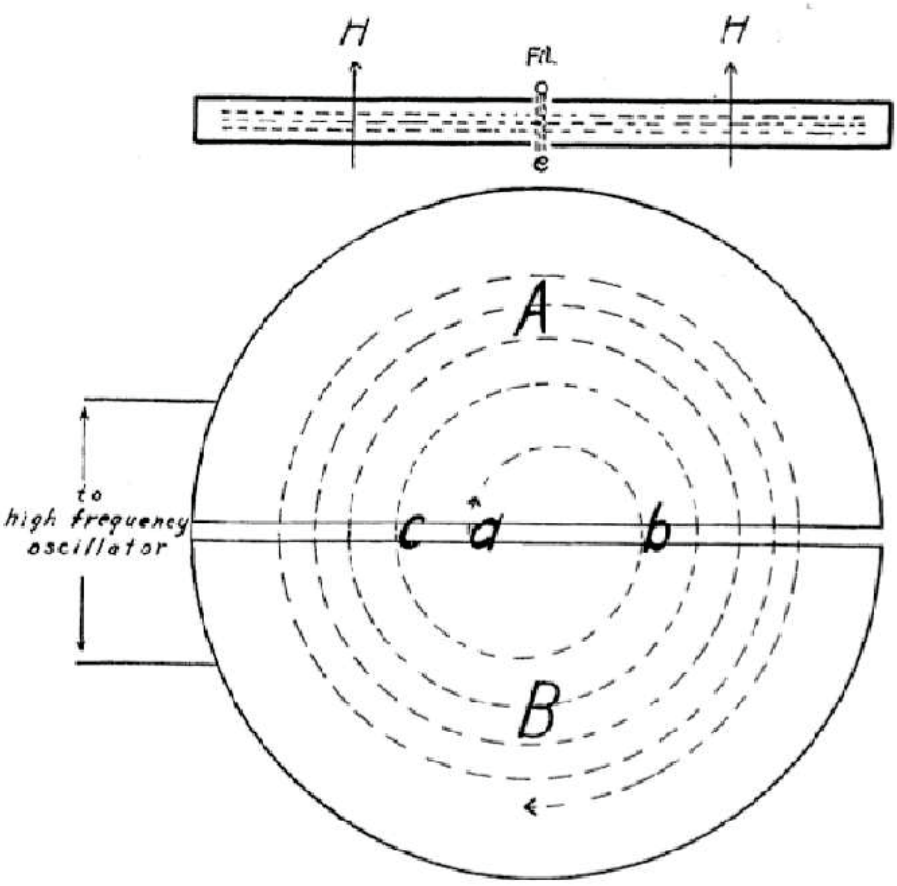

Figure 3: Scheme of a cyclotron (Picture taken from Ref. [30]). The particles are accelerated in between the section A and B, while a magnetic field is applied inside the two sections in order to bend the trajectories of the particles.

To maintain the particles in the accelerating phase of the drift section, it is therefore necessary either to apply an rf field with a variable frequency (as in the case of the synchrocyclotron), or a non constant magnetic field that compensate the increasing Lorentz factor (that is the case of the isochronous cyclotron).

One of the downside of the cyclotron and the further developments was the necessity to maintain the magnetic field on the whole surface of the disks since the gyroradius, also in the case of the isochronous cyclotron, was not constant but proportional to the velocity of the particle, $r = m_0\gamma v/qB = p/qB$. The development of the synchrotron aimed to solve this problem.

The main feature of the synchrotron is the use of time-dependent magnetic fields (Fig.4). The variation of the magnetic field follows the variation

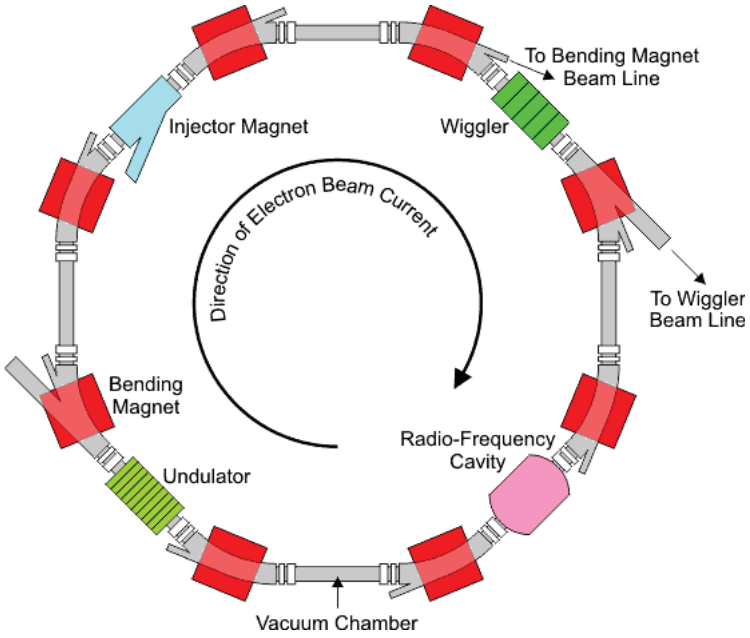

Figure 4: Sketch of a synchrotron (Picture taken from Ref. [31]). The ring is composed by bending magnets that provide the necessary time-dependent magnetic field used to bend the beam direction, accelerating sections and focusing magnet to compress the beam.

of the particles momenta, so that is not only achieved the matching with the accelerating phase of the rf field, but the gyroradius is constant, reducing the space in which the magnetic field must be applied.

The main issue of the synchrotron, and more in general of circular accelerating machines, is the energy lost by synchrotron radiation, occurring on relativistic particles moving on a curved path. The energy lost in circular machines is approximately

$$\Delta W \propto \frac{E^4}{r^2(mc^2)4} \tag{1}$$

therefore light particles suffer more of the loss due to synchrotron radiation rather then heavy particles. The state of art for synchrotron nowadays is the Large Hadron Collider (LHC) at CERN, in which protons are accelerated up to energies of the center of mass $\sqrt{s} \propto 7\text{TeV}$.

The development of accelerators facilities have seen an exponential growth of the energies achieved in the center of mass (Fig.5), together with an increase of the size of the accelerators.

Nevertheless the actual acceleration techniques, relying always in rf fields, are still limited by the material breakdown and it is still a great challenge to

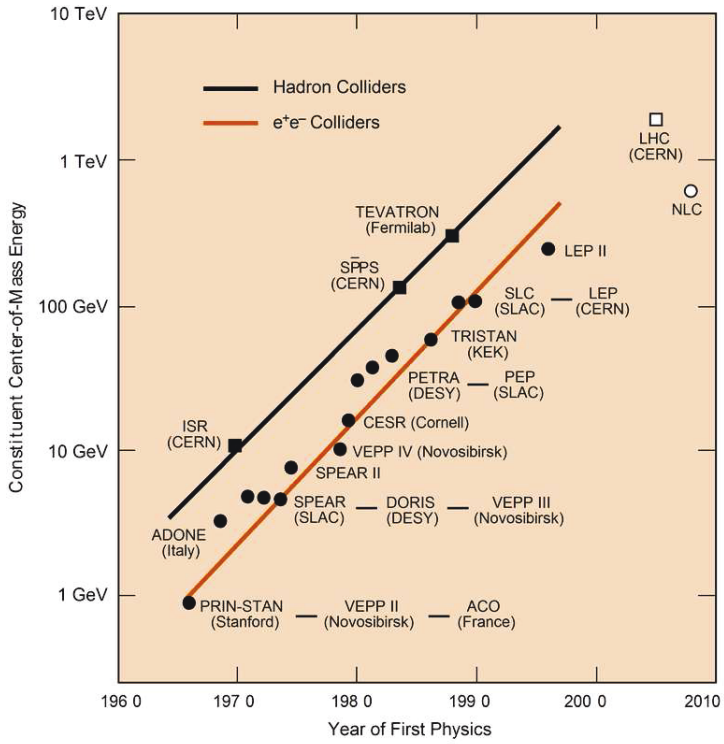

Figure 5: Livingston plot representing the increasing energy at the center of mass for the developed accelerating facilities as a function of the years (Picture taken from Ref. [32]).

brings electrons and positrons to high energies since it is only possible using linear colliders and so huge accelerating facilities.

A different approach that would allows to reach higher energy than accessible nowadays, together with a reduction of the accelerating structure, could be the use of plasma-based accelerators, in which particles are accelerated by the fields developed by a perturbed plasma. A more detailed description of this approach will be provided in Section 4.

3 Basic plasma physics

Although plasma is widely present in nature, about 99% of the matter in the universe is in plasma state, its understanding and control has always been a great challenge.

This is a consequence of its unique characteristics that can be evinced by its own definition: a plasma is a quasi neutral gas of charged and neutral particles which exhibits collective behavior [33].

The quasi neutrality implies that the plasma is able to screen out any local variation of the charge density at a certain distance L greater than the scale of the perturbation. The collective behavior instead arises from the variation in the charge and current densities that lead to the generation of electromagnetic fields. The long-range nature of these interactions provides for the plasma non-local attributes.

This interplay between different scales requires specific tools for the description of the dynamics of the plasma and its interaction with external sources. This chapter is aimed to review some well known concepts of plasma physics that formalize what described above and are necessary for a better understanding of the next sections.

3.1 Plasma dynamics

3.1.1 Kinetic theory

System composed by a large number of particles are described using statistical mechanics, namely tracing the evolution of the average quantities of the system. The fundamental quantity on which relies such approach is the distribution function $f(t, \mathbf{r}, \mathbf{p})$, where $\mathbf{r}$ and $\mathbf{p}$ are the generalized coordinates and momenta characterizing the phase space $\Gamma = (\mathbf{r}, \mathbf{p})$ [34].

The quantity $f(t, \mathbf{r}, \mathbf{p})d\Gamma = f(t, \mathbf{r}, \mathbf{p})d\mathbf{r}d\mathbf{p}$ is the mean number of particles in a given volume element of the phase space.

The dynamics of the distribution function is described by the Boltzmann equation:

$$\frac{df}{dt} = \frac{\partial f}{\partial t} + \mathbf{v} \cdot \nabla_{\mathbf{r}} f + \mathbf{F} \cdot \nabla_{\mathbf{p}} f = C(f) \tag{2}$$

where $\mathbf{F}$ is any macroscopic force acting on the system and $C(f)$ is the rate of change of the distribution function due to collisions.

The macroscopic forces $\mathbf{F}$ can be either externally induced, or self-generated by the system itself, as those providing the collision term. The difference between the two is in the scale at which they change compared to the scale of the system. Macroscopic forces vary on a scale comparable to that of

the system while collisions are provided by interactions occurring on a much smaller scale.

For a collisionless system holds the Liouville's theorem, providing:

$$\frac{\partial f}{\partial t} + \mathbf{v} \cdot \nabla_{\mathbf{r}} f + \mathbf{F} \cdot \nabla_{\mathbf{p}} f = 0. \tag{3}$$

Plasmas as well can be described by such approach, providing a Boltzmann equation for both electrons and ions. For collisionless plasma this yields:

$$\frac{\partial f_\alpha}{\partial t} + \mathbf{v} \cdot \nabla_{\mathbf{r}} f_\alpha + \frac{q_\alpha}{m_\alpha} \left(\mathbf{E} + \frac{\mathbf{v}}{c} \times \mathbf{B} \right) \cdot \nabla_{\mathbf{p}} f_\alpha = 0 \tag{4}$$

with $\alpha = e, i$ for electrons and ions respectively.

The electric and magnetic fields in the Lorentz force are both the external ones and those self-generated by the plasma. For a self-consistent description of the system therefore, it is necessary to couple the Boltzmann equation with the Maxwell equations for the fields:

$$\nabla \cdot \mathbf{E} = 4\pi\rho \tag{5}$$

$$\nabla \times \mathbf{E} = -\frac{1}{c}\frac{\partial \mathbf{B}}{\partial t} \tag{6}$$

$$\nabla \cdot \mathbf{B} = 0 \tag{7}$$

$$\nabla \times \mathbf{B} = \frac{4\pi}{c}\mathbf{J} + \frac{1}{c}\frac{\partial \mathbf{E}}{\partial t} \tag{8}$$

where the charge and current densities are related to the distribution function by the equations:

$$\rho = e \int (Z f_i - f_e) d\mathbf{p} \tag{9}$$

$$\mathbf{J} = e \int \mathbf{v} (Z f_i - f_e) d\mathbf{p}. \tag{10}$$

The full set of equations (4-10) forms the Vlasov equations.

As for gases, the fields generated by the plasma and providing the Lorentz force, has to be considered as mean fields over the scales of the system, therefore as macroscopic fields. All the others, whose mean is zero, are sources of collisions as soon as the scales of the system are comparable with those of the interactions.

3.1.2 Fluid theory

A macroscopic description of the plasma can be formulated in terms of fluid equations. The dynamics in this case is described by the equation of motion

for the average quantities characterizing the plasma, defined as:

$$n_\alpha = \int f_\alpha d\mathbf{p} \qquad \textit{Particle density} \tag{11}$$

$$\bar{\mathbf{v}}_\alpha = \mathbf{u}_\alpha = \frac{1}{n_\alpha}\int \mathbf{v} f_\alpha d\mathbf{p} \qquad \textit{Average velocity} \tag{12}$$

$$\mathbf{\Pi}^{ij}_\alpha = m_\alpha \int (\mathbf{v} - \mathbf{v}^i_\alpha)(\mathbf{v} - \mathbf{v}^j_\alpha) f_\alpha d\mathbf{p} \qquad \textit{Pressure tensor} \tag{13}$$

$$\tag{14}$$

The equations of motion are obtained by taking the moments of Eq.(4), obtaining:

$$\frac{\partial n_\alpha}{\partial t} + \nabla(n_\alpha \mathbf{u}_\alpha) = 0 \qquad \textit{Continuity equation} \tag{15}$$

$$\frac{\partial \mathbf{u}_\alpha}{\partial t} + (\mathbf{u}_\alpha \cdot \nabla)\mathbf{u}_\alpha = \frac{q_\alpha}{m_\alpha}\left(\mathbf{E} + \frac{\mathbf{u}_\alpha}{c} \times \mathbf{B}\right) - \frac{1}{m_\alpha n_\alpha}\nabla \cdot \mathbf{P}^{ij}_\alpha \qquad \textit{Euler equation.} \tag{16}$$

In order to close the system it is necessary to obtain an equation of motion for the second moment of the distribution function. This will relate the pressure tensor with the energy flux $\mathbf{q} = \frac{m_\alpha}{2}\int (\mathbf{v} - \mathbf{v}_\alpha)^2 \mathbf{v} f_\alpha d\mathbf{p}$. It is nevertheless possible to truncate the hierarchy by discarding dissipative effects in the system and setting an equation of state that relates the pressure with the plasma temperature (and so its energy).

3.2 Fundamental quantities

3.2.1 Plasma frequency

One example of the collective behavior mentioned previously emerges perturbing a plasma initially at the equilibrium. For sake of simplicity it is considered an infinite, homogeneous, cold electron plasma in a neutralizing background, so the ions motion is discarded. The fluid equations (15-16) turns therefore into:

$$\frac{\partial n}{\partial t} + \nabla(n\mathbf{u}) = 0 \tag{17}$$

$$\frac{\partial \mathbf{u}}{\partial t} + (\mathbf{u} \cdot \nabla)\mathbf{u} = -\frac{e}{m}\left(\mathbf{E} + \frac{\mathbf{u}}{c} \times \mathbf{B}\right) \tag{18}$$

where the subscript for the species has been dropped since the model includes only electrons. The electromagnetic fields are only those self-induced by the plasma and have to be evaluated through the Maxwell equations (5-8).

Considering a linear perturbation from the equilibrium, it is possible to expand the quantities as

$$n = n_0 + n_1 \qquad \mathbf{u} = \mathbf{u}_0 + \mathbf{u}_1 \qquad \mathbf{E} = \mathbf{E}_0 + \mathbf{E}_1 \qquad \mathbf{B} = \mathbf{B}_0 + \mathbf{B}_1 \tag{19}$$

where the subscript 0 denotes the equilibrium condition and 1 the linear perturbation. Replacing the quantities in Eq.(17-18) provides two sets of equations, one for the equilibrium and one for the perturbation. Without lacking of entirety, a possible solution for the equilibrium is obtained by setting $\mathbf{u}_0 = \mathbf{E}_0 = 0$. Under these assumptions the dynamics of the perturbation is described by:

$$\frac{\partial n_1}{\partial t} + n_0 \nabla \cdot \mathbf{u}_1 = 0 \tag{20}$$

$$\frac{\partial \mathbf{u}_1}{\partial t} = -\frac{e}{m}\mathbf{E}_1 \tag{21}$$

$$\nabla \cdot \mathbf{E}_1 = -4\pi e n_1. \tag{22}$$

Performing a Fourier transformation to the perturbed quantities according to the prescription $f(t, \mathbf{r}) = \int_{-\infty}^{\infty} \tilde{f}(\omega, \mathbf{k}) e^{-i(\omega t - \mathbf{k}\cdot\mathbf{r})} d\omega d\mathbf{k}$ provides:

$$-i\omega\tilde{n}_1 + n_0 \mathbf{k} \cdot \tilde{\mathbf{u}}_1 = 0 \tag{23}$$

$$-i\omega\tilde{\mathbf{u}}_1 = -\frac{e}{m}\tilde{\mathbf{E}}_1 \tag{24}$$

$$\mathbf{k} \cdot \tilde{\mathbf{E}}_1 = -4\pi e \tilde{n}_1. \tag{25}$$

The system is fulfilled with the non trivial solution

$$\omega = \omega_p = \sqrt{\frac{4\pi e^2 n_0}{m}} \tag{26}$$

with ω_p being the *plasma frequency* [35].

The physical mechanism ongoing is rather simple but extremely important to understand the basic properties of plasmas. A small perturbation of the plasma electrons, drives an electrostatic force exerted by the ions composing the background, in order to restore the equilibrium conditions. The small inertia of the electrons induce them to oscillate around the equilibrium position, with a frequency equal to ω_p. The periodic charge bunching produces as well a periodic electric field.

It is worth to be mentioned that this behavior has been derived from the fluid description of the plasma, meaning that is a macroscopic feature of the system and so involves the collective interaction of a large number of particles.

3.2.2 Debye length

Another important example of the collective behavior of the plasma is the Debye screening, namely the ability of the plasma to macroscopically neutralize local charge perturbations.

This effects clearly emerges considering a single component plasma initially in equilibrium, perturbed by a single charge [36]. The unbalance charge induces an electric field that provides a local density perturbation. The total electrostatic potential is therefore the sum of that of the single charge and that arising from the density perturbation. The Poisson equation becomes therefore:

$$\nabla^2\Phi(\mathbf{r}) = -4\pi e(\delta(\mathbf{r}) + \langle\delta n(\mathbf{r}\rangle). \tag{27}$$

Since the perturbation is small it is reasonable to assume a Boltzmann distribution for the average density perturbation and therefore:

$$\langle\delta n(\mathbf{r})\rangle = n_0\left(\exp\left(-\frac{e\Phi(\mathbf{r})}{k_bT}\right) - 1\right) \simeq -\frac{n_0 e\Phi(\mathbf{r})}{k_bT} \tag{28}$$

where n_0 is the equilibrium plasma density, k_b is the Boltzmann constant and T is the plasma temperature. Replacing the result of Eq.(28) in (27) brings to the solution for the electrostatic potential:

$$\Phi(\mathbf{r}) = \frac{e}{r}\exp\left(-\frac{4\pi n_0 e^2}{k_bT}r\right) = \frac{e}{r}\exp\left(-\frac{r}{\lambda_D}\right) \tag{29}$$

with λ_D being the *Debye length* [37].

The behavior of the plasma emerges clearly from Eq.(29). For distances $r \ll \lambda_D$ the dominant term in the potential $\Phi(\mathbf{r})$ is the Coulomb-like one, meaning that the perturbation has to treated like a single-particle interaction. On the contrary, when $r \gg \lambda_D$, the potential is exponentially screened, meaning that macroscopically the plasma is not affected by the local perturbation.

A direct comparison between the Debye length and the inverse of the plasma frequency shows that are related for thermal electrons traveling with velocity $v_{th} = k_bT/m$.

4 Plasma wakefield

As explained in Section 2, standard technologies for accelerating particles involves the use of rf fields. Although the great success achieved in different fields of physics through this technology, the always higher energies required for fundamental physics research and the large accelerating facilities needed, opened to the research of new accelerating techniques. One of the most promising one is the plasma wakefield acceleration (PWFA).

In the PWFA a driver, either a laser or a particle beam, is used for perturbing a plasma initially in equilibrium, exciting a plasma wave. The electric field of the wave is used then for the acceleration of a witness bunch injected on the trail of the driver [38].

The work of Tajima and Dawson [21], using a laser pulse as a driver, first suggested the possibility to use plasmas as efficient medium to accelerate particles. The main reason for such conclusion is the intense accelerating gradient that can be provided, of the order of the non relativistic wavebreaking field $E_0 = m_e c\omega_p/q_e$.

Shortly after Chen [39], proved the possibility to employ a particle beam as a driver for the plasma wakefield.

From that pioneering articles, huge progresses have been made (Fig.6) both theoretical and experimental [22, 23, 40, 41], proving the wide range of applications for such mechanism, ranging from medical physics [42, 43] to experimental particle physics [44, 45].

The basic scheme for PWFA involves the use of a single short driver (Fig.7a). In the case of a short laser pulse, the pondemorative force of the laser is responsible for the perturbation of the background plasma. This is provided,in the linear regime, by $\mathbf{F}_p = -m_e c^2 \nabla(a^2/2)$ where m_e is the rest electron mass, c is the speed of light and $|a| = e|A|/m_e c^2 \ll 1$ is the normalized amplitude of the vector potential of the laser. The wave is resonantly excited if the pulse duration is approximately $\tau \simeq \omega_p^{-1}$.

The same considerations applies to the case in which the driver is a short particle bunch. In this case the space-charge force of the bunch is the perturbing source of the plasma wave. This is given by $\mathbf{F}_{sc} = -m_e c^2 \nabla\phi$ where $\phi = e\Phi/m_e c^2$ is the normalized scalar potential generated by the beam and plasma perturbation. In the linear regime the motion of the plasma electrons occurs in order to neutralize the space-charge potential of the bunch.

In order to improve specific features of the PWFA or to overcome limitations provided by the available technologies, different configuration of PWFA can be performed using different shapes of the drivers or more than a single ones (Fig.7). Some examples of the possible techniques, different from those involving a single short driver, are:

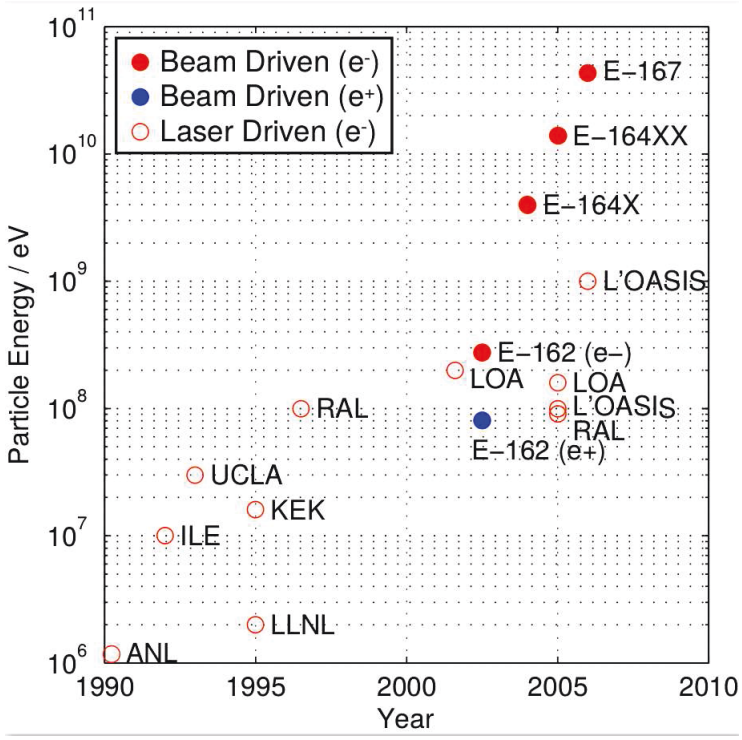

Figure 6: An analogous plot as the Livingston plot for accelerators, showing the progresses of plasma based accelerators in term of reached particle energies as a function of the years (Picture taken from Ref. [46]).

- Plasma beat-wave accelerator: the drivers of the wave are two long laser pulses with frequencies $\omega_1 - \omega_2 \simeq \omega_p$ [47–49]. This technique was first suggested in [21] since short laser pulses where not achievable with the available technology (Fig.7b);

- Multiple pulses/bunches: the driver is a train of laser pulses (or particle bunches) who resonantly excite a plasma wave [50, 51]. The intensity of the resulting accelerating field after the driver is a linear function of the number of drivers involved (Fig.7c);

- Self-modulated regime: the wakefield is excited by a long driver (either a laser or a particle beam again). Due to its length the driver is affected by the plasma wave resulting in a modulation of the driver. The configuration obtained after fully modulated is analogous to a train of pulses [52, 53] (Fig.7d).

A further improvement of the acceleration performances can be achieved in the nonlinear regime of plasma wakefield, so called "bubble regime" [54] in

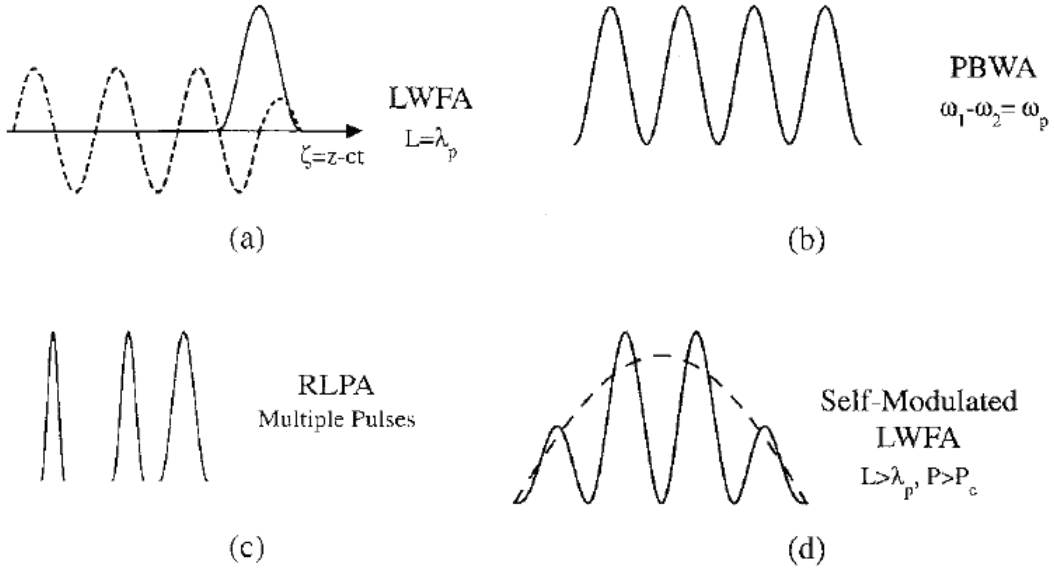

Figure 7: Possible schemes of generation of a plasma wakefield as presented in Ref. [38]: a) laser wakefield accelerator (or beam driven plasma wakefield accelerator as well); plasma beat wave accelerator; c) multiple pulses (or multiple bunches) accelerator; d) self-modulated laser wakefield accelerator (or self-modulated beam driven plasma wakefield accelerator)

which the strong pondemorative force of the laser breaks the wave already after the first oscillation, producing a electron free cavity just behind the driver. One of the key features of this configuration is the self-trapping of the plasma electrons in the accelerating phase, removing so the use of a second witness bunch.

The goal of this chapter is to provide a brief introduction on the physics of plasma wakefield accelerator. A particular emphasis will be given on the linear theory of particle driven plasma wakefields, especially in the self-modulated configuration and in the multiple bunch one, closely related to the topic of this manuscript.

4.1 Linear theory of PWFA

4.1.1 Quasi-static approximation

The quasi-static approximation is a widely used assumption in the framework of the plasma wakefield acceleration [55,56]. The approximation relies on the possibility to describe the interaction of the external driver with the plasma

taking into account only effects occurring at a specific time scale.

Assuming a driver propagating in the z direction, the dynamics of the interaction can be described through a coordinates system moving together with the driver, according to the transformation $\xi = \beta ct - z$ and $\tau = t$, where $\beta = v_b/c$ with v_b being the beam velocity and c the speed of light.

The relevant scales involved in the dynamics are the duration of the driver $\tau_L = v_b L_d$, being L_d the length of the driver, the evolution time of the driver τ_E and the inverse of the plasma frequency ω_p^{-1}.

If holds the relation $\tau_L \ll \tau_E \ll \omega_p^{-1}$, then it is reasonable to assume that the plasma interacts with a non-evolving driver. Therefore, concerning just the plasma dynamics, it is possible to discard any dependency by the proper time τ.

It is worth to underline that this assumption is valid only for the response of the plasma, while the dynamics of the driver explicitly depends by the time τ and has to be taken into account for a full self-consistent treatment of the system.

4.1.2 1-dimensional theory

The description of the plasma wakefield relies in the fluid approach presented in section 3.1.2 and follows steps analogous to those described in section 3.2.1.

Without loss of generality is considered here the interaction with a single electron bunch. The validity of the model holds assuming the ions as a static neutralizing background. Moreover, the linear approach demands the beam density to be much lower than the plasma density $n_b \ll n_p$. This allows to include the beam like an external perturbation whose dynamics can be discarded. Lastly the quasi-static approximation holds.

In such a framework, the dynamics of the perturbed plasma density is described by the equation of a driven harmonic oscillator (for sake of simplicity the index referring to the first order perturbation is removed):

$$\frac{\partial^2 n_p}{\partial \xi^2} + k_p^2 n_p = -k_p^2 n_b \tag{30}$$

where $k_p = \omega_p/v_b$. The solution for an arbitrary beam density profile is:

$$n_p(\xi) = -k_p \int_0^\xi n_b(\xi') \sin[k_p(\xi - \xi')] d\xi'. \tag{31}$$

The expression of the perturbed electric field can be evaluated by coupling Eq.(31) with the Poisson equation (5):

$$E_z(\xi) = 4\pi \int_0^\xi \rho_b(\xi') \cos[k_p(\xi - \xi')] d\xi'. \tag{32}$$

The Green functions of the two perturbed quantities are $\pi/2$ out of phase. Moreover the longitudinal field acts decelerating the driver bunch. This is expected since the driver is transferring its energy to the plasma(Fig.8).

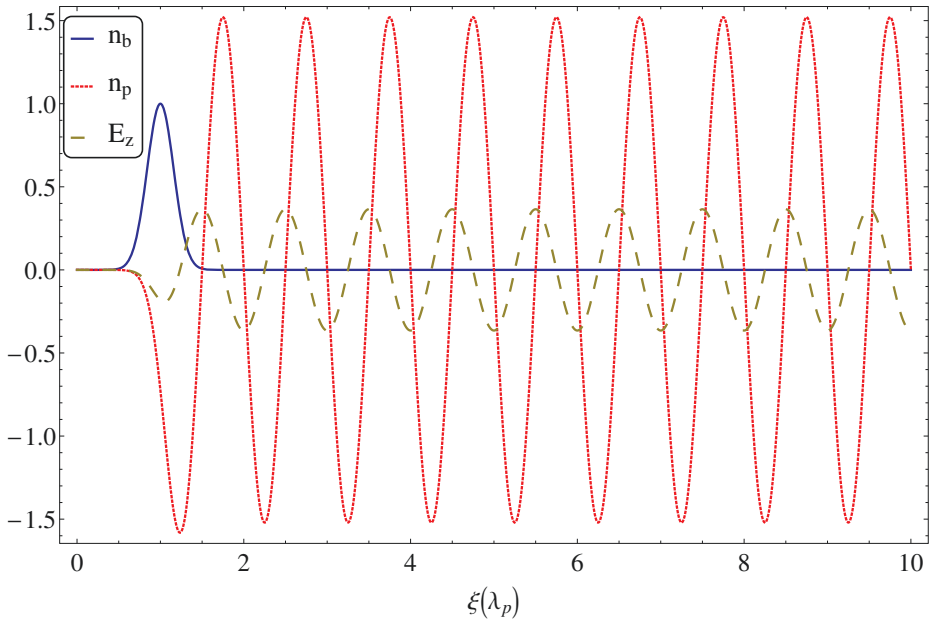

Figure 8: Driver density, perturbed plasma density and perturbed electric field for the 1-dimensional model of PWFA.

The wave generated can be then used for accelerating a second witness bunch placed in the accelerating phase of the electric field.

The role of the plasma is therefore that of a transformer medium: the plasma wave takes energy from the driver, depositing it then on the witness bunch. Ideally the process ends when the driver has given all its energy to the witness bunch. On the other hand in real experiments other problems occur such as the dephasing of the witness bunch or the deterioration of the driver due to the onset of instabilities.

4.1.3 2-dimensional theory

The equations describing the 2-dimensional dynamics of the plasma wakefield can be as well obtained from the fluid equations Eq.(15,16) coupled together with the Maxwell equations Eq.(5-8). The model [57], developed in a cylindrically symmetry, is based on the assumptions:

- Quasi-static approximation (see Section 4.1.1). The plasma dynamics occurs on a faster time-scale than that of the driver. The latter can be therefore considered adiabatically invariant;
- Cold plasma. The plasma temperature is low enough to not play a relevant role in the dynamics;
- Linear plasma perturbation. Between the driver and plasma density holds the relation $n_b < n_p$, therefore the perturbation driven by the particle bunch can be considered small enough to be treated linearly;
- Azimuthal symmetry. The plasma dynamics does not depend on the angle ($\partial_\theta \simeq 0$).

Here are provided the final equations derived from the model. For a complete evaluation of these equations we refer to Appendix A.

The longitudinal and transverse fields are:

$$E_z(r,\xi) = -4\pi k_p^2 \int_0^\infty \int_0^\xi \rho_b(r',\xi') r' \, \mathrm{I}_0(k_p r_<) \, \mathrm{K}_0(k_p r_>) \cos[k_p(\xi - \xi')] d\xi' dr' \tag{33}$$

$$W(r,\xi) = 4\pi k_p \int_0^\infty \int_0^\xi \frac{\partial \rho_b(r',\xi')}{\partial r'} r' \, \mathrm{I}_1(k_p r_<) \, \mathrm{K}_1(k_p r_>) \sin[k_p(\xi - \xi')] d\xi' dr' \tag{34}$$

with $r_{</>} = \min / \max(r, r')$ and $\mathbf{W} = \hat{r}(E_r - \beta B_\theta)$.

Both the longitudinal and transverse field present a similar structure: a longitudinal and transverse Green function and a source term. In the case of the longitudinal field the source is the beam density, while in the transverse field it is the radial derivative.

While the oscillatory behavior of the longitudinal field is associated with its accelerating/decelerating phase, in the transverse field is related to focusing/defocussing effects. The plasma wave therefore, together with accelerating the witness bunch, provides as well a compression.

The interesting difference that emerges is the different phase of the longitudinal Green function between the two fields. This is extremely important

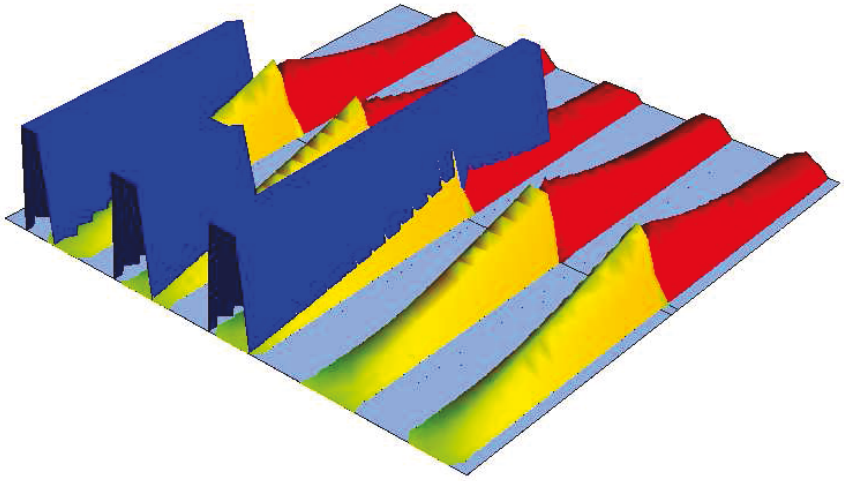

Figure 9: Sketch of the transverse field excited by a flat-top driver. The blue boxes are the flat-top bunches, being the leading one the driver of the wakefield. The wakefield is represented by a yellow section for the inner part, with $r < r_b$ and a red section for the outer part, with $r > r_b$. The field presents the oscillatory behavior induced by the plasma oscillation in the direction of propagation of the driver. On the transverse direction it reaches the maximum on the beam edge, corresponding to the maximum number of particles contributing to the wakefield, then decreasing outside the beam.

since it means that particles in the accelerating phase (with positive E_z therefore) are subjected to a focusing field (with negative W).

The radial Green function is represented for both the fields by the product of modified Bessel functions (of different order for the two fields). The different behavior of the two Bessel functions describes the quasi-exponential increasing and decreasing of the wakefield inside and outside the driver. Inside the beam the field intensity increases with the radius due to the increasing number of particles contributing to the generation of the wave. Once $r > r_b$ the source term disappear and therefore the waves becomes evanescent. A sketch of the behavior of the transverse field is presented in Fig.9.

The exact characteristic of the fields are presented in Fig.10 can be seen the longitudinal and transverse field generated by a short and narrow Gaussian bunch. The main features described previously emerge here clearly.

Both the fields are sinusoidal, driven by the plasma oscillation, but as

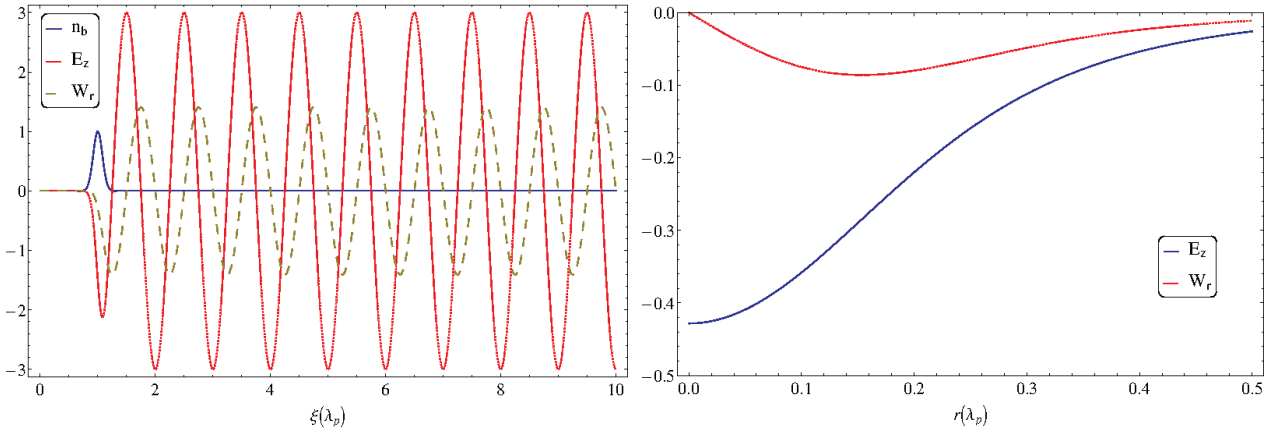

(a) (b)

Figure 10: Longitudinal and transverse field excited by a short Gaussian bunch. a) Driver density, longitudinal electric field and transverse field as a function of the longitudinal direction for $r \simeq 0.2\lambda_p$; b) longitudinal electric field and transverse field as a function of the transverse direction at the center of the bunch.

mentioned previously, they are out of phase.

The radial dependence by the Bessel function implies a rapid decay of the fields shortly after the center of the bunch in the radial direction.

In Fig.11 are presented the full 2-dimensional wakefields varying both the longitudinal and the transverse direction. The features depicted previously appear once again in this figure, with the longitudinal field that has a maximum on axis (the bunch is centered in $r = 0$) and the rapidly decays in the transverse direction.

The transverse field presents a maximum on the bunch radius, when the whole bunch density contributes to the generation of the wakefield.

Although the model is based on several assumptions it is able to properly describe the basic dynamics of the plasma wakefield in two dimensions.

It is worth noting that the model does not take into account the dynamics of the driver explicitly, solving only the fluid equations for the plasma. This might not be relevant for short particles bunches, but becomes more important when the driver length is longer than λ_p. In this case it is necessary to study the evolution of the wakefield coupled with the evolution of the driver. In Section 5 will be provided the tools to properly include the dynamics of the particle beam as well.

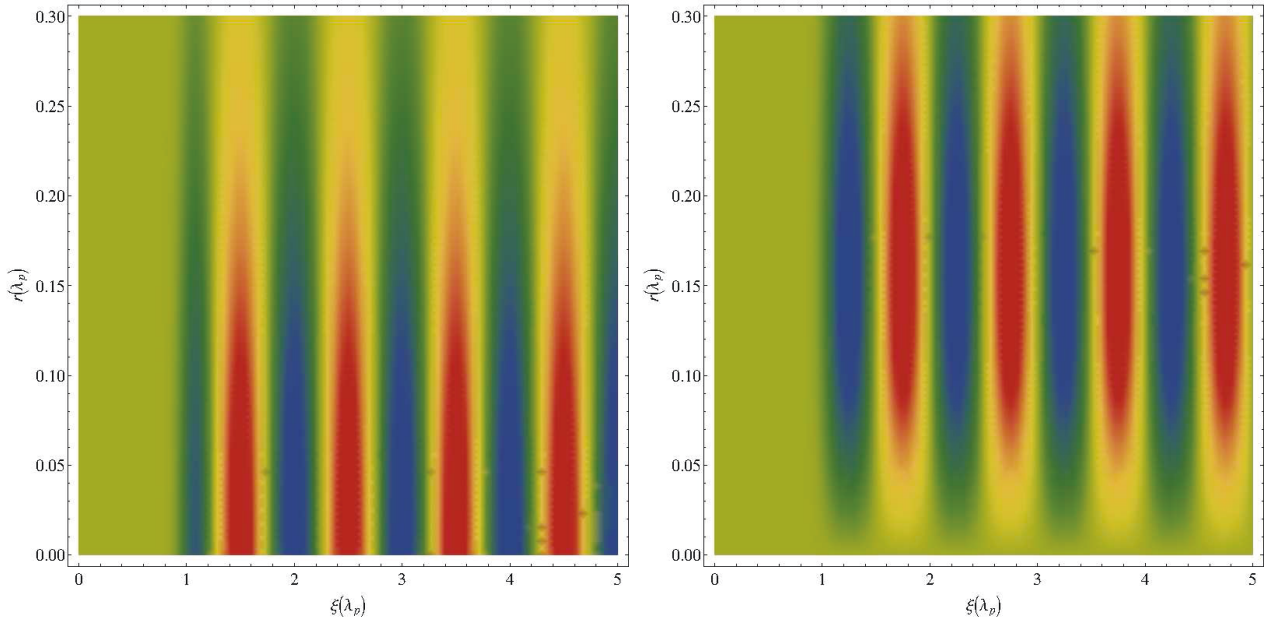

(a) (b)

Figure 11: 2-dimensional density plot of the longitudinal and transverse fields excited by a short Gaussian bunch

4.2 Scale ordering in a plasma wakefield

The analysis presented in Section4.1.1 showed the importance of the different scales involved in the plasma wakefield in order to develop a simplified analysis. As well in the previous section we mentioned as the evolution of the driver can be discarded in the model for the 2-dimensional plasma wakefield only under the particular conditions of a short driver. We want to present here a deeper insight to the different relevant scales for beam driven plasma wakefields [58], so that appears more clearly when the assumptions made are reasonable.

The three relevant scales in a PWFA are:

- The plasma wavelength $\lambda_p = c/\omega_p$. This is the shortest scale in such a framework;
- The focusing/defocussing length $L_f \simeq c(\gamma m r_b/|F_r|)^{\frac{1}{2}} \simeq c/\omega_\beta$ being F_r the transverse force acting on the beam and ω_β the betatron frequency. This is the length over which there is a change in the beam radius;
- The deceleration length of the driver L_d being the length over which the driver loses half of its energy.

By assuming $E_z \simeq E_0$ and $F_r \simeq eE_0$ being E_0 the wavebreaking limit and $r_b \simeq \lambda_p$ the following ordering is obtained:

$$L_d \simeq \gamma\lambda_p \gg L_f \simeq \sqrt{\gamma}\lambda_p \gg \lambda_p. \tag{35}$$

This shows the requirement in order to have the possibility to perform specific approximations. On the smallest scale λ_p, it is reasonable to assume a non evolving beam, a rigid beam, so that its dynamics does not have to be included on the study of the plasma wakefields.

If the scale analyzed is increased up to the point of being comparable with the focusing/defocusing length, then the transverse beam dynamics has to be included as well. The transverse evolution of the beam due to the transverse fields excited, as well as externally applied, sensibly modifies the wakefields. This self-consistent treatment has to be included by a proper model for the beam evolution, such as the envelope one presented in Section5.

On the other hand such scale is still smaller than the decelerating one, the beam does not lose much of its energy while experiencing a transverse modulation. It is therefore reasonable to perform a quasi-static analysis in such conditions.

Finally when the length are even longer, comparable to the decelerating length, the energy lost by the beam becomes relevant and a full dynamics description of the physics is needed.

This short analysis proves the importance of a deep understanding of the physical processes occurring in the interaction between a beam and the plasma and the importance to distinguish the several scales playing a role in order to simplify the description of the mechanism.

4.3 Properties of plasma wakefield

4.3.1 Transformer ratio

A relevant aspect of the plasma wakefield accelerators is the efficiency of energy transfer from the driving beam to the witness one. This is an extremely important issue especially if the length of the plasma cell, and so the duration of the interaction between the driver and the plasma, is long.

The parameter that take into account such an issue is the transformer ratio, defined as:

$$R = \frac{\Delta\gamma_{witness}}{\Delta\gamma_{driver}} \tag{36}$$

where $\Delta\gamma_{witness}$ is the energy gained by the witness bunch from the plasma and $\Delta\gamma_{driver}$ is the energy deposited by the driver in the plasma.

If we assume a non evolving bunches we can approximate the energies loss and gains as $\Delta\gamma_{driver} \sim E^- L$ and $\Delta\gamma_{witness} \sim E^+ L$ where $E^{-/+}$ are respectively the peak decelerating field under the driver and the peak accelerating field behind the driver and L is the traveled distance. This way the transformer ratio can be recast as:

$$R = \frac{E^+}{E^-}. \tag{37}$$

A major issue related to the transformer ratio and so to the energy transfer is that the maximum value that can be reached for a linearly perturbed plasma by symmetric bunches is $R = 2$. In order to prove this we can rely on a simple 1-dimensional model employing Eq.(32).

The longitudinal electric field is:

$$E_z(\xi) = 4\pi \int_0^{\xi} \rho_b(\xi') \cos[k_p(\xi - \xi')] d\xi'. \tag{38}$$

If the driver is short the electric field behind the driver can be rewritten as:

$$\begin{aligned} E_z(\xi) &= 4\pi \int_{-\infty}^{\infty} \rho_b(\xi') \cos[k_p(\xi - \xi')] d\xi' = \\ &= 4\pi \left(\cos(k_p\xi) \int_{-\infty}^{\infty} \rho_b(\xi') \cos(k_p\xi') d\xi' + \sin(k_p\xi) \int_{-\infty}^{\infty} \rho_b(\xi') \sin(k_p\xi') d\xi' \right). \end{aligned} \tag{39}$$

If the bunches is symmetric, then the second integral is zero because the integrand is an odd function integrated on a symmetric range. Therefore the maximum electric field achieved behind the driver is:

$$|E^+| = 4\pi \int_{-\infty}^{\infty} \rho_b(\xi') \cos(k_p\xi') d\xi' \simeq 2|E_z(0)| \leq 2|E^-|. \tag{40}$$

In the last passage we have used the fact that the electric field in $\xi = 0$ must be either equal or smaller to the maximum decelerating field. Therefore we obtain the limiting relation for the transformer ratio for symmetric bunches linearly perturbing the plasma $R \leq 2$.

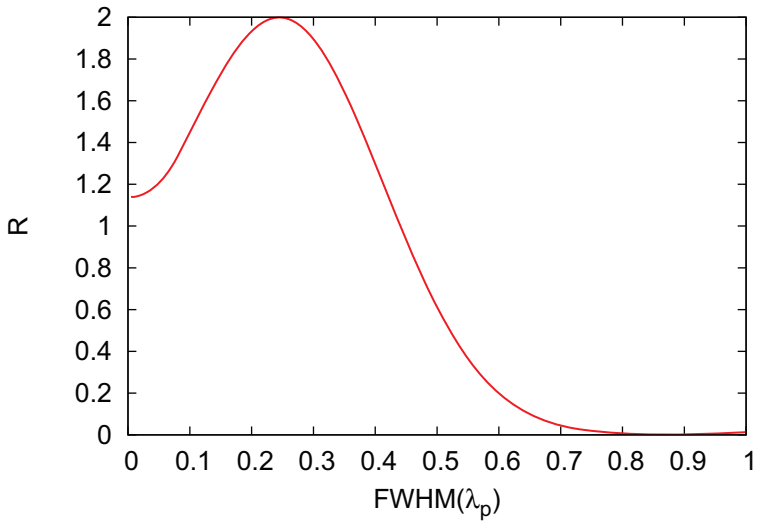

Figure 12: Dependence of the transformer ratio by the FWHM of a Gaussian driver.

As an example in Fig.12 is represented the transformer ratio achieved with a single Gaussian driver by changing its length. The maximum achievable is as expected $R = 2$ for a FWHM$= 0.4898\ \lambda_p$ [59].

4.3.2 Beam loading and energy spread

Reasonably the witness bunch as well is able to excite a plasma wakefield. Increasing the charge of the witness bunch increases as well the intensity of the excited wave, up to the point in which becomes as relevant as the wakefield of the driver, affecting the efficiency of the wakefield. Such a problem is known as beam loading and is one of the limit occurring in PWFA [60].

The beam loading efficiency is defined as the fractional energy gained by the witness bunch:

$$\eta_b = \frac{\Delta\gamma_{in} - \Delta\gamma_{out}}{\Delta\gamma_{in}} \tag{41}$$

where $\Delta\gamma_{in/out}$ are the energies of the wake before and after the witness bunch. In [61] has been evaluated in a simplified model the expression for the beam loading efficiency:

$$\eta_b = \frac{N}{N_e}(2 - \frac{N}{N_e}) \tag{42}$$

where N is the number of particles in the witness bunch and N_e is the beam loading limit for which the efficiency is maximum. N_e is defined as the

maximum number of particle for the witness bunch that can be stored in a small segment $l \ll \lambda_p$ in order to excite a wave that would cancel the one of the driver. The value evaluated in [61] is:

$$N_e = \frac{n_p A_b}{k_p} \frac{E_z}{E_0} \tag{43}$$

where $A_b \gg \pi/k_p^2$ is the cross-section of the witness beam.

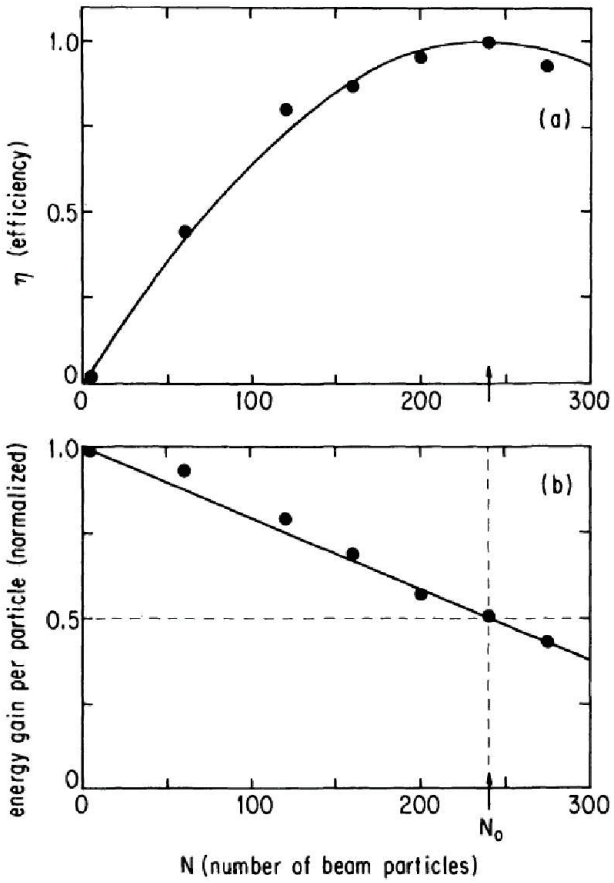

Figure 13: Beam loading and energy spread as a function of the number of particles in the beam (Picture taken from Ref. [61]).

Although is desirable to load a witness bunch with N_e particles, so that the whole wakefield energy is deposited in the bunch, for a symmetric unshaped bunch this might lead to an high energy spread. In [61] has been shown that the maximum energy spread is actually achieved when the beam loading limit is reached. This appears reasonable since in such a simplified

model, the front of the witness bunch experiences the maximum wave, that linearly decreases because of the energy deposited, up to the end of the bunch in which is zero (Fig.13).

Such problems can be nevertheless overcome by using a tailored bunch.

5 Beam dynamics

In the previous sections the explicit dynamics of the driver has not been taken into account by considering the wakefield excited by short bunches. This is not the case in configurations involving the onset of the self-modulation instability for example [26], in which the driver is much longer than the plasma wavelength. In such cases the driver is affected as well by the plasma wave generated that therefore reshape the whole configuration. For a full description of the dynamics it is therefore necessary to couple the beam evolution with that of the wave.

In particular, due to the framework depicted previously, the relevant dynamics that must be taken into account is the transverse one, occurring on a faster time scale than the longitudinal one.

It is necessary therefore to develop a model that takes into account the evolution of the beam including the self-fields generated and the external one.

5.1 Emittance pressure

Before going in the details of the dynamics of the beam it is worth first to give a brief description on the nature of the emittance and its effects on the beam evolution. For the purpose of this work we describe only the transverse emittance.

The emittance is a parameter related to the "quality" of the beam, taking into account on the evolution of the transverse projection of the beam driven by the intrinsic thermal spread [62].

There is not a unique definition for the emittance. Considering a two dimensional system with paraxial approximation, $v_x \ll v_z$ with z the direction of propagation, the emittance is defined as [63]:

$$\epsilon = \frac{1}{\pi} \int dx dx' \tag{44}$$

where $x' = v_x/v_z$. The emittance therefore is related to the area occupied by the beam particles in the trace-space $x - x'$ as can be seen in Fig.14. Such definition nevertheless does not describe appropriately the beam quality in term of beam degradation since the area in the trace-space remains constant during the beam evolution for the Liouville theorem. A far better definition for the emittance that is closely related to the thermal motion of the beam particles is the rms emittance [62]:

$$\epsilon_{RMS} = \sqrt{< x^2 >< x'^2 > - < xx' >^2}. \tag{45}$$

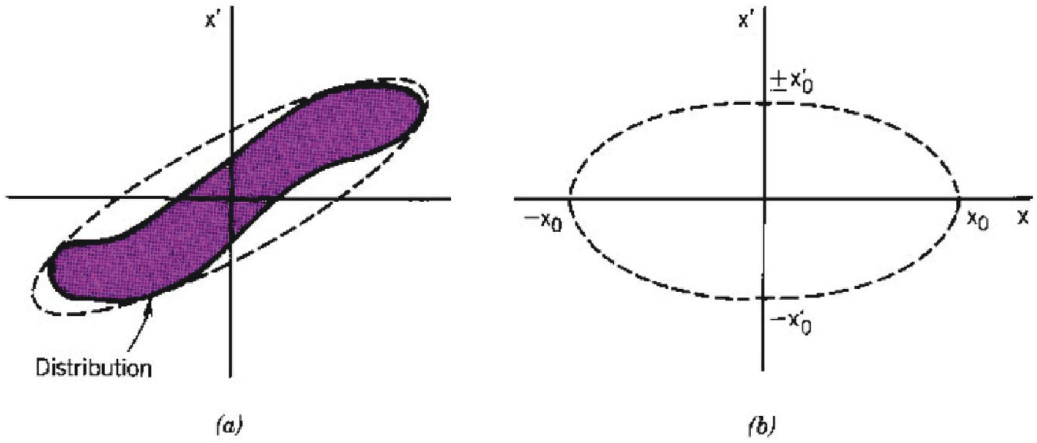

Figure 14: Example of the emittance for a specific distribution of particles (Picture taken from Ref. [63]).

The downside of such definitions of the emittance it is the reduction induced by increasing the longitudinal momentum, although eventually there is no change in the transverse distribution of the beam. In order to avoid this problem is generally used the normalized emittance $\epsilon_n = \beta\gamma\epsilon$. This way the growth of the emittance is explicitly related to a transverse degradation of the beam.

The emittance is not only a useful tool for characterizing the quality of the beam, but since it is related to the transverse velocity spread of the beam particles, plays a role as well in the dynamics.

Following [63] it is possible to express the force exerted by the emittance on the beam. A set of assumptions has to be fixed:

- Azimuthal symmetry for a cylindrical beam;
- Beam particles are confined inside a radius R;
- Paraxial approximation for the beam.

Assuming that the emittance would provide an expanding force to the beam, due to the diffusion-like nature of the force, in order to compensate this effect a linear force confining the beam has to be applied, specifically $F(r) = -F_0(r/R_0)$. If this is the only force acting on the beam particles, these perform radial oscillations with frequency:

$$\omega_r = \sqrt{\frac{F_0}{\gamma m R_0}}. \tag{46}$$

By definition the emittance is related to the transverse displacement as:

$$\epsilon = R\frac{v_{r0}}{v_z} = \omega_r \frac{R^2}{v_z}. \tag{47}$$

Replacing in the last expression that for the frequency we obtain the necessary radial force to compensate the emittance pressure:

$$F_0\left(\frac{r}{R}\right) = \frac{\epsilon^2 v_z^2 \gamma m}{R^3}. \tag{48}$$

This represents an effective force acting on the beam due to the thermal motion of the beam particles. When evaluating the full dynamics of the beam, including self-generated fields and external ones, the contribution due to the emittance has to be taken into account as well.

5.2 Envelope model

It is possible now to set a model for describing the full dynamics of a beam, including the effects of the self-generated fields as well the external applied one.

A simple approach is to consider the transverse motion of a single beam particle according to Newton's law:

$$\frac{d^2}{dt^2}(\gamma m \mathbf{r}) = F_r \hat{r} \tag{49}$$

where we have assumed the beam propagating along the z direction.

In order to simplify the model we can set a series of assumptions that are in line with the previous one related to the emittance force and the plasma wakefield. We can therefore assume an axisymmetric model. Moreover we consider a beam with constant velocity, therefore $\gamma = const$. Under these assumptions, the equation for the transverse motion turns into:

$$\hat{r}\left(\frac{d^2 r}{dt^2} - r\left(\frac{d\theta}{dt}\right)^2\right) + \hat{\theta}\left(2\frac{dr}{dt}\frac{d\theta}{dt} + r\frac{d^2\theta}{dt^2}\right) = \frac{F_r}{m\gamma}\hat{r}. \tag{50}$$

Since no forces are applied in the $\hat{\theta}$ direction, we have the conservation of the angular momentum:

$$L = r^2 \frac{d\theta}{dt} \tag{51}$$

that replaced in the previous equation considering just the motion in the $\hat{r}$ direction gives:

$$\frac{d^2 r}{dt^2} - \frac{L}{r^3} = \frac{F_r}{m\gamma}. \tag{52}$$

The nature of F_r involves both the forces arising from the self-generated fields of the beam, that have to be included through the Maxwell equations in the model, both the external fields applied. This equation holds for the single charged particle composing the beam. A simple extension to the dynamics of the whole beam can be done by replacing $r = r_b$ and including the emittance pressure in the model:

$$\frac{d^2 r_b}{dt^2} - \frac{L}{r_b^3} - \frac{\epsilon^2 v_z^2}{r_b^3} = \frac{F_r}{m\gamma}. \tag{53}$$

It is worth noting that such a procedure is valid only for homogeneous beam subject to a linear transverse force.

A more accurate procedure to obtain the beam dynamics in term of the RMS emittance, has been provided by [64] evaluating the equation of motion for the second moment of the charged particles, but the development of that model goes beyond the aim of this work.

6 Transformer ratio enhancement

In section 4.3.1 we have defined the transformer ratio R as the parameter that describes the efficiency of energy transfer from the driver to the witness bunch. In linear theory, using symmetric driver, the parameter is limited to 2.

In early experiments of plasma wakefield such limit was not an important issue due to the short distances the driver used to interact with the plasma, limiting the amount of energy that was deposited. On the other hand actual experiments may involve a longer interaction time between the driver and the plasma, therefore the efficiency of energy transfer becomes a relevant parameter as well.

There are different ways to improve the transformer ratio in a plasma wakefield accelerator. A solution consists in exciting nonlinear wakefield [59, 65]. Another possibility is the use of an asymmetric driver [66, 67], like a triangular shaped beam density profile. Lastly there is the possibility to employ a train of bunches with a ramped density profile [68, 69]. The last two concepts are actually similar each other, the ramped train of bunches resembling the triangular shaped driver.

In this section we deal with the use of the ramped sequence of bunches for enhancing the transformer ratio. We first describe the theoretical background that suggested the possibility to use the ramped sequence of symmetric bunches. The limit of the theoretical description it is the applicability only to bunches with finite support, such as flat-top bunches.

We then extend therefore the analysis to the case of a driver defined by a train of realistic Gaussian bunches. This new approach leads to rather different results compared to the well established case of flat-top bunches.

We develop a different instrument to analyze the new results, being able this way to properly compare them with the theoretical model and to improve the final transformer ratio in the new configuration by a proper reshape of the driver.

The results presented in this section are based on the work [70].

6.1 Transformer ratio of a train of flat-top bunches

A complete analysis of the transformer ratio should involved the 2-dimensional equations for the wakefield expressed in section 4.1.3. Assuming a non-evolving driver on the other hand, with fixed radius, it is possible to factorize the beam density profile:

$$\rho_b(r, \xi) = f_b(r) g_b(\xi). \tag{54}$$

This assumption is rather strong since the driver, especially a modulated one, is affected by the wakefield as well, therefore the radius of the driver experiences focusing and defocussing forces according to the position ξ inside the driver. On the other hand this is a reasonable assumption if we look for the proper initial conditions for the driver in order to improve the transformer ratio.

Under this assumption the longitudinal field itself can be separated in its radial and longitudinal component:

$$E_z(r,\xi) = F(r)\int_0^{\xi} g_b(\xi')\cos[k_p(\xi-\xi')]d\xi'. \tag{55}$$

The expression resembles the one for the 1-dimensional case, with an additional contribution given by the transverse factor. On the other hand when evaluating the transformer ratio, the prefactor will be canceled out since does not depends on the longitudinal position and therefore is the same inside and outside the driver. It is reasonable so to perform the analysis assuming a 1-dimensional wakefield as in section 4.1.2.

We look first at the wakefield excited by a train of flat-top bunches with equal lengths. Such configuration corresponds to a density profile:

$$g_b(\xi) = \sum_{m=1}^{M} \rho_m \left[H(\xi - \xi_m + \frac{L}{2}) - H(\xi - \xi_m - \frac{L}{2}) \right] \tag{56}$$

where ρ_m is the charge density of the individual bunches, M is the total number of bunches, ξ_m is the position of the mth bunch and L is the length of the bunches.

The total wakefield generated is the sum of the wakefields generated by every single bunch. We can evaluate the expression analytically for such density profiles, obtaining so inside and outside the Mth bunch the longitudinal fields:

$$E_{in}(\xi) = -2\sum_{j=1}^{M-1} \rho_j \sin\left(\frac{k_p L}{2}\right)\cos\left[k_p\left(\xi-\xi_j\right)\right] - \rho_M \sin\left[k_p\left(\xi - \xi_M + \frac{L}{2}\right)\right] \tag{57}$$

$$E_{out}(\xi) = -2\sum_{j=1}^{M} \rho_j \sin\left(\frac{k_p L}{2}\right)\cos\left[k_p\left(\xi-\xi_j\right)\right]. \tag{58}$$

The value of the longitudinal fields, and as a consequence that of the transformer ratio, depends on the choice of the three parameters ρ_j, L and ξ_j.

In order to reduce the number of parameters involved in the analysis we can assume $L = \lambda_p/2$. This is a reasonable assumption since it provides the maximum transformer ratio for the case of a single bunch.

The other two parameters has to be set according to the final result that the configuration should achieve. If the goal is to maximize the final accelerating field behind the driver, then the density has to be the same for all the bunches ($\rho_j = \rho_m = \rho$) and the periodicity has to be equal to a plasma wavelength(or a multiple integer, $\xi_j - \xi_{j-1} = k\lambda_p$).

$$E_{in}(\xi) = -(2M-1)\rho\cos\left[k_p\left(\xi-\xi_1\right)\right]) \tag{59}$$

$$E_{out}(\xi) = -2M\rho\cos\left[k_p\left(\xi-\xi_1\right)\right]. \tag{60}$$

The downside of such configuration is that it does not bring any improvement at the transformer ratio. Even worst the transformer ratio decreases with the number of bunches as $R = 2M/(2M-1)$.

Such configuration for a train of bunches involves the constructive interference among the wakefields generated by the single bunches. This guarantees an increasing intensity of the accelerating field behind the driver, but also an increasing decelerating field under the bunches. The transformer ratio cannot be improved therefore by such configuration (Fig.15).

The configuration that guarantees instead an improvement in the transformer ratio is the train of bunches with a ramped peak density. The cornerstone of such configuration is the same decelerating field generated under every bunch. This way it is not anymore a function of the number of bunches as in the previous case.

In order to derive the scaling for the parameters one can simply impose the desired condition, resulting in the equation:

$$2\sum_{j=1}^{M-1}\rho_j\sin\left(\frac{k_pL}{2}\right)\cos\left[k_p\left(\xi-\xi_j\right)\right] + \rho_M\sin\left[k_p\left(\xi-\xi_M+\frac{L}{2}\right)\right] =$$
$$= \rho_1\sin\left[k_p\left(\xi-\xi_1+\frac{L}{2}\right)\right]. \tag{61}$$

The equation states that the decelerating field under the Mth bunch has to be the same as under the first bunch. Assuming again a bunch length $L = \lambda_p/2$, the solution of the equation provides the scaling for the bunch densities and periodicity as:

$$\rho_j = (2j-1)\rho_1 \tag{62}$$

$$\xi_j = \xi_{j-1} + \frac{3}{2}\lambda_p. \tag{63}$$

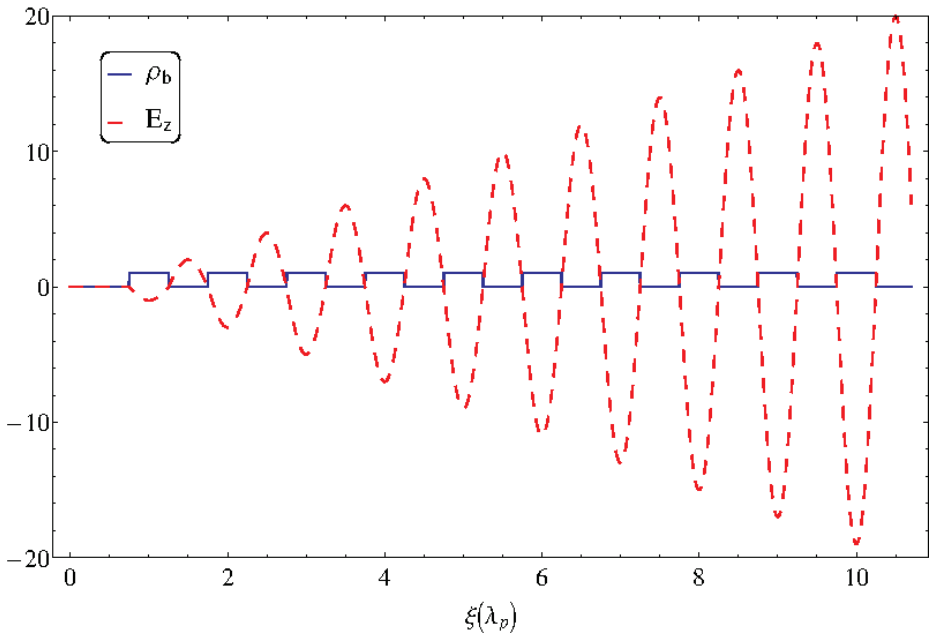

Figure 15: Electric field for a train of ten bunches with periodicity λ_p. The constructive interference among the electric field generated by the single bunches enhances both the decelerating and the accelerating fields.

It is worth to be noting that this is just one of the possible solutions for the previous equation since there are two parameters involved for one single equation.

Nevertheless this choice of the parameters guarantee a solution of the Eq.(61) for any longitudinal position. This can be seen easily in the case of the bunches, for which the equation can be rewritten as:

$$1 + \tilde{\rho}_2 \left(\cos[k_p \Delta] + \tan[k_p(\xi - \xi_1) \sin[k_p \Delta]]\right) = 0 \tag{64}$$

where $\tilde{\rho}_2$ is the charge density of the second bunch normalized to the density of the first bunch and $\Delta = \xi_2 - \xi_1$ is the displacement of the second bunch respect to the first.

It appears clearly that the only solution independent by the position ξ is obtained only when $\sin[k_p \Delta] = 0$, therefore the solution provided previously.

For such choice of the parameters, the resulting electric field behind the driver turns into:

$$E_{out}(\xi) = 2M\rho_1 \cos\left[k_p(\xi - \xi_1)\right]. \tag{65}$$

The transformer ratio with such configuration scale as $R = 2M$ since the accelerating field behind the driver is a linear function of the number of bunches while the decelerating field is constant.

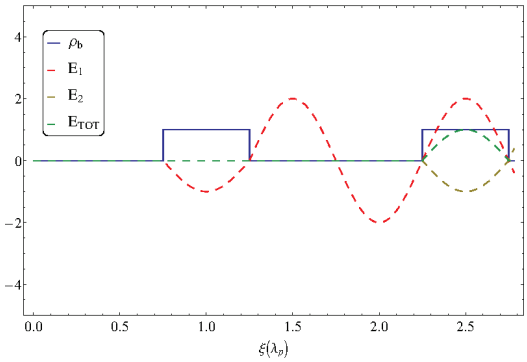

(a)

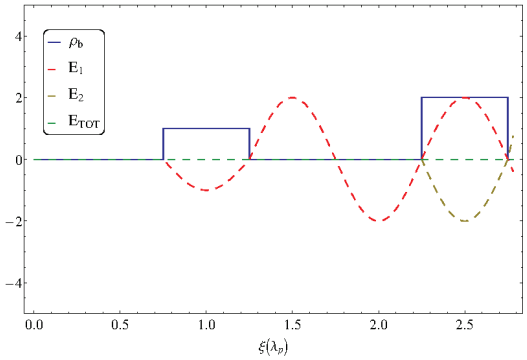

(b)

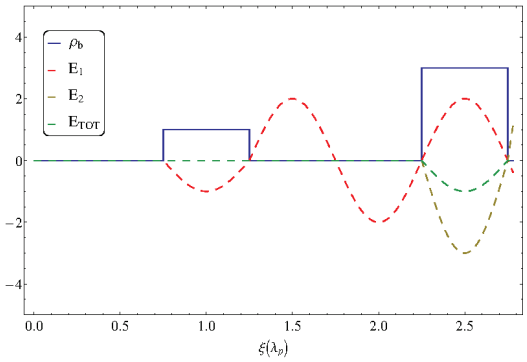

(c)

Figure 16: Electric field under the second bunch for different values of the second bunch density. The red line represent the electric field generated by the first bunch, the green line the electric field generated by the second bunch and the brown line the combination of the two. a)$\rho_2 = \rho_1$, b)$\rho_2 = 2\rho_1$, c)$\rho_2 = 3\rho_1$

In such configuration, contrary to the previous one, a destructive interference among the wakefields generated by the single bunches takes place, due to the separation of half integer of the plasma wavelength (Fig.16). The increasing bunch density is necessary to provide the required decelerating field: placing bunches with the same density would actually accelerates the next bunches (Fig.16a), that so would take energy from the system; doubling the density would compensate the previous wakefield, therefore the next bunches does not provide energy to the system at all (this is the case in which the limit for the beam loading is reached as explained in Section 4.3.2(Fig.16b); the ramped density instead allows to compensate the previous wakefield and still provides energy to the system (Fig.16c). to the system.

The aspect that might appear surprising is the linear scaling for the accelerating field with the number of bunches, as in the case of a coherent interference among the wakefields. On the other hand, although the scaling is the same in the two configurations, in the last one the required density in order to excite the wakefield is increased since part of the charge is necessary to compensate the previous longitudinal field.

6.2 Transformer ratio of a train of Gaussian bunches

The framework depicted in the previous section holds for flat-top bunches. Real experiments on the other hand usually deal with different density profiles, for example Gaussian bunches. It is necessary therefore to check if the same results hold also for different density profiles.

The model used for the analysis of Gaussian bunches is still a 1-dimensional one, holding the same assumptions made in the previous section on the static nature of the configuration.

Gaussian bunches are defined as

$$f(\xi, \xi_1, \sigma) = e^{-\frac{(\xi-\xi_1)^2}{2\sigma^2}}. \tag{66}$$

As in the previous case, the field inside the Nth bunch can be considered as being the sum of an external field provided by the combined wake of the preceding bunches, and the internal field self-generated by the bunch itself:

$$E(\xi) = E_{in}(\xi, \rho_N, \xi_N, \sigma_N) + \sum_{n=1}^{N-1} E_{out}(\xi, \rho_n, \xi_n, \sigma_n). \tag{67}$$

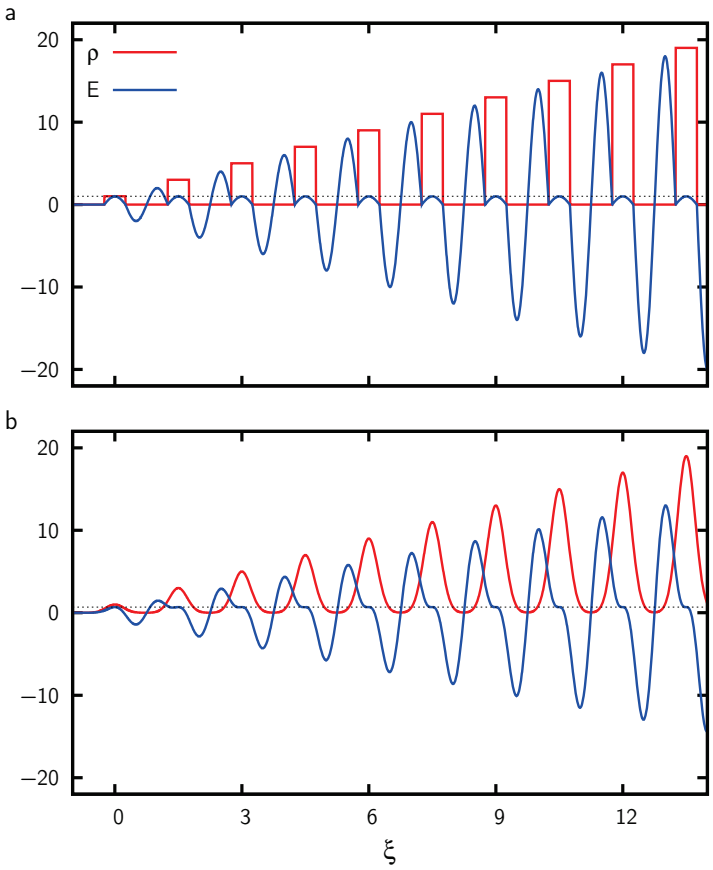

Figure 17: Driving beam and associated electric field for a train of a) flat-top and b) Gaussian profile bunches. In both cases the periodicity and density scales according to the optimal scaling for flat-top bunches. The dotted black line marks the maximum decelerating field under the first bunch. The flat-top profile allows the same decelerating field under every bunch, while the Gaussian profile does not.

For Gaussian bunches this results in:

$$E_{in} = \rho_0 \sqrt{\frac{\pi\sigma^2}{2}} e^{-\frac{\sigma^2}{2}} \,\mathrm{Re}\left(e^{-i(\xi-\xi_1)} \,\mathrm{erfc}\left(-\frac{\xi - \xi_1 - i\sigma^2}{\sqrt{2\sigma^2}} \right) \right) \tag{68}$$

$$E_{out} = \rho_0 \sqrt{\frac{\pi\sigma^2}{2}} e^{-\frac{\sigma^2}{2}} \cos(\xi - \xi_1) \tag{69}$$

where E_{out} corresponds to the limit $\xi - \xi_1 \gg \sigma$.

Differently from the case of flat-top bunches, only the external field is sinusoidal for Gaussian bunches. The internal field therefore cannot compensate the external field in the same fashion of flat-top bunches at every point. In Fig.17 the difference between the two cases appears more clearly.

For Gaussian bunches the constraint of the same decelerating field under every bunch is fulfilled only at the bunch center. On the other hand the rest of the bunch experiences a different decelerating field, eventually greater than the one at the center. A direct application of the same scaling of the parameters as for flat-top bunches does not bring the same result using Gaussian bunches.

Further, we note that the property of having a sinusoidal internal field is unique to the flat-top profile, with the result that the scaling $R \sim N$ cannot be achieved for any other density profile.

6.3 Weighted Transformer Ratio

Since the same scaling of the flat-top profile for the bunch parameters does not provide an increasing transformer ratio for Gaussian bunches, it is necessary to find a different way to improve the transformer ratio in this case.

First of all it is necessary to reconsider the definition of the transformer ratio for profiles different from flat-top. For example for Gaussian bunches, is not well defined the maximum decelerating field "acting on the driver", since they does not have a finite support. One possible solution is to consider the maximum decelerating field within a finite range of the bunch center. This corresponds to applying an homogeneous weighting to the field, but this is somewhat arbitrary, as it is expected that higher-density parts of the bunch contribute more to the wake.

In order to find a better definition for the transformer ratio, we need to keep in mind the definition of this variable. As shown in Section 4.3.1, the parameter provides an estimate of the efficiency of energy transfer between the driver and the witness bunch. The definition as the ratio between the accelerating and decelerating fields is a consequence of the assumption of non evolving drivers that generate the same electric field and as well are all affected in the same way by this one.

In the case of inhomogeneous driver, different slices of the beam provide different energies to the wakefield, and as well they are subjected in a different way from the external field.

From these considerations results natural to weight the decelerating electric field to the relative bunch density, $E_W(\xi) = E(\xi) f(\xi, \xi_1, \sigma)$. The weighted transformer ratio for a single bunch is then

$$R_W = \frac{\max_\xi |E_{out}(\xi)|}{\max_\xi |E_W(\xi)|}, \tag{70}$$

It is worth noting that the new definition of transformer ratio returns the same value for flat-top profiles as in the unweighted case, and that the optimal

transformer ratio for a symmetric pulse is still 2, without any contradiction to the previous theory.

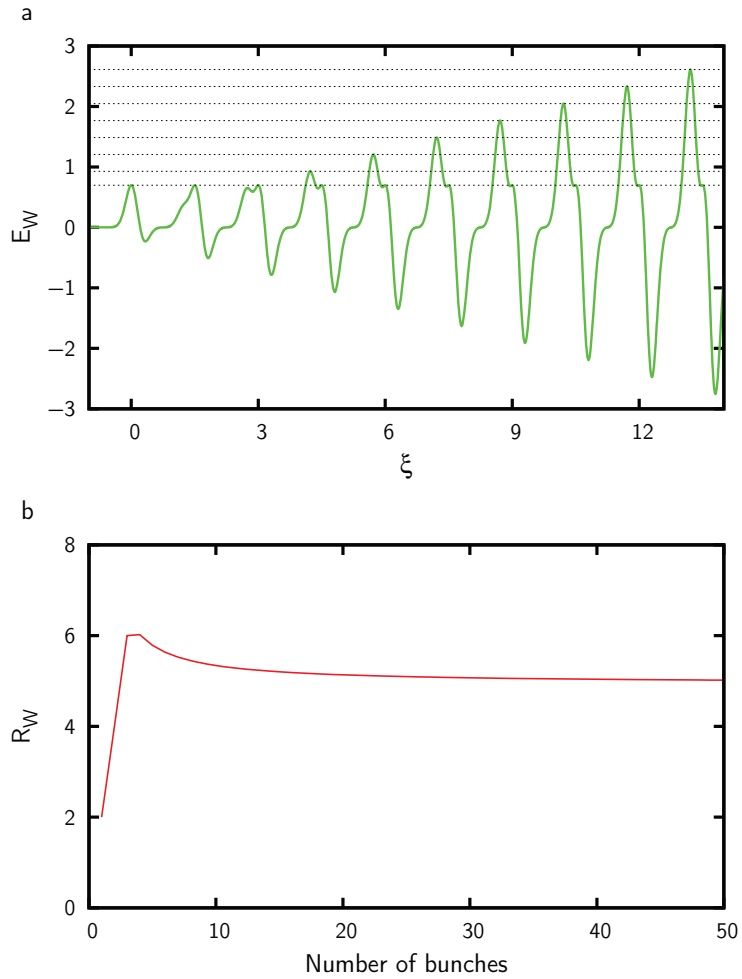

Figure 18: a) Weighted electric field, E_W, for the train of Gaussian bunches considered in Fig.17. The periodicity and the density are chosen to match the optimal scaling for flat-top bunches. The dotted black line represent the peak decelerating field. b) Weighted transformer ratio, R_W, as a function of number of bunches for the same configuration.

For a train of bunches, the weighted electric field is:

$$E_W(\xi) = \max_n \big(f(\xi, \xi_n, \sigma_n)\big) E(\xi). \tag{71}$$

and therefore the weighted transformer ratio:

$$R_W = \frac{\max_\xi |\sum_n E_{out}(\xi)|}{\max_\xi |E_W(\xi)|}. \tag{72}$$

Fig.18a shows the weighted electric field for the same configuration of Gaussian bunches considered in Fig.17b. The first three bunches experience the same maximum decelerating field. On the other hand from the fourth bunch the decelerating field increases linearly.

As the maximum accelerating field E^+ grows linearly, $E^+ \sim N$, this leads to the behavior seen in Fig.18b for the transformer ratio: a linear increase for the first three bunches then decreasing from the fifth bunch.

In order to understand this behavior for the transformer ratio we still remember that the decelerating field is composed by a sinusoidal component due to the wakefield excited by the previous bunches, and a non-sinusoidal perturbation due to the nonlinear wakefield excited by the bunch itself.

The sinusoidal component is constant despite increasing the number of bunches since it is compensated by the destructive interference of the wakefield in a similar fashion as for flat-top bunches, providing the same decelerating field at the center of the bunch.

On the other hand, the nonlinear component is not affected by the destructive interference in the same way as the sinusoidal component and still linearly increase as $\sim (2N-1)$, until it becomes the dominant term. This emerges clearly from Fig.18a, where the maximum of the decelerating field shifts from the center to the side due to the increasing nonlinear contribution of the decelerating field caused by the increasing bunch density on the front of the bunch.

6.4 Optimization of the Transformer Ratio

The results of the previous section underline the different behavior, for what concerns the transformer ratio, between Gaussian and flat-top bunches. Since we have been able to define a new measure for the transformer ratio that better fits with a more general condition rather than flat-top bunches, we can now perform an extended analysis in order to find the proper parameters to enhance the transformer ratio also for Gaussian bunches.

Due to the nonlinear nature of the wakefield excited inside the bunch, the optimal parameters must be found by a code developed to scan the entire parameters space. The maximum accelerating field is obtained from the expression for E_{out} in Eq.(69), while the maximum decelerating field is evaluated numerically from Eqs.(68,69) and (67).

This semi-analytical approach resulted to be faster than the full numerical evaluation of Eq.(55), with a computation time scaling linearly with the number of bunches.

First of all we consider a periodic train of bunches. The reason for such choice is the wide use of this configuration in the experiments and as well

being the one achieved using the self-modulation technique described in [26].

A parameter scan is carried out over the three independent variables: the bunch length σ_n, the periodicity $\Delta\xi$, such that $\xi_n = n\Delta\xi$ and the density scaling, $\Delta\rho$, such that $\rho_n = 1 + (n-1)\Delta\rho$.

The optimal transformer ratio and the corresponding parameters as a function of the number of bunches, are shown in Fig.19. The transformer ratio tends to saturate, reaching $R_W = 23$ for 50 bunches. Although the result is not comparable to that achieved by flat-top bunches, $R_W = 100$, is still a remarkable improvement respect to a direct application of the optimal scaling for a flat-top profile to Gaussian bunches that would result in a transformer ratio $R_W \sim 6$ as shown in Fig.18b.

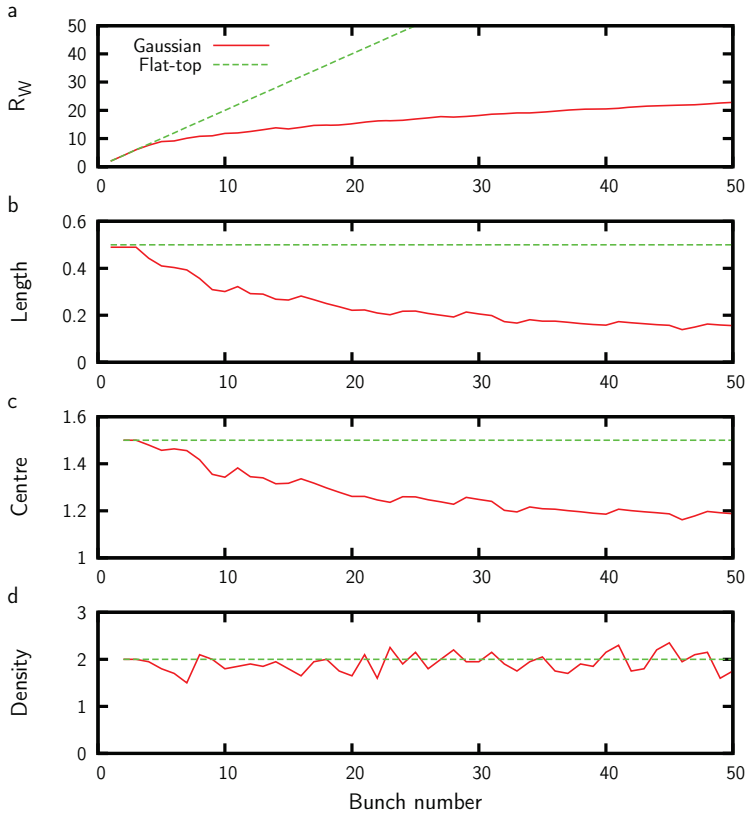

Figure 19: Optimal transformer ratio and the corresponding scaling parameters for a periodic bunch train, as a function of total number of bunches. a)Weighted transformer ratio, R_W, b)FWHM bunch length, c)Bunch periodicity, such that $\xi_n = n\Delta\xi$, and d)Density scaling, such that $\rho_n = 1+(n-1)\Delta\rho$. Numerical results for Gaussian bunches are compared to the analytical solutions for the flat-top profile.

An even better result can be reasonably achieved removing the constraint

on the periodicity of the bunches and performing a full parameter scan. Such a train of bunches could be achieved experimentally, for example, by using an electron mask [71] or a photoinjector with a laser pulse shaper [72].

The optimization is performed one bunch at the time, finding the optimal parameters of the last bunch once fixed the previous upstream to the already evaluated fitting parameters. The results, presented in Fig.20, show an even better transformer ratio for a fully-optimized bunch train respect to the previous cases, giving $R_W = 40$ for 50 bunches.

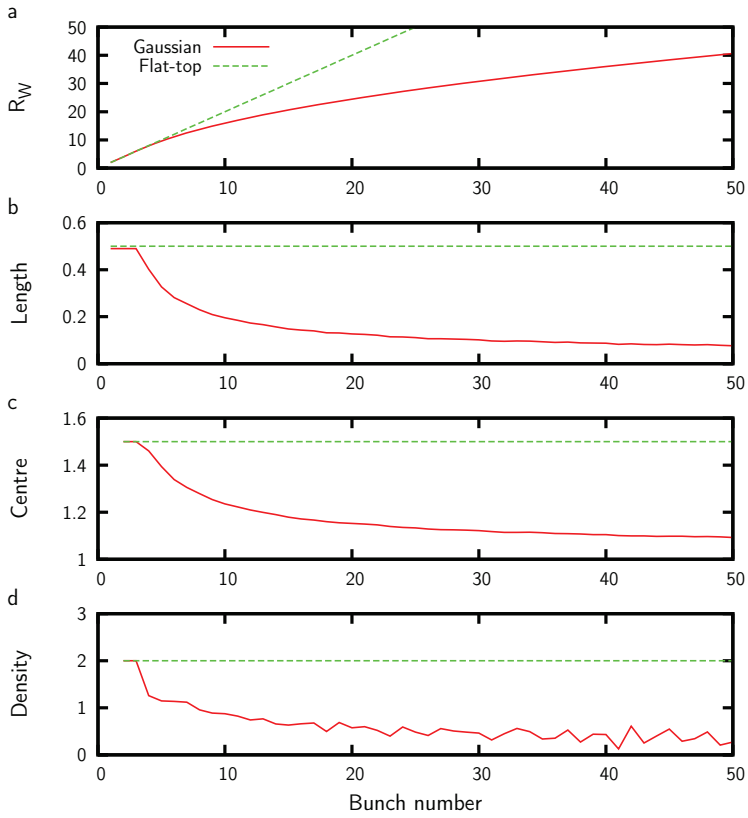

Figure 20: Optimal transformer ratio and the corresponding scaling parameters for a fully optimized beam. a)Weighted transformer ratio, R_W, b)FWHM bunch length, c)Bunch position, ξ_n, and d)Bunch density, ρ_n. Numerical results for Gaussian bunches are compared to the analytical solutions for the flat-top profile.

For 50 bunches the transformer ratio in this case does not show yet a full saturation, leaving margins for a further improvement. On the other hand a different problem arises when looking on the parameter space increasing the number of bunches (Fig.21).

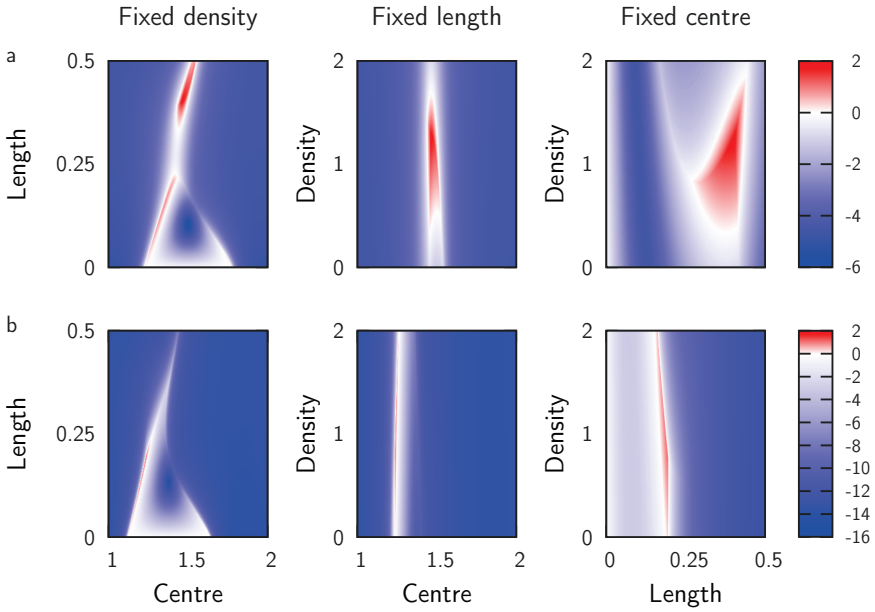

Figure 21: Change in the weighted transformer ratio varying two out of three parameters for a configuration with a) fourth and b) 10th bunch. The third parameter is fixed to the optimal value, corresponding to a)$\Delta\rho$=1.26, FWHM length=0.403, $\Delta\mu$=1.46, and b)$\Delta\rho$=0.790, FWHM length=0.193, $\Delta\mu$=1.24. Red areas show an increase in transformer ratio.

Increasing the number of bunches in the configuration, the parameter space that provides a large transformer ratio becomes smaller and smaller: for the fourth bunch, a small deviation from the optimal parameters does not strongly affect the resulting transformer ratio, while for the 10th bunch there is a much larger reduction by smoothly deviating from the optimal parameters.

It does not seem reasonable therefore to extend the analysis beyond the 50th bunch since, although the saturation in the transformer ratio is not yet achieved, the optimal parameters for an increasing number of bunches become increasingly difficult to achieve experimentally and the fast decay of the transformer ratio for a small deviation for the matching parameters does not provide margin for mistakes.

Although the final result in term of transformer ratio is different between the periodic and fully-optimized case, the behavior of the individual parameters can be explained in a similar fashion.

The optimal bunch length (Figs.19c, 20c) becomes shorter for increasing bunch number. This can be understood from Fig.17 noting, as previously mentioned, that the maximum decelerating field occurs at the leading edge of

the bunch. Decreasing the bunch length therefore reduces the bunch exposure to the maximum decelerating field.

The reduction of the bunch length drives the reduction in the bunch spacing (Figs.19b, 20b). For Gaussian bunches in fact, as emerges from Eqs.(68, 69), the phase of the internal field depends on the bunch length. This is on the other hand not true for the external field, in which it affects only the amplitude.

Therefore by reducing the bunch length, the internal field is affected by a phase-shift relative to the bunch center. In order to compensate this effect, in order to have the absolute maximum of the decelerating and accelerating field align in the next bunch, the periodicity needs to be tuned as well. This leads to the decreasing bunch periodicity.

Finally the behavior of the density is related again to the compensation of the effects driven by the other two parameters.

In the fully-optimized case, shown in Fig.20d, the decreasing density can be understood from the reduced growth of the external field. While for flat-top bunches the density has to scale linearly in order to compensate the linear scaling of the external field, for Gaussian bunches this is not required since the external field growth is reduced by the modified periodicity. This results in the end in a lower density required increasing the number of bunches.

A more complex behavior emerges for the density in the periodic case (Fig.19d). This effect persists increasing the resolution of the parameter scan, meaning that it depends by the strong nonlinear response of the system. Changing the density scaling modifies both the relative weight of the drive bunches, and so the phase and amplitude of the external field, and the amplitude of the internal field, leading to a strongly nonlinear dependence of the transformer ratio on the density.

On the other hand, we note that this dependence is extremely weak for both the periodic and fully-optimized case. Choosing a fixed density scaling of $\Delta\rho = 2$ results in a decrease in R_W of $< 4\%$ for any number of bunches.

The results presented, although not comparable to those that can be achieved theoretically with flat-top bunches, are of key importance for the study of the transformer ratio for PWFA.

The different behavior of a generic density profile, in particular Gaussian, respect to the flat-top one, required an accurate analysis in order to understand the nature of the differences and a way to mitigate them.

A great improvement of the transformer ratio can now be achieved as well for bunches with a generic density profile, leading to a more efficient energy transfer, especially when the driver can interact with the plasma for long distance. More important, the analysis developed brings a better understanding of the transformer ratio for a generic density profile.

On the other hand, the analysis still required strong assumptions, in particular the non evolving nature of the driver. This is of course not true, especially in the situations in which the improvement of the transformer ratio can be important, i.e. interaction for long distances.

In the next section therefore we study the stability of a modulated beam, analyzing the effects of the wakefield on the driver itself, its equilibrium configuration and its duration.

7 Stability of a modulated beam

In the previous section we have assumed a non evolving driver in order to study the transformer ratio. This is rather a strong assumption, since the driver while propagating in the plasma is subjected to both the self-generated fields and the wakefield excited.

It is therefore a key aspects in PWFA is the stability of the driver. In order to maintain the excited wave for long distances, achieving so a higher final energy for the the witness bunch, the driver has to be preserved from the deterioration.

In the case of a single short bunch this is not one of the main problems, but becomes relevant for configuration with a long driver. This is the case for example of modulated beams.

A long driver is subject to the wakefield generated by the interaction with the plasma and would eventually leads to the onset of a various range of instabilities that can then cause a fast deterioration. The more the driver deteriorates, the less particles coherently contribute to the wakefield, eventually reducing its intensity up to the complete disappearance.

It is of key importance therefore to properly study the stability of the driver during its propagation in the plasma and find the optimal conditions that provide a strong wakefield together with a longer driver duration.

The aim of this section is to provide such analysis for a configuration involving a modulated driver. This approach is achieving greater interest [24, 73–76] due to the high intensities of the wakefield that can be excited, together with a freedom in the specific characteristics of the wakefield due to the tunability of the driver.

This section looks in particular at the transverse stability of the driver a problem already studied in previous works [58, 77–79] and still object of deep analysis.

It is reasonable to consider just the transverse dynamics due to the different time scale at which the longitudinal and transverse dynamics develop, being the first much slower than the second.

The analysis is performed using the 2-dimensional model described in Section 4.1.3 for the wakefields. The equations are self-consistently coupled with the envelope description of the beam dynamics presented in Section 5.

In the first part of the analysis we deal with the transverse equilibrium of a train of flat-top bunches. Such configuration is more feasible for an easy understanding of the physical phenomena occurring, removing some of the numerical issues that can arise from more complicated bunch shapes.

The results concerning the equilibrium configuration are then extended to Gaussian bunches, comparing the similarities with the previous configuration.

Once the equilibrium configuration is defined, the stability of the modulated beam is taken into account. The most relevant aspect that is studied in this analysis, is the role of the emittance in the driver stability. As explained in Section 5, the beam is always subject to the emittance-driven pressure. Due to the coupling between the driver and the plasma, this effect influences as well the excited wakefield.

A relevant emphasis will be given therefore to the effects on the wakefield of the emittance-driven expansion of the front of the bunch, the so called "emittance-driven erosion".

Once analyzed the problem of the stability, we perform an optimization of the modulated beam, aimed to mitigate the deterioration caused by the emittance-driven erosion.

The results of the next sections are based on the works [80, 81].

7.1 Beam envelope model in a plasma wakefield

In the previous sections have been already described the 2-dimensional model we are going to use for the study of the stability. The main assumptions described previously therefore still hold in the actual development, in particular the azimuthal symmetry of the system.

In this section we briefly review the model, showing the coupling with the envelope model for the beam.

For sake of clearance we write again the two-dimensional transverse wakefield generated inside the driver:

$$W(r,\xi) = 4\pi k_p \int_0^{\infty} \int_0^{\xi} \frac{\partial \rho(r',\xi')}{\partial r'} r' \, \mathrm{I}_1(k_p r_<) \, \mathrm{K}_1(k_p r_>) \sin[k_p(\xi - \xi')] d\xi' dr' \tag{73}$$

where $k_p = \omega_p / c$ is the plasma wavenumber, $\rho(r,\xi)$ is the bunch charge density, I_1 and K_1 are the modified Bessel functions and $r_{</>} = \min / \max(r, r')$.

We consider the wakefield excited by a flat-top bunch in the transverse direction:

$$\rho(r,\xi) = n_b q_b \left(\frac{r_0}{r_b(\xi)} \right)^2 \mathrm{H}(r_b(\xi) - r) f(\xi) \tag{74}$$

where n_b is the peak bunch density, q_b is the bunch charge, r_0 is the initial bunch radius, $r_b(\xi)$ is the radius of the beam-envelope, H is the Heaviside function and $f(\xi)$ is the longitudinal bunch profile. Although a flat-top transverse profile might not be feasible for experiments, it is useful for an easier development of the model, granting a deeper understanding of the main physical features.

The wakefield generated by such a distribution can be therefore formulated as:

$$W(r,\xi) = -4\pi k_p n_b q_b r_0^2 \begin{cases} \mathrm{I}_1(k_p r) \int_0^\xi f(\xi') \frac{\mathrm{K}_1(k_p r_b(\xi'))}{r_b(\xi')} \sin[k_p(\xi-\xi')] d\xi' \text{ for } r < r_b \\ \mathrm{K}_1(k_p r) \int_0^\xi f(\xi') \frac{\mathrm{I}_1(k_p r_b(\xi'))}{r_b(\xi')} \sin[k_p(\xi-\xi')] d\xi' \text{ for } r > r_b. \end{cases} \tag{75}$$

To self-consistently include the transverse dynamics of the driver we couple the field equations with the beam-envelope equation for the beam radius as explained in Section 5.

We already mentioned in the previous section that a more rigorous analysis of the beam dynamics should take into account of the rms radius of the beam, developing so a statistical description. Nevertheless, for the aim of this work, we stick to the previous model developed in Section 5, in particular assuming that the transverse motion of the driver can be described by the motion of its boundary like in a water-bag model. This is a valid approximation as long as the force acting inside the beam is approximately linear like in this analysis. Moreover the assumptions on the basis of the envelope model so derived, are not in contradiction with that of the 2-dimensional model for the wakefield.

Denoting with $r_b = r_b(\xi,\tau)$ and with $r_b' = r_b(\xi',\tau)$, the resulting equation for the envelope radius evolution is:

$$\begin{aligned} &\frac{\partial^2 r_b}{\partial \tau^2} = F(\xi,\tau) = \frac{\epsilon^2 c^2}{\gamma^2 r_b^3} + \\ &- \frac{4\pi k_p n_b q_b^2 r_0^2}{m_b \gamma} \begin{cases} \mathrm{I}_1(k_p r_b) \int_0^\xi f(\xi') \frac{\mathrm{K}_1(k_p r_b')}{r_b'} \sin[k_p(\xi-\xi')] d\xi' \text{ for } r_b < r_b' \\ \mathrm{K}_1(k_p r_b) \int_0^\xi f(\xi') \frac{\mathrm{I}_1(k_p r_b')}{r_b'} \sin[k_p(\xi-\xi')] d\xi' \text{ for } r_b > r_b' \end{cases} \end{aligned} \tag{76}$$

with ϵ being the normalized beam emittance, $\gamma = 1/\sqrt{1-\beta^2}$ the beam relativistic Lorentz factor and m_b the mass of the beam particles.

We are dealing with PWFA in overdense plasma $n_b < n_p$, so the dynamics described by the model can be readily interpreted as a charge neutralization of the bunch particles by the oscillating plasma electrons.

The charge neutralization weakens the Coulomb force arising from the bunch particles and therefore the pinching force generated by the bunch current is not anymore balanced. This leads eventually to a periodical focusing of the bunch. The emittance force is always defocussing, leading so to a bottom limit on the pinching derived from the neutralization.

It is worth noting that the charge neutralization is not the only requirement to obtain the pinching of the driver. It is necessary as well that the

return plasma current flows outside the beam. If this is not the case, the magnetic field induced by the plasma current can react to that of the beam reducing the effect of the pinching. This might happen in wide drivers, having a radius larger than the plasma skin depth c/ω_p.

The periodical focusing of the beam leads to a local increase of the bunch density providing therefore a stronger wakefield.

7.2 Equilibrium configuration

On the ground of the model presented in the previous section it is possible to analyze now the transverse equilibrium of a bunch interacting with a plasma. As previously mentioned, effects occurring in the longitudinal direction are discarded since they occurs on a slower time scale than the transverse motion [58].

The equilibrium configuration is first studied for a train of longitudinal flat-top bunches. Although these bunch shape is common in real experiment, provides a more clear interpretation of the physical process occurring.

The analysis is then developed as well for Gaussian bunches as well, checking for differences in the behavior between the two configurations.

7.2.1 Equilibrium configuration for flat-top bunches

We study now the equilibrium configuration for a modulated beam with flat-top longitudinal density profile. Although this is not the common driver used in experiments, it provides an easier understanding of the physical problem, removing possible nonlinear effects that can arise using different bunch shapes.

The density profile is therefore:

$$f(\xi) = \mathrm{H}\left(\xi - \xi_0 + \frac{L}{2}\right) - \mathrm{H}\left(\xi - \xi_0 - \frac{L}{2}\right) \tag{77}$$

with ξ_0 the center of the bunch and L its length. The parameters used for the analysis, for both the bunch and the plasma, correspond to the baseline of the AWAKE experiment [25] with the exception of the bunch length (Table 1).

In a similar fashion as in [58], we look for the equilibrium configuration starting from a bunch seed that in this case is the flat-top bunch defined above and then modeling it in order to reach the transverse equilibrium condition.

In the cited approach on the other hand, an optimization of the equilibrium configuration took place, removing the sections of the bunch in the defocussing phase or in the accelerated phase of the wakefield. This way

Table 1: Simulation parameters for plasma and bunch.

Parameter	Value
Plasma density (n_p)	7×10^{14} cm^{-3}
Bunch length (L)	1.2 cm
Initial bunch radius (r_0)	0.02 cm
Peak bunch density (n_b)	4×10^{12} cm^{-3}
Bunch relativistic Lorentz factor (γ)	400
Normalized bunch emittance (ϵ)	3.5 mm mrad

the obtained equilibrium configuration is initially trapped and resonantly contributes to the constructive interference of the wakefield.

In the present analysis this optimization is not performed. We look at the transverse equilibrium configuration obtained from the initial long flat-top bunch, without removing the sections that would not contribute efficiently to the wakefield. The reason for such difference is in the resulting equilibrium configuration obtained in our analysis, that resembles the one achievable in a self-modulated framework.

The transverse equilibrium is achieved when the force exerted by the wakefield is able to balance the emittance force that is always defocussing, playing a role similar to a centrifugal force.

Before going in the details of the equilibrium configuration it is worth mention some features of the dynamics.

As can be seen from Eq.(73), the head of the bunch is not subject to the wakefield since there is no perturbed plasma ahead. The dynamics of the front of the bunch therefore is described by only the emittance pressure, providing so a purely expanding front. This mechanism is known as emittance-driven erosion [82, 83] and we will see in the next sections that plays an important role in the stability of the driver.

The evolution of the head of the driver, since it is governed by just the emittance pressure, can be easily solved leading to:

$$r_b(\xi = 0, \tau) = r_{b0}(\tau) = r_0 \sqrt{1 + \frac{\epsilon^2 c^2 \tau^2}{r_0^4 \gamma^2}}. \tag{78}$$

Such a dynamics occurs to the whole beam, not only the head, but for the rest of the bunch the wakefield react to such an expansion.

Nevertheless, according to the initial condition for the bunch, the wakefield can be too weak for triggering the focusing force immediately after the front. This might lead to an entire section of bunch that experience a similar dynamics as the head, with a slower growth rate due to the increasing

contribute of the wakefield. On the other hand moving further behind the front of the bunch more and more particles contribute to the generation of the wake that therefore becomes more intense and able to focus the bunch.

In the case of flat-top bunches it is possible to obtain an expression for the pinchiping point ξ_p, at which the focusing of the bunch first occurs for given initial conditions. The expression is obtained by setting to zero Eq.(76), considering a radius independent by ξ, since there is not yet the onset of the focusing.

This leads to:

$$\frac{\epsilon^2 c^2}{\gamma^2 r_b^3(\tau)} = \frac{4\pi k_p n_b q_b^2 r_0^2}{m_b \gamma} \mathrm{I}_1(k_p r_b(\tau)) \int_0^{\xi_p} \frac{\mathrm{K}_1(k_p r_b(\tau))}{r_b(\tau)} \sin[k_p(\xi_p - \xi')] d\xi' \quad (79)$$

and therefore:

$$\xi_p(\tau) = \frac{1}{k_p} \arccos\left[1 - \frac{\epsilon^2 c^2}{\omega_b^2 r_0^2 \gamma^2 r_b^2(\tau)\, \mathrm{I}_1(k_p r_b(\tau))\, \mathrm{K}_1(k_p r_b(\tau))}\right] \quad (80)$$

with $\omega_b^2 = 4\pi n_b q_b^2 / m_b \gamma$. The position of the pinching point is a decreasing

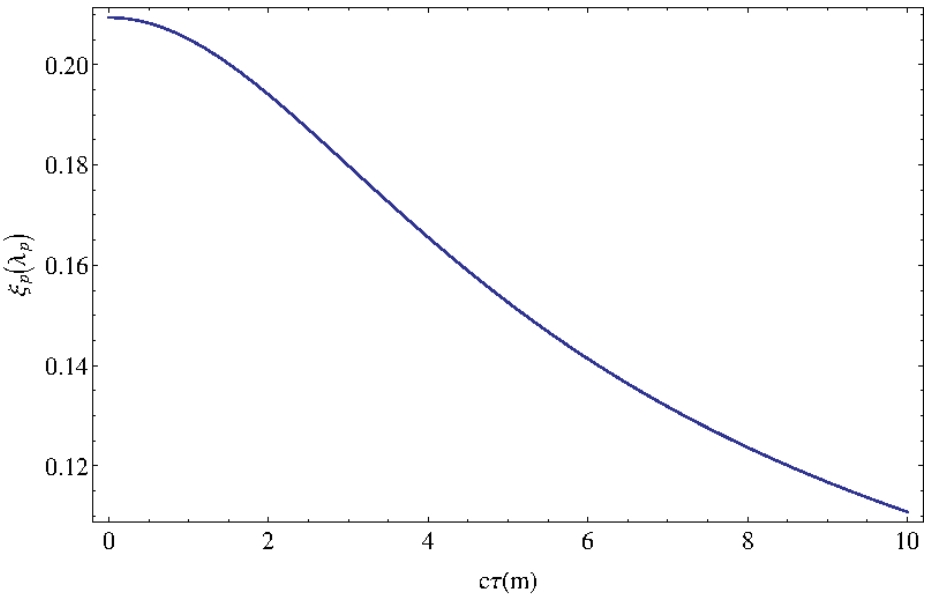

Figure 22: Position of the pinching point ξ_p as a function of the propagation distance according to Eq.(80), for the baseline of AWAKE.

function of the bunch density. This is reasonable since a higher density provides a stronger wakefield that then can rapidly generate the pinching.

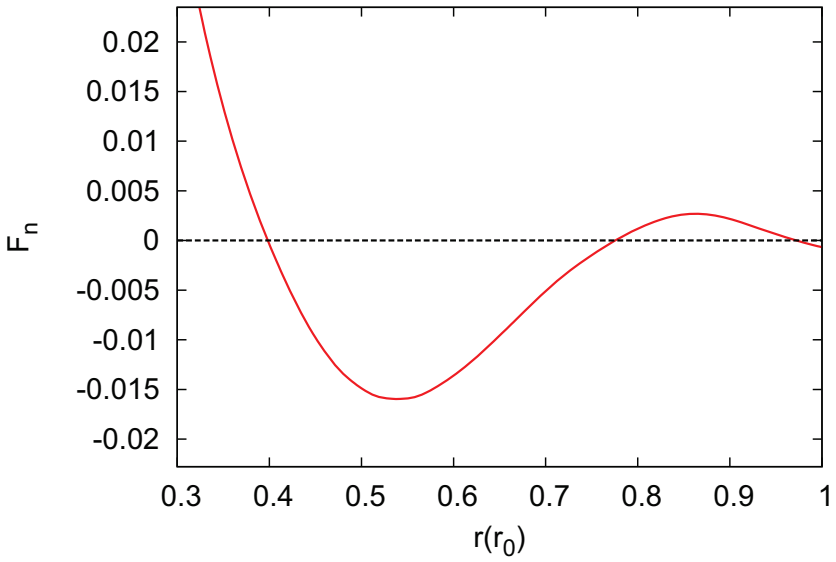

Figure 23: Normalized force $F_n = F/m_b E_0$ at $\xi = 5.3\lambda_p$. $E_0 = m_e c\omega_p/e$ is the wave-breaking field.

The pinching point is as well a decreasing function of the initial radius of the bunch. This might be counterintuitive since an increasing bunch radius provides a decreasing bunch density and so a weaker wakefield. On the other hand the emittance pressure as well is a decreasing function of the bunch radius. Increasing the initial bunch radius would provide a much weaker emittance pressure respect to the reduction in the wakefield, resulting in the end in a faster onset of the pinching.

Since the front of the bunch is always expanding while propagating in the plasma channel, according to Eq.(78), the non-neutralized section of the bunch is a decreasing function of the propagating distance in plasma (Fig.22).

The neutralization of the charge provides a focusing force acting on the bunch once reached the position ξ_p. This means that the maximum radius achievable while propagating in the plasma is the one corresponding to the free expansion in vacuum in Eq.(78) for the same propagation distance. This reflects the case in which the focusing field is zero.

Another important issue that emerges from the simple model depicted above, is the presence of multiple roots of the equilibrium equation, i.e. multiple equilibrium radii for the bunch at the same position ξ. This is a consequence of the piece-wise nature of the wakefield excited by a bunch with sharp boundaries (Fig.23). This last issue implies a non unique solution for

the equilibrium radius therefore additional conditions must be set in order to fix an equilibrium configuration.

The prescriptions on the equilibrium conditions for the beam radius can be obtained by the physical properties we want the beam to fulfill.

A first assumption, in view of the focusing nature of the field, is that the equilibrium radius must be equal or smaller than the radius of the free expanding bunch $r_b(\xi) \leq r_b(\xi = 0)$. Any solution of the equilibrium radius occurring over this limit has to be discarded.

The second assumption is to consider just stable equilibrium configuration under small perturbations. This is a reasonable request in view of the aim to obtain a long-lasting bunch configuration for the whole propagation distance in the plasma.

These two assumptions alone might not be sufficient to define an equilibrium configuration for the whole bunch and an additional one has to be set according to the physical properties we demand the bunch to posses. A possible choice consists of an equilibrium solution lying in the global minimum of the potential for every slice of the bunch, or else in the smaller equilibrium radius achievable.

In the first case we demand the beam to be more stable. The deeper the minimum in the potential, the more energy is required to the beam particles to escape from it while oscillating due to external perturbations. We can expect in this case therefore a more stable configuration under small perturbations.

In the second one, taking the smallest of the two solutions, we favor the intensity of the produced wakefield since a strongly focused driver reach a higher density and therefore excites a stronger wave.

It might be reasonable actually to think that the smaller the radius, the more intense the wakefield and therefore the more deeper the potential well, having so no distinction between the two cases. On the other hand, a larger radius mean more particles contributing to the wakefield that can actually provide a deeper trapping potential but without contributing much to the accelerating field on axis.

We carry the analysis of the equilibrium structure under the previous assumptions for both the "focused" and "global minimum" cases, comparing the differences between the two.

As shown in Fig.24 the bunch experiences a periodical focusing force at which corresponds consequently a modulated equilibrium structure. The equilibrium configuration achieved is analogous to that obtained after the onset of the self-modulation instability (Fig.25).

It is possible to see the initial section of the bunch that is not affected by the modulation. Up to the pinching point the beam does not excite a

strong enough field to drive the focusing as presented previously. The same behavior occurs as well in the second and third bunch, up to the point in which an intense enough wakefield is always obtained and the beam is always modulated.

The interesting aspect that emerges, is the different final configuration for the modulated beam for the two choices of the equilibrium radius. The difference results from the fourth bunch. The difference respect to the previous bunch is the appearance of the third root inside the range $r_b(\xi) \leq r_b(\xi = 0)$ defined above. The new root guarantees a deeper trapping potential, leading therefore to a different configuration respect to the one with the minimum radius.

The shift in the modulation due to the sudden jump to the new equilibrium position persists then for the rest of the bunch.

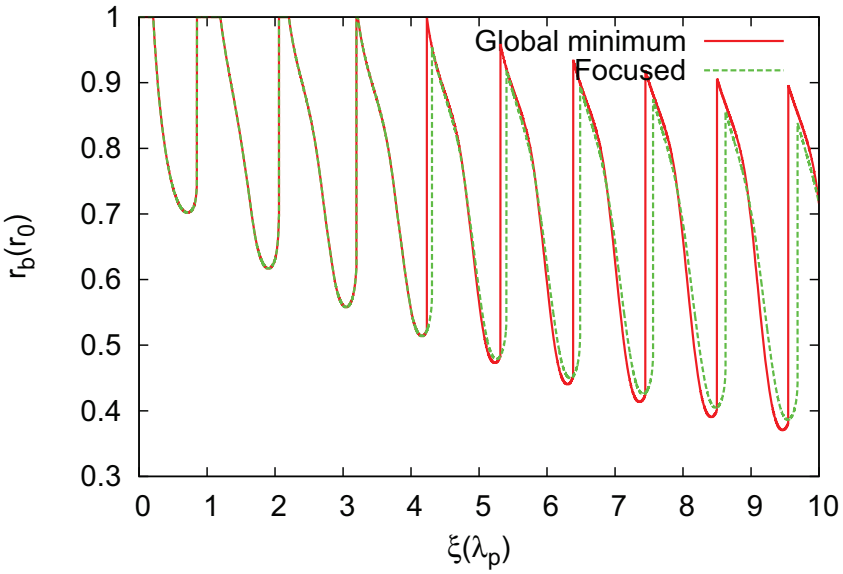

Figure 24: Normalized equilibrium beam radius for the "global minimum case (continuous line) and "focused" case (dashed line).

As mentioned previously, the different structure for the two cases corresponds to a different behavior of the potential for every slice ξ in the bunch.

For the case of "global minimum" solution the modulation occurs at the formation of a new global minimum eventually far from the previous one.

In the case in which the focusing of the bunch is favored instead, the modulation is related to the complete disappearance of the solution corresponding to the smallest radius and consequently jump to the closest possible

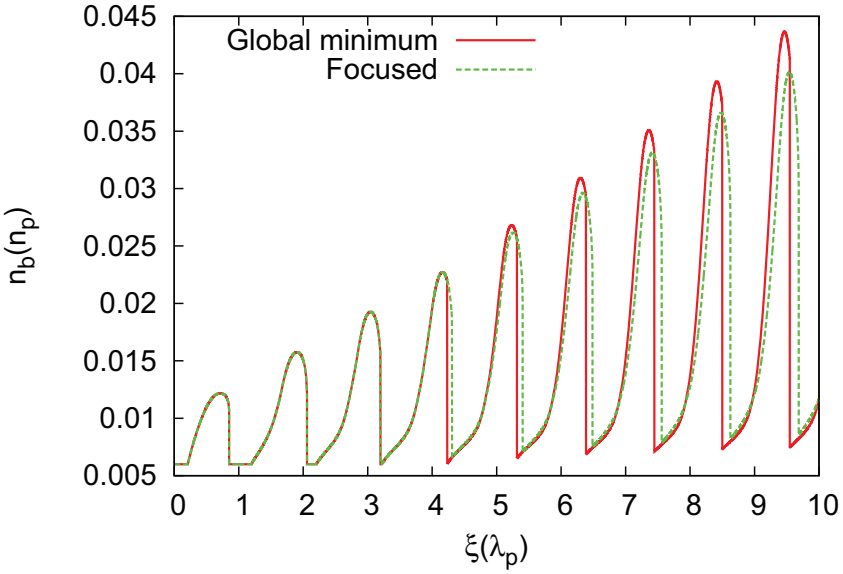

Figure 25: Equilibrium configuration for a modulated beam in the "global minimum" case (continuous line) and "focused" case (dashed line).

solution.

In both the configurations the peak density of the bunches grows moving towards the end of the bunch as a consequence of the constructive interference acting on the transverse field generated by the single bunches.

Nevertheless we can see that the configuration corresponding to the highly focused case does not provide a higher peak density for the bunches. This is a result of the phase shift in the transverse field respect to the "global minimum" case, due to the different lengths of the fourth bunch for the two configurations.

The total transverse field at every point is a result of the superposition of the fields generated by the single bunches. The different length of the forth bunch in the "focusing" configuration provides an imperfect matching of the phase of the transverse field, resulting in a weaker total focusing force and therefore in a lower peak density for the bunches.

According to this last result therefore we can carry the rest of the work just considering the "global minimum" equilibrium configuration since it provides both a stronger focusing and consequently a higher peak density for the bunches as well as a more stable configuration.

7.2.2 Equilibrium configurations for Gaussian bunches

We perform now a similar analysis as that proposed in the previous section but considering bunches with a Gaussian longitudinal profile. The different profile does not provide new interesting features that where not present as well in the flat-top case, but nevertheless is useful to present since real experiments usually deal with Gaussian bunches.

Since the defocusing force driven by the emittance does not depend on the shape of the bunch, we can apply exactly the same model also for Gaussian bunches represented by the longitudinal density profile:

$$f(\xi) = \sum_{j=1}^{N} e^{-\frac{(\xi-\xi_j)^2}{2\sigma_j^2}} = \sum_{j=1}^{N} e^{-\frac{(\xi-\xi_0-j\Delta)^2}{2\sigma^2}} \tag{81}$$

with N being the number of bunches, ξ_j the center, σ_j the length and Δ the periodicity.

The analysis is developed in the same way as the previous one, by solving numerically, for every bunch slice, Eq.(76) for the desired longitudinal density profile. Once obtained the transverse field for the specific slice, we then evaluate the equilibrium radius as the global minimum of the potential providing Eq.(79), with the prescription $r_b(\xi, \tau) \leq r_b(\xi = 0, \tau)$. The algorithm is then repeated for every bunch slice.

The complete set of the parameters characterizing both the plasma and the beam, with the exclusion of the beam length, is based again on the baseline of the AWAKE project (Table 1).

Although this analysis refers explicitly to the AWAKE experiment, the mechanism that leads to the modulation can be general. Therefore the same results hold for both a pre-modulated and a self-modulated beam.

As expected (Fig.26), the interaction with the plasma leads to the focusing of the modulated beam, increasing the peak density of the bunches as compared to the case of pure vacuum. The focusing force increases towards the tail of the configuration due to the coherent interference among the transverse fields generated by the single bunches.

The main difference between the two density profiles is the smaller peak bunch density obtained in the Gaussian case. This is due to the weaker wakefield excited initially by the Gaussian bunches due to the rapidly decrease of the density far from the bunch center. The resulting wakefield is therefore weaker than for flat-top bunches.

The weaker wakefield excited is also the cause of the delayed onset of the focusing force respect to flat-top bunches. It emerges clearly the difference between the initial Gaussian profile of the bunch, as in the vacuum case, and

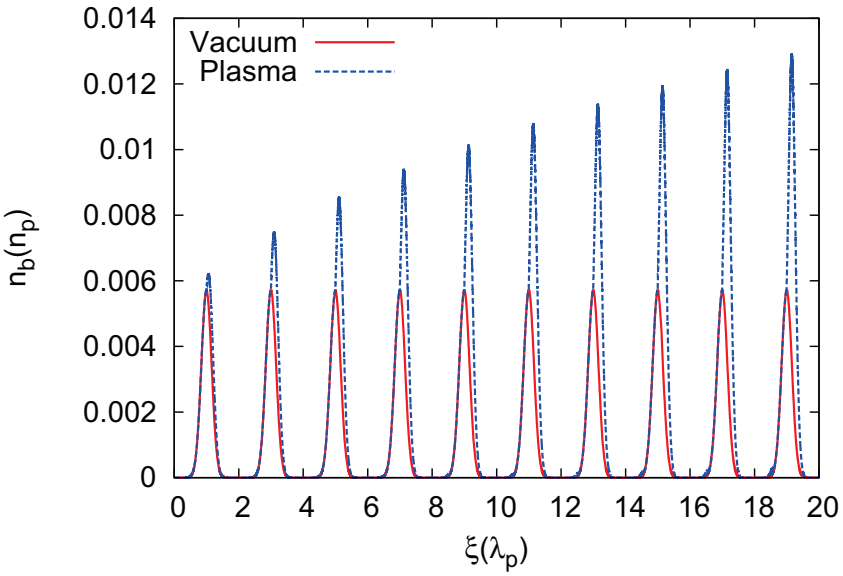

Figure 26: Quasi-equilibrium configuration for a modulated Gaussian bunch with periodicity $2\lambda_p$ in vacuum and in plasma (top) and for different propagation distances in the plasma (bottom).

the pinched section of the bunch as soon as the focusing force becomes strong enough to compensate the emittance force.

Nevertheless for Gaussian bunches is not possible to obtain an exact oppression for the position of the pinching point as in the case of flat-top bunches due to the inhomogeneity of the profile.

7.3 Emittance-driven evolution of the modulated beam

As previously mentioned, the front of the bunch is never able to reach an equilibrium position since its dynamics is controlled by just the emittance pressure and not also by the excited wakefield. Therefore the equilibrium configurations defined previously cannot be stable, subjected at least to an evolution driven by the expansion of the head of the bunch.

Moreover, since the dynamics at every point in the bunch depends on the upstream section, the expansion of the head of the beam leads to an evolution of the equilibrium configuration for the whole driver.

In this section we study the evolution of the equilibrium configuration due to the emittance-driven head expansion, discarding all other time dependencies.

Analysis involving the emittance erosion of the beam has been already

performed in [82–84] for beam transport in plasma in the ion-focused regime, as well in [85, 86] for field-ionized plasma in the context of the bubble regime of PWFA. In these work nevertheless the analysis was devoted on the erosion of the head of the bunch only. The relevant effect taken into account in this section involves the evolution of the wakefield, and so of the beam modulation, driven by the erosion.

The effects of the head expansion on the rest of the driver are analyzed for both the previous configurations, flat-top and Gaussian bunches.

7.3.1 Evolution for longitudinal flat-top bunches

We start studying the emittance-driven evolution for the configuration of flat-top bunches.

A clear influence of the head expansion on the whole beam configuration appears immediately in Fig.27 where the potential map for the whole beam it is shown for three different propagation distances in the plasma.

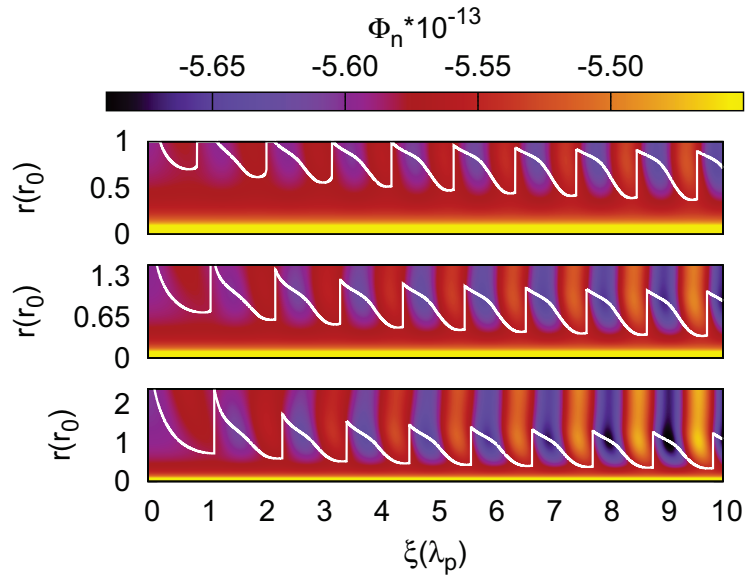

Figure 27: Potential surfaces after propagating for 0, 5 and 10 meters in the plasma. The white lines correspond to the beam radius defined by the minimum of the potential at every position ξ

Although the only time-dependent mechanism is the head expansion, there is an evolution of the potential map on the whole bunch size. The potential structure appears to experience a shift toward the back of the bunch. Moreover the potential wells become deeper.

Since the equilibrium configuration is defined by the minima of the potential, a backward drift in its structure implies a backward drift as well in the equilibrium configuration for the train of bunches.

An analogous backward drift of the potential wells has been already observed for the self-modulation instability [79]. In this analysis we are able to address the emittance force as the responsible mechanism for such a drift, since it is the only dynamical effect occurring in the beam.

The backward shift appears more evident in Fig.28 where the different equilibrium configuration obtained for different propagation distances are presented.

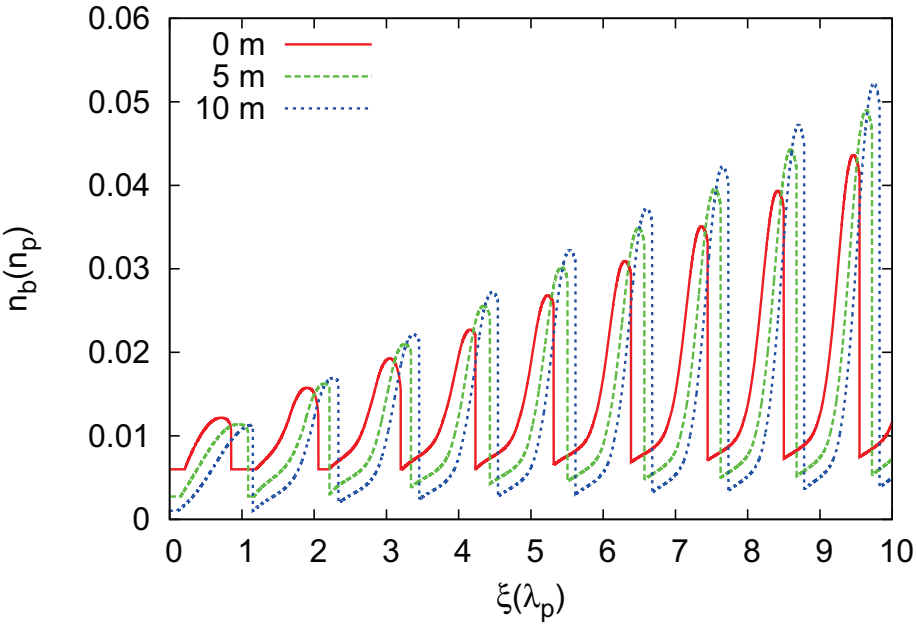

Figure 28: Equilibrium configuration after 0 (continuous line), 5 (dashed line) and 10 (dotted line) meters of propagation in the plasma. The minimum densities achieved correspond to the absence of a focusing field and therefore to a purely-expanding bunch due to the emittance-driven force

The modulated structure is still preserved, with periodicity and length of the bunches approximately equals the plasma wavelength as for the initial condition. The whole configuration on the other hand, exhibits a drift towards the back of the bunch respect to those at previous propagation distances. Moreover there is as well an increase of the peak densities of the bunches for increasing propagation distances.

The first bunch appears to behave differently in respect to the rest of the

configuration. The peak density is in fact decreasing for increasing propagation distances in the plasma. The length as well is not constant but it is rather increasing.

In order to characterize the evolution of the equilibrium structure and understand the reason for such a behavior we track the position of the peaks of the bunches for different propagation distances. The first feature that emerges from Fig.29 is an approximately equal variation of the bunch positions respect to their initial one for all the bunches.This means that the equilibrium configuration rigidly moves backward while propagating in the plasma and that the period of the modulation therefore does not change. Moreover the variation is initially a linear function of the propagation distance, becoming smoother after approximately 7 m.

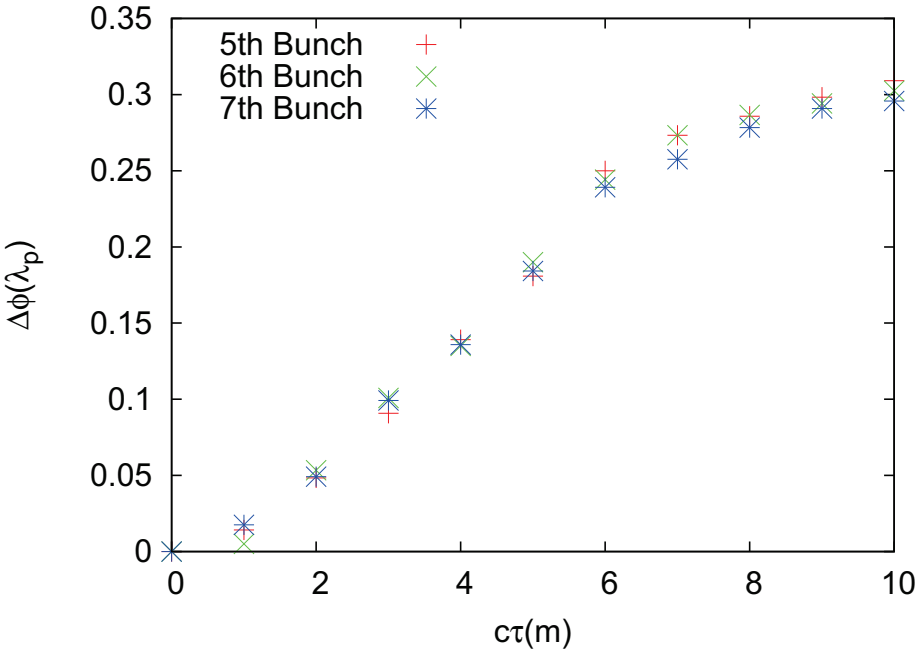

Figure 29: Shift of the 5th, 6th and 7th bunch respect to its initial position for different propagation distance.

As we pointed previously the divergence of the beam driven by the emittance is the only time-dependent mechanism in this analysis, therefore the reason for the presence of such a drift has to be found there.

An interesting difference that we mentioned above in the evolving equilibrium configuration, is the anomalous behavior of the first bunch respect to the rest of the modulated beam. In particular the length of the first bunch is increasing while propagating in the plasma.

There are two main reasons for such phenomenon related each other as can be seen in Fig.30. The first one, as previously mentioned, is the recession of the pinching point. The beam rarefaction due to the head expansion weaken the emittance force that can be therefore compensated by the wakefield sooner than for previous propagation distances.

The second reason lies in the weaker wakefield that can be excited for different propagation distances due to the decreasing bunch density. Although the emittance force is more affected by the decreasing density, the wakefield is as well reduced. This means that for different propagation distances, it is necessary a longer section of the bunch to generate a wakefield of the same intensity (more charges are contributing to the wakefield).

This last issue is responsible for a phase shift of the transverse field and therefore of a longer length of the first bunch.

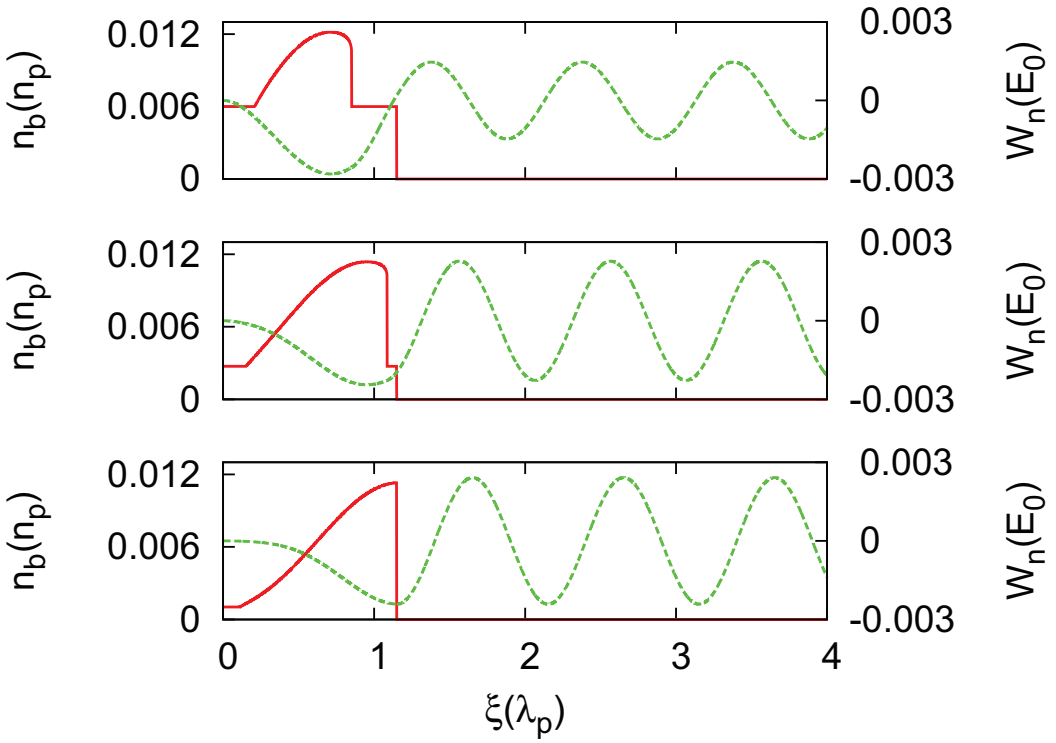

Figure 30: Bunch density and transverse wakefield at $r = r_0/2$ after 0, 5 and 10 meters of propagation for a short bunch.

This phase shift in the transverse field occurring on the first bunch is the cause of the backward drift for the entire configuration.

The transverse field is responsible for the modulation of the beam, there-

fore a change in the phase of the wakefield leads to a change as well of the equilibrium configuration.

Moreover, although the maximum field inside the first bunch is a decreasing function of the propagation distance, the different length results in an increasing maximum field outside the bunch. This results in a stronger focusing force and therefore in the increasing peak density of the bunches observed.

The mechanism, studied in [80], can be summarized as follows: the bunch experiences an expansion driven by the emittance pressure. The expansion leads to a reduction of the bunch density and therefore to the intensity of the wakefield. In order to obtain wakefield of the same intensity for different propagation distances it is necessary therefore to include a longer section of the bunch for compensating the reduction of the density. This leads to a phase shift of the transverse wakefield that is responsible for the focusing and defocussing of the rest of the beam. The phase shift in the wakefield results so in a phase-shift in the global equilibrium configuration of the modulated driver.

7.3.2 Evolution for longitudinal Gaussian bunches

The use of flat-top bunches made easier the understanding of the physical mechanism that provides the evolution of the equilibrium configuration. We want to check if the same behavior occurs as well for Gaussian bunches or it is suppressed by the nonlinear wakefield excited by such density profile.

As can be seen in Fig.31, Gaussian bunches experience a slightly different behavior respect to flat-top ones.

In order to avoid effects due to the overlapping of the single bunches, the periodicity of the train of bunches has been set to $\Delta = 2\lambda_p$.

The similarity with the previous case is the backward drift experienced by the equilibrium configuration while propagating in the plasma. The drift increases as well with the propagation distance as in the previous analysis, although the displacement appears to be smaller than in the flat-top case.

The difference respect to the previous case is in the peak bunch densities that is actually decreasing with the propagation distance.

Although such a difference between the two configurations, the mechanism inducing such behavior is actually the same, as can be seen in Fig.32.

Also in the case of a Gaussian bunch the expansion of the bunch induced by the emittance corresponds to a decreasing bunch density and therefore to a reduction of the wakefield. This reduction once again has to be compensated by a larger section of bunch required to obtain the same charge for different propagation distances. This process delays the onset of the focusing force.

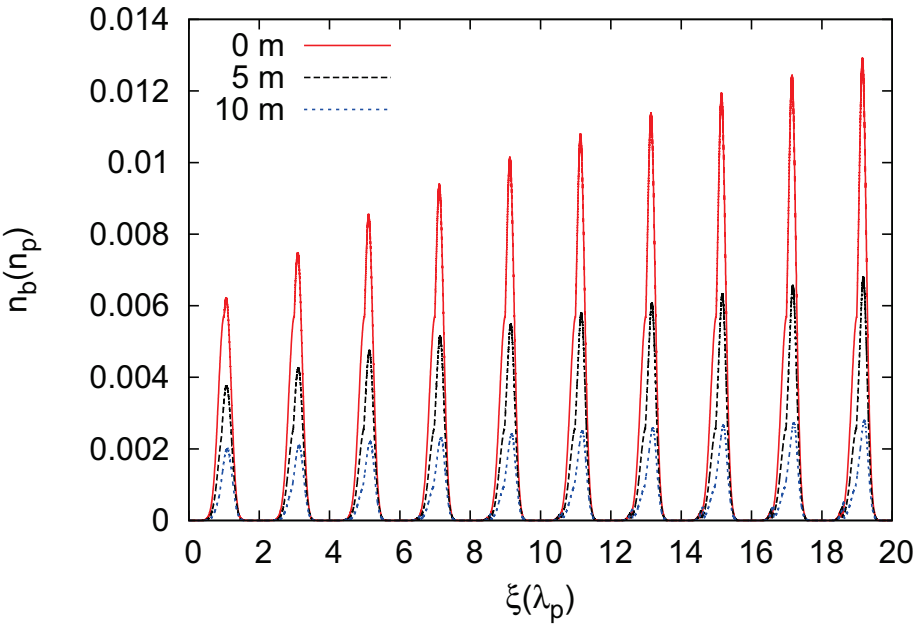

Figure 31: Drift of the equilibrium configuration for a train of Gaussian bunches for 0, 5 and 10 m of propagation in the plasma.

The reason for the different amount of drift experienced by the Gaussian bunches, as can be clearly seen in Fig.32, is the inhomogeneity of the density profile in this case, with a strong decay moving away from the bunch center.

The lower density of the front excites a weaker wakefield, bringing to a delay of the onset of the pinching respect to flat-top bunches. Moreover, while flat-top can easily compensate the density decrease induced by the emittance pressure, since the density of the bunch is constant, Gaussian bunches are constrained by the rapid decrease of the density profile. It can occur that there is not enough density in the rest of the bunch to reach the same intensity of the transverse field as for previous propagation distances. This is the reason of the decreasing peak density of the bunches for Gaussian profile.

This problem can be of course overcome by increasing the length of the Gaussian bunches.

This is the reason for the quantitative different behavior of the backward drift for Gaussian bunches respect to flat-top ones, although the mechanism inducing the drift is still the same. In Fig.33 it is possible to see the different amount of the drift for the two cases. Nevertheless, the drift is still rigid for Gaussian bunches as it was for flat-top ones since they are both driven by

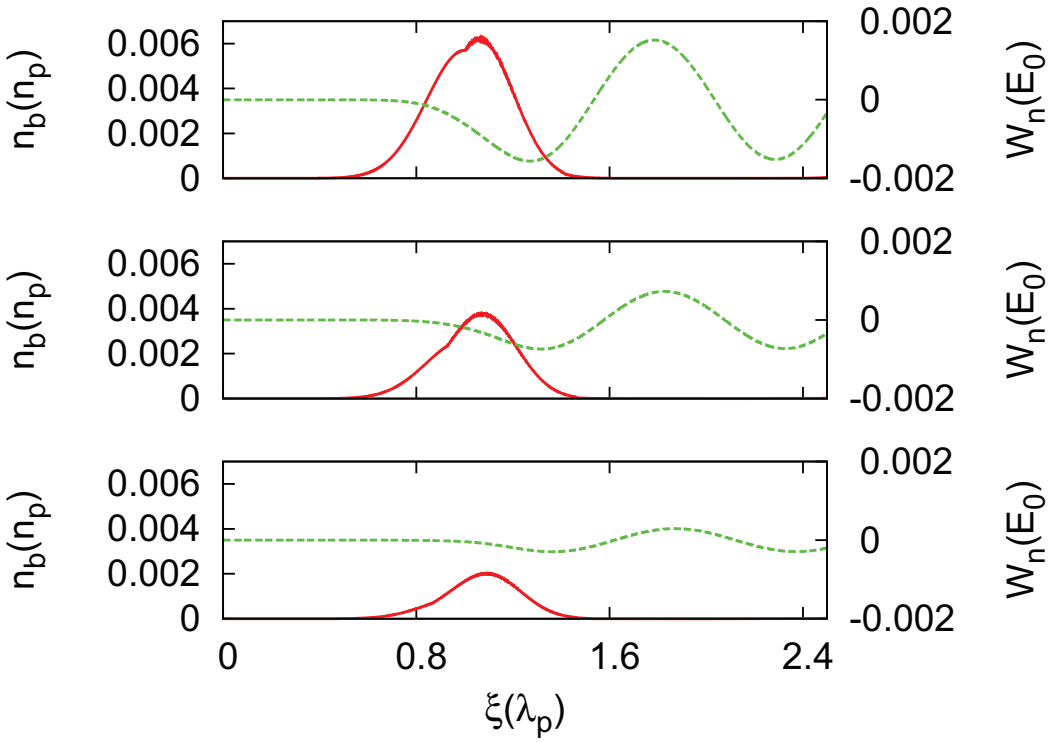

Figure 32: Transverse field excited by a Gaussian bunch for 0, 5 and 10 m of propagation in the plasma.

the same effect.

This drift caused by the emittance-driven head erosion is qualitatively analogous to those studied in previous works [82–86]. On the other hand, the previous analysis focused just on the deterioration of the beam front driven by the emittance [82–84], without considering its effects on the rest of the bunch.

In the same way, the works [85, 86] took into account only the drift of the ionization front and the consequent interaction of the beam with a not completely ionized plasma.

In the present analysis we look to how this drift affects the phase of the wakefield and therefore the evolution of a train of bunches initially in equilibrium.

This might be relevant also in context in which the emittance is nevertheless small enough to not provide any relevant deterioration of the driver compared to other physical effects [87].

The emittance-driven evolution of the equilibrium configuration implies

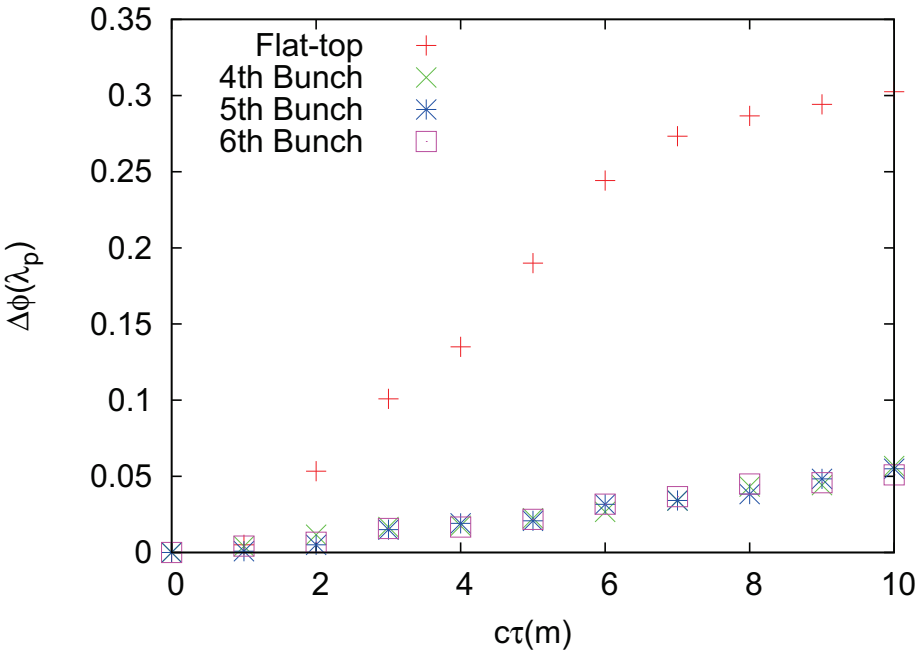

Figure 33: Shift of the 4th, 5th and 6th bunch respect to its initial position varying the propagation distance in the plasma. The result is compared with the shift experienced by flat-top bunches.

serious consequences for the stability and the duration of the modulated beam.

A bunch particle initially in an equilibrium position, will find itself in an unstable one while propagating in the plasma as a consequence of the rearrangement of the trapping potential caused by the expansion of the front.

The displacement experienced by the initial bunch radius with respect to the new equilibrium configuration results in a gain of transverse momenta. If the displacement is large enough, the bunch particles can even escape the trapping potential.

The more driver particles are depleted, the lower is the wakefield amplitude, resulting in the lower efficiency of the process.

It is worth underline that this is only one of the mechanism of degradation of a periodic modulated driver, since full simulations shown that the instability is caused by the partially slippage of the bunches in the defocussing phase of the wake [79].

7.4 Optimization of a train of Gaussian bunches

In the previous section emerged a problem of stability for a modulated beam caused by the simply expansion of the front of the driver. This might lead to a serious issue since the evolution of the beam configuration might induce a deterioration of the driver.

A possible way to ease this problem is to reshape the modulated configuration in order to provide a better stability. There are three parameters that are tunable in order to obtain a different configuration, the bunch densities, the bunch length and the distance between the bunches.

It is true indeed that a train of bunches with periodicity $\Delta = \lambda_p$ provides an intense accelerating field behind the driver, due to the coherent interference among the wakefield generated by the single bunches. Nevertheless, the simple expansion of the front of the bunch causes its degradation. The more particles the bunches lose while propagating in the plasma, the weaker is the final accelerating field.

Might be eventually of more advantage reshape the driver configuration, moving away from that providing the maximum accelerating field, obtaining a longer lasting driver that can accelerate the witness bunch with a lower acceleration gradient but for longer distances.

Although the analysis can be performed on all the three parameters characterizing the configuration, as in Section 6.4, we look only to the proper position of the single bunches in order to maximize the number of particles keeping trapped while propagating in the plasma.

We drop therefore the scan on the bunch densities and lengths. This is due to the more difficulties provided in the control of these two parameters.

The analysis is performed only for bunches with longitudinal Gaussian density profile, since are more feasible for experiment and the analysis for flat-top bunches was performed just for an easier understanding of the problem.

This approach has been performed in previous works [58, 87] including further physical effects in the analysis. We show here that also the phase-shift of the wakefield caused by the expansion of the head can be mitigated by finding a new proper configuration of the modulated beam by changing the periodicity of the bunches.

The trapping of the beam particles is studied between the initial and final position in the plasma channel. Since the backward shift increases with the propagation distance, improving the trapping respect to the final stage guarantees as well an improvement for the whole evolution.

It is worth noting that with such approach we do not take into account the transverse momenta acquired by the bunch particles at every time step. Therefore the deterioration might be even worst in a full time-dependent

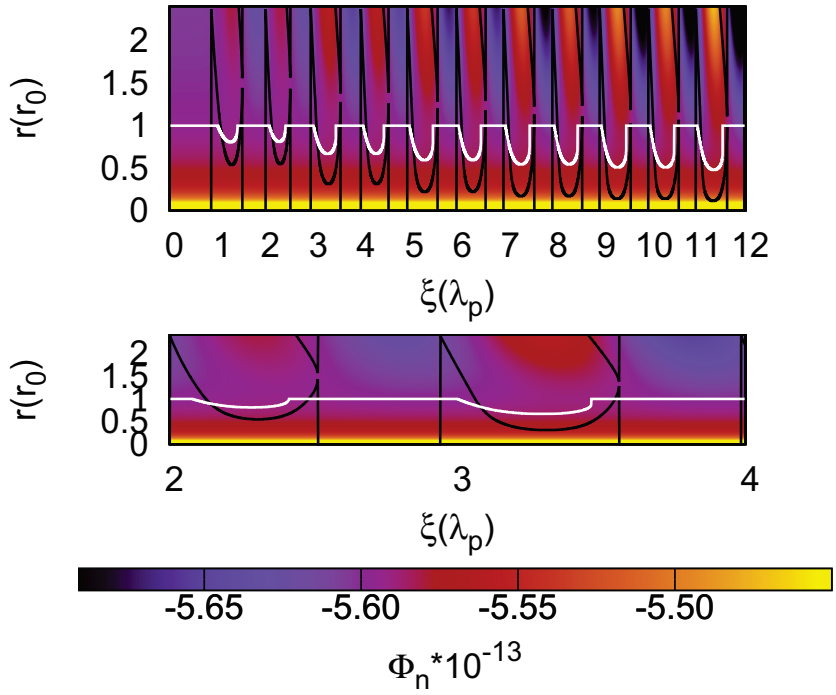

Figure 34: Potential surface after 10 m of propagation in the plasma. The white line corresponds to the equilibrium beam radius at 0 m, while the black lines are the boundaries for which the particle stay trapped after 10 m of plasma.

analysis. Nevertheless such approach guarantees the proper initial shape of the modulated beam in order to mitigate the deterioration driven by the emittance pressure.

To establish which sections of the bunches are unstable, we compare the initial radial configuration with that at the end of the propagation. The bunch particles are lost if the difference between the two is large enough to provide the necessary transverse momentum to escape the trapping potential.

In Fig.34 we can see an example of the method applied: the trapping boundaries defined the region of the potential in which the bunch should lies in order to remain trapped. It appears clearly like some sections of the initial equilibrium configuration are, at the end of the propagation distance, out of the trapping region, meaning that those slices of the bunches are lost.

Since the bunches are Gaussian, so inhomogeneous, it is not enough to look for the section of the bunch lost, but it is necessary to evaluate the exact number of bunch particles that escape the trapping potential, since the slices defocussing might be of low density.

According to this criterion we look for the matching periodicity of the configuration that guarantees the highest number of particles trapped between the initial and final step. The analysis is performed one bunch at the time for all those composing the periodic driver. For every bunch analyzed, the configuration upstream is fixed to the matching one previously evaluated.

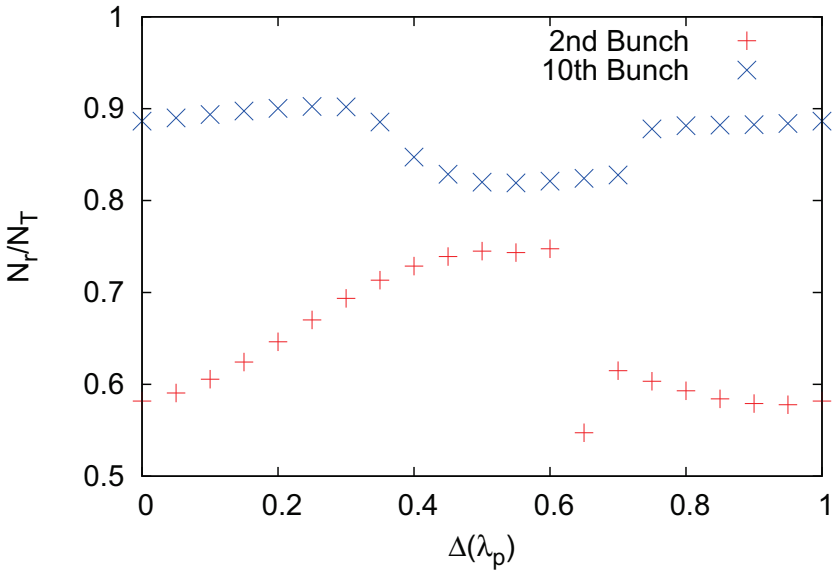

Figure 35: Relative number of particle trapped after 10 m of propagation varying the position of the last bunch of the configuration.

In Fig.35 we can see the relative number of particle trapped changing the position of the last bunch of the configuration over a plasma wavelength.

As expected the maximum number of particle trapped is not achieved with a periodicity $\Delta = \lambda_p$. The reason has to be looked in the expression of the transverse field that guarantees the focusing.

The maximum of the Green function for the transverse field in Eq(74) lies at $\Delta = \lambda_p/2$, so as explained in Section 4.1.3, the accelerating and focusing fields are out of phase. Moreover, the Gaussian profile induces a nonlinear shift on the wakefield due to the inhomogeneous density. Another reason is the additional phase shift induced by the single bunches involved in the configuration, changing the phase between two bunches. Lastly, the backward drift driven by the expansion of the front of the bunch causes an additional shift of the optimal position, the one we are trying to mitigate.

The final position of the maximum of the focusing field, and therefore of the maximum number of particle trapped, is provided by the sum of all this

contributes.

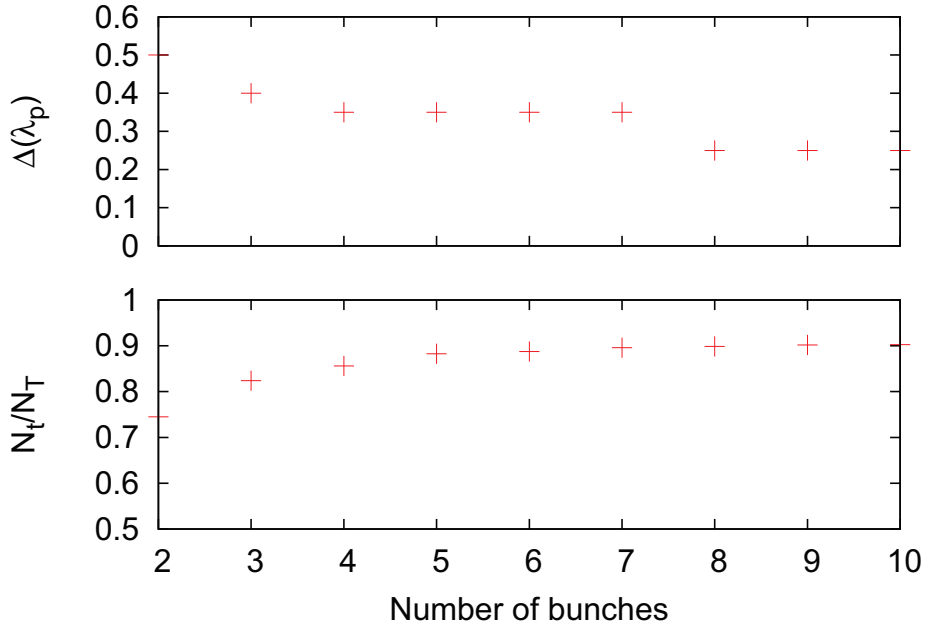

Figure 36: Matching position of every bunch to improve the trapping (top) and relative number of particle trapped (bottom).

By looking for the matching position that mitigates the deterioration, it appears immediately like the displacement is not constant for every bunch, meaning that it is not enough to rigidly move the configuration backward, but an analysis for every bunch is required (Fig.36). This is as well expected since placing a bunch on the tail of a previous one provides a shift in the phase of the wakefield [79].

On the other hand the stability of the configuration, defined as the relative number of particle trapped, increases with the number of bunches involved. This is a consequence of the increasing total transverse field due to the superposition of the single ones generated by all the upstream bunches. The potential well characterizing the trapped particles becomes deeper and therefore an increasing transverse field is necessary for the bunch particle to escape.

It is worth noting that the approach performed above provides an increasing final total charge of the beam. This does not necessarily implies as well an intense accelerating field behind the driver. There is the possibility that the new position of the bunches lies in the accelerating phase of the wakefield, therefore the bunches does not deposit coherently the energy in

the wave.

This can be understood also by looking at Eq.(74), since the Green function for the longitudinal and transverse fields are $\pi/2$ out of phase, meaning that the maximum of the first will be close to the minimum of the second.

In order to obtain a configuration suitable for particle acceleration, it is necessary to improve the stability of the train of bunches together with the final accelerating field behind the driver. It is reasonable to expect that is not possible to obtain the best of the two conditions at the same time, but nevertheless we look for a configuration that guarantees a coherent interference between the longitudinal fields generated by the single bunches, as well as a slow deterioration.

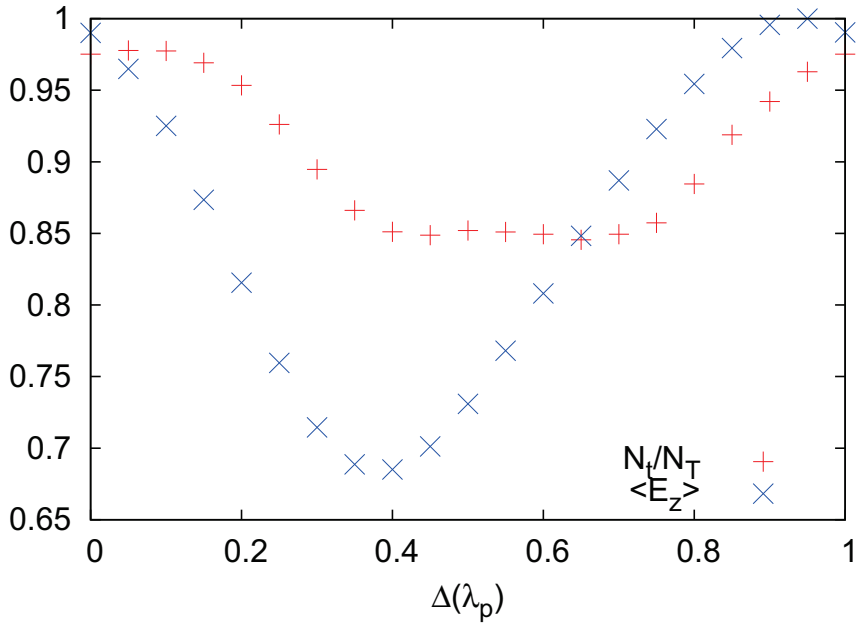

Figure 37: Relative number of trapped particle with average accelerating field behind the driver for a configuration with ten bunches.

To do this we perform an analogous analysis as the previous one, taking into account this time also the average of the accelerating field behind the driver over the propagation distance. The analysis is performed again for one bunch at the time, fixing the configuration upstream to the matching one. Fig.37 displays clearly the behavior mentioned previously.

The position that guarantees the maximum number of trapped particles does not correspond to that improving also the longitudinal field behind the driver. In order to obtain the best of the two behaviors, the matching

condition is set at the crossing between the lines representing the relative number of trapped particle and the average accelerating field behind the driver. The position is highly conditioned by the different effects mentioned previously and must be evaluated numerically.

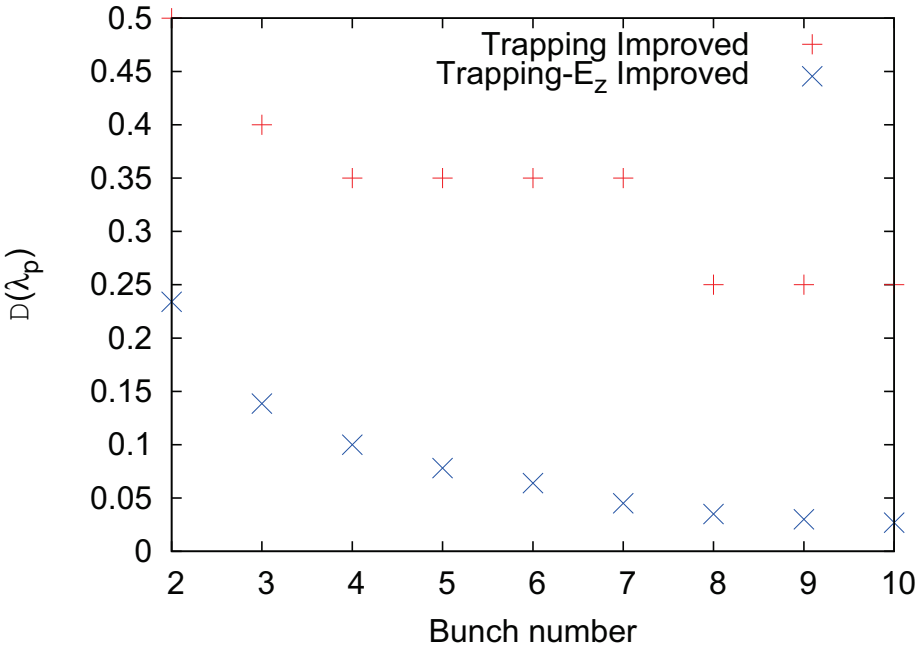

Figure 38: Matching position of every bunch in order to improve both the stability of the driver and the final accelerating field. The result is compared with the previous one in which only the stability was guaranteed.

As can be seen in Fig.38, the needed shift of the initial bunch position is clearly different comparing the case improving only the stability of the configuration and that improving as well the final accelerating field. Both of them on the other hand show a decreasing function of the number of bunches involved in the configuration, eventually leading to a saturation of the shift increasing more the number of bunches.

The analysis developed so far is based nevertheless on a simplified model and does not take into account additional effects that might influence the stability of the configuration, especially nonlinear effects. The additional exclusion of a full time-dependent simulation of the dynamics might affect the final results on the optimal configuration.

In order to confirm the results therefore, we have performed a three dimensional PIC simulation using the quasi-static VLPL code [88]. We compare both the bunch densities and the longitudinal electric field for a modula-

tion of λ_p and the newly obtained modulation. A more extensive explanation of the code used will be provided in Appendix B.

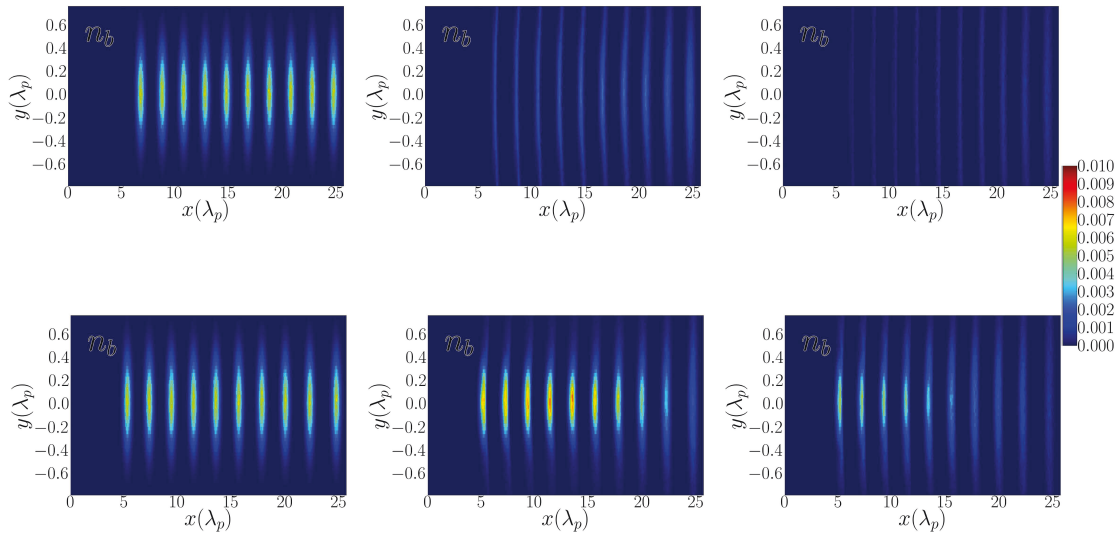

Figure 39: Bunch densities after 0, 5 and 10 m of propagations in plasma for the rigid train of bunch configuration (top) and the optimized configuration (bottom). The new configuration provides an increasing density for the bunches at the end

As can be seen in Fig.39, the results from the PIC simulations confirm those obtained by the simplified model. It emerges clearly that the optimized configuration preserves the bunch densities, obtaining a final charge higher than that in the periodic case. There is still a deterioration of the driver, but this was expected since the approach aims to mitigate the effects of the defocussing forces.

The other main feature desired, a strong accelerating field behind the driver, is as well obtained.

This characteristic as well provides the behavior expected by the improved configuration as can be seen in Fig.40. Indeed the modulation of λ_p guarantees a stronger electric field initially, but on the other hand, the optimized configuration provides an improved focusing field acting on the single bunches. The focusing force enhances the peak bunch density, providing therefore a more intense accelerating field. Moreover the improved trapping allows to sustain such electric field for longer propagation distances respect to a periodicity of λ_p in which the deterioration of the driver rapidly reduce as well the final accelerating field.

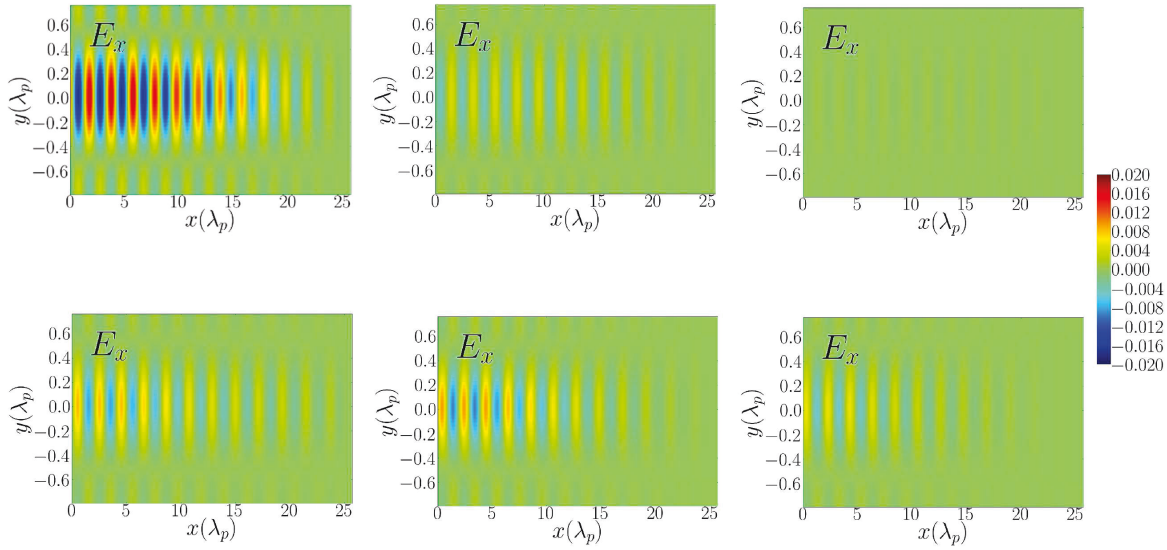

Figure 40: Accelerating field after 0, 5 and 10 m of propagation in plasma for the rigid train of bunch configuration (top) and the optimized configuration (bottom). The new configuration provides a more intense accelerating field for the second half of propagation in plasma.

The difference in the intensity of the longitudinal field can be clearly observed in Fig.41. The new configuration shows an initial rise of the accelerating field due to the focusing force acting on the bunches that increases their peak density. At that stage, the bunch configuration reach the transverse equilibrium described in the previous sections.

After about 3 meters of propagation in the plasma, the accelerating field behind the driver becomes stronger in this new configuration due to the highly focused bunches and to the mitigation of the bunch deterioration.

Finally the deterioration of the driver occurs also in the optimized case, but nevertheless it is slower than the previous case, still providing an intense electric field at the end of the propagation.

The analysis developed in this sections has shown the importance of a properly shaped train of bunches in order to preserve the stability of the driver and as well improve the final accelerating field.

The simple periodicity of $\Delta = \lambda_p$ is not anymore satisfactory when broader effects, beyond the improvement of the initial accelerating field, are included in the analysis.

Such analysis might suggest further improvement that can be achieved, in a similar fashion as for the optimization of the transformer ratio, by expand-

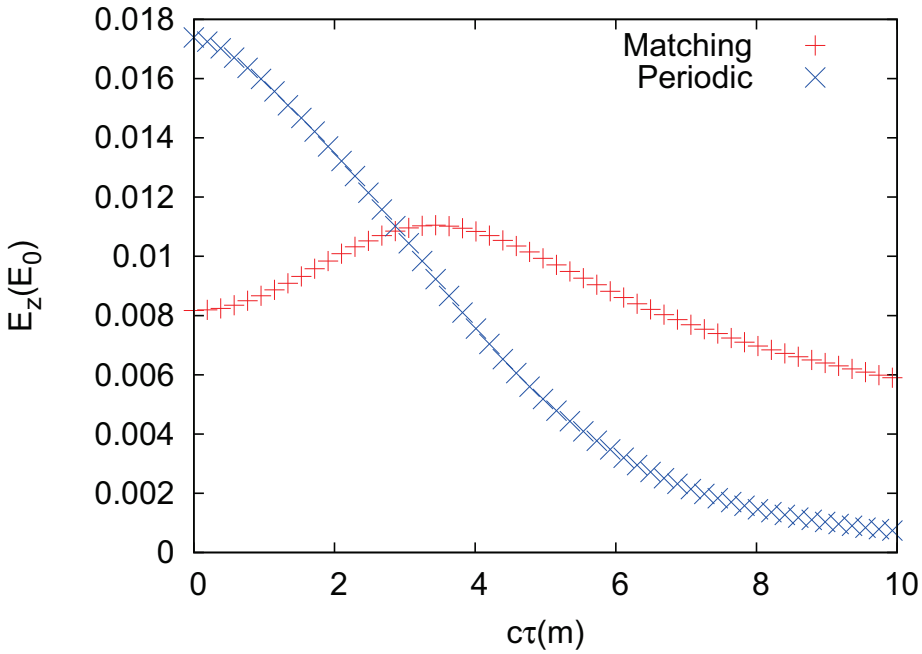

Figure 41: Comparison of the accelerating field behind the driver for the periodic and optimized case as a function of the propagation distance.

ing the parameter scan to the bunch densities and lengths as well, opening eventually new regime for the stability of the driver in the linear PWFA.

Another important application of such analysis, might be the effects of the transverse field on the stability of the witness bunch, as well the eventual beam loading and energy spread. The issue of the accelerating field in this case is not important anymore, but there are other important features that must be preserved or improved for the witness bunch, features that are affected as well by the wakefield generated by the newly shaped driver.

8 Conclusion

We have shown in this work the importance of plasma wakefield accelerator as a possible alternative to standard rf accelerator. This is not just due to the high acceleration gradients that the plasma can sustain, but also for the additional features emerging in such a framework, like the focusing of the beam by the transverse field excited.

Nevertheless important issues have to be solved in order to substitute actual accelerator by this technique.

In particular, for what concerns beam driven plasma wakefield, the first problem to be solved for a kilometer long accelerator is the stability of the driver. Nowadays one of the severe limit of such mechanism is the deterioration of the driver due to the interaction with the wakefields generated. The length scale at which the deterioration occurs is usually shorter than the depletion length at which the driver has deposit all its energy in the plasma.

It is therefore pointless to use a driver with a large energy stored such as the 400 GeV proton beam of the SPS for the AWAKE project, if the beam cannot transfer all its energy to the plasma and then to the witness bunch.

We try therefore to address the problem of the stability of the driver in this work, in particular the stability of a modulated beam. The reason for an emphasis to such a driver is due to the promising possibilities that can be achieved with this configuration. The coherent interference of the wakefields excited by the single bunches can large improve the final accelerating field. Moreover, the tunability of the configuration, especially in term of periodicity of the bunches, allows a better manipulation in order to improve the performances.

A practical reason is that modulated beams, and in general long driver, are more subject to instabilities caused by the interaction with the wakefield generated.

In this work we have first of all characterized the equilibrium configuration for such a driver. We have seen that there are different choices in order to obtain a stable equilibrium configuration, that would provide different features of the wakefield.

Among them we have chosen the one with the best performances and we have studied the influence of the head expansion due to the emittance in term of stability of the configuration.

The problem of the emittance-driven erosion of the beam is already a well known one, being responsible for the drift of the pinching point of the beam or of the ionization front in the beam-ionized plasma configurations. Nevertheless this is the first time that the emittance effects are included in the evolution of the wakefield.

We have shown that the expansion of the front of the beam leads to a backward drift of the whole equilibrium configuration due to the phase shift of the wakefield induced by the reduced density of the beam.

The phase shift induces an instability, since particles that where in an equilibrium point initially might acquire enough transverse momentum to escape the trapping potential and so be lost, causing the deterioration of the driver.

We observed the same behavior, although quantitatively different, for a train of flat-top bunches as well Gaussian bunches.

We look therefore to a way for mitigate such deterioration for a train of Gaussian bunches, being more feasible for experimental applications.

We found out that a possible solution consists in removing the constraint of a series of bunches with fixed periodicty. Properly changing the distance between each bunch , it is possible to reduce the deterioration of the driver. Moreover, due to the highest number of particles that remain trapped and so contribute to the wakefield, the final accelerating field on-axis is enhanced as well respect to the case of a strictly periodic modulated beam with periodicity $\Delta = \lambda_p$. Such feature shows the importance to improve the quality of the driver in order to increase as well the performances as accelerator mechanism.

Another important issue in such a framework is the efficiency of the energy transfer between the driver and the witness bunch. This might be less relevant nowadays due to the short acceleration distances that can be achieved right now, but becomes an important figure of merit when discussing of kilometers long plasma wakefield accelerators.

The characteristic describing the efficiency in the transfer of energy is the transformer ratio, the ratio between the energy gained from the witness bunch over the energy deposit by the driver.

Linear plasma perturbations, using symmetric drivers have the rather unpleasant limit of $R = 2$. On the other hand this limit can be overcome using nonlinear plasma wakefields, asymmetric drivers or a properly shaped train of bunches.

Dealing with this last configuration, we have shown that the ramped configuration providing a transformer ratio $R = 2N$ is feasible only using flat-top bunches. For non homogeneous bunch such behavior is not satisfied anymore.

Even worst, by applying the same scaling for length, periodicity and peak density to a configuration of Gaussian bunches we obtained a far smaller transformer ratio.

Such results required a further analysis for the transformer ratio using a train of Gaussian bunches. We shown that inhomogeneous bunches require a different parameter to properly quantify the energy exchange efficiency,

namely the weighted transformer ratio, that takes into account of the specific number of particles that are subjected to the wakefield: the more particles are affected by the wakefields, the more important is that slice of the bunch (rather than having the same weight as in the case of flat-top bunches).

Using this new parameter that provides the already established result for flat-top bunches, we performed a parameter scan on the configuration of Gaussian bunches, in order to find the optimal length, peak density and periodicity of the single bunches to improve the transformer ratio.

The results are far from being as good as those for flat-top bunches, but on the other hand are a great improvement respect to a simply application of the scalings for flat-top bunches to Gaussian ones.

The enhancement of the transformer ratio required, as in the improvement of the driver stability, a fine tuning of the parameters of the driver, showing once more the great possibilities that can be obtained by using a modulated beam as a driver for plasma wakefield.

Although the promising results presented in this work, there are still important issues to be addressed. In term of the driver stability, for example, several effects has been discarded in the present analysis that might be important for mitigating the deterioration of the bunch.

Moreover the quality of the accelerated witness bunch should be also taken into account. In order to be feasible for applications it should have not only an high energy, but also a small emittance so to increase the luminosity of the bunch. These are problems that have to be taken into account as well for a plasma wakefield accelerator that can replace the actual technologies.

The present work shows the wide possibilities obtained by a fine tuning of the parameters of a train of bunches used as a driver. Such freedom in the shape of the driver configuration might be a possible solution to a lot of problems related to plasma wakefield accelerators.

Another way to improve the characteristic of such framework might be the tuning of the plasma parameters, not mentioned at all in this work. Previous analyses have already shown the improvement of the concept by using a density gradient for the plasma for example. A more accurate study of the effects of the plasma parameters, in term of density and velocity, might open additional possibilities to improve the quality of the plasma wakefield.

A Derivation of the 2-dimensional wakefield equations

This chapter provides a complete derivation of the 2-dimensional electric and magnetic fields arising from the interaction of a particle beam with a plasma. The evaluation greatly relies on the work of Kenigs and Jones [57].

The model considers immobile plasma ions, based on their greater inertia respect to the electrons. Moreover the sources are azimuthally symmetric, so that the analysis can be reduced to a 2-dimensional one. Lastly, $n_b \ll n_p$, the plasma is overdense, so it is reasonable to consider a linear response of the perturbed plasma, discarding higher order terms.

The first step is to evaluate the wave equations for the electric and magnetic fields from the Maxwell equations Eq.(5-8).

Taking the curl of the Faraday law Eq.(6) and replacing the Ampere equation Eq.(8) one obtains:

$$\nabla \times (\nabla \times \mathbf{E}) = -\frac{1}{c}\frac{\partial(\nabla \times \mathbf{B})}{\partial t} = -\frac{4\pi}{c^2}\frac{\partial \mathbf{J}}{\partial t} - \frac{1}{c^2}\frac{\partial^2 \mathbf{E}}{\partial t^2}. \tag{82}$$

Using the identity $\nabla \times (\nabla \times \mathbf{A}) = \nabla(\nabla \cdot \mathbf{A}) - \nabla^2 \mathbf{A}$ and the Poisson equation Eq.(5) in the previous expression provides:

$$\frac{1}{c^2}\frac{\partial^2 \mathbf{E}}{\partial t^2} - \nabla^2 \mathbf{E} = -\frac{4\pi}{c^2}\frac{\partial \mathbf{J}}{\partial t} - 4\pi\nabla\rho \tag{83}$$

where the sources providing the electric field are both the plasma and the particle beam($\mathbf{J} = \mathbf{J}_p + \mathbf{J}_b,\ \rho = \rho_p + \rho_b$). An analogous equation can be obtained in a similar fashion for the magnetic field, by taking the curl of Eq.(8) and replacing Eq.(6,7) together with the previous operator identity. The final results is:

$$\frac{1}{c^2}\frac{\partial^2 \mathbf{B}}{\partial t^2} - \nabla^2 \mathbf{B} = \frac{4\pi}{c}\nabla \times \mathbf{J}. \tag{84}$$

To self-consistently close the system the wave equations have to be coupled with the fluid equations describing the dynamics of the plasma Eq.(16,17).

Assuming that the perturbation is small, it is possible to linearly expand the quantities involved, discarding second order effects:

$$n_p \simeq n_0 + n_1 \tag{85}$$

$$\mathbf{v}_p \simeq \mathbf{v}_0 + \mathbf{v}_1 = \mathbf{v}_1 \tag{86}$$

$$\mathbf{E} \simeq \mathbf{E}_0 + \mathbf{E}_1 \tag{87}$$

$$\mathbf{B} \simeq \mathbf{B}_0 + \mathbf{B}_1 \tag{88}$$

where we have assumed an initially static plasma.

The fluid equations for the perturbed quantities turns therefore into:

$$\frac{\partial n_1}{\partial t} + n_0 \nabla \cdot \mathbf{v}_1 = 0 \tag{89}$$

$$\frac{\partial \mathbf{v}_1}{\partial t} = -\frac{e}{m_e}\mathbf{E}_1 \tag{90}$$

$$\frac{1}{c^2}\frac{\partial^2 \mathbf{E}_1}{\partial t^2} - \nabla^2 \mathbf{E}_1 = -\frac{4\pi}{c^2}\frac{\partial}{\partial t}(\mathbf{J}_1 + \mathbf{J}_b) - 4\pi\nabla(\rho_1 + \rho_b) \tag{91}$$

$$\frac{1}{c^2}\frac{\partial^2 \mathbf{B}_1}{\partial t^2} - \nabla^2 \mathbf{B}_1 = \frac{4\pi}{c}\nabla \times (\mathbf{J}_1 + \mathbf{J}_b). \tag{92}$$

It is possible to rearrange the expression by explicitly expressing the current source term in the wave equations. For the equation of the electric field this turns into:

$$\frac{\partial}{\partial t}(\mathbf{J}_b + \mathbf{J}_1) = \frac{\partial \mathbf{J_b}}{\partial t} - e n_0 \frac{\partial \mathbf{v}_1}{\partial t} = \frac{\partial \mathbf{J_b}}{\partial t} + \frac{e^2 n_0}{m_e}\mathbf{E}_1. \tag{93}$$

where we have used Eq.(90). Substituting the result in the wave equation gives:

$$\frac{1}{c^2}\frac{\partial^2 \mathbf{E}_1}{\partial t^2} - \nabla^2 \mathbf{E}_1 + \frac{\omega_p^2}{c^2}\mathbf{E}_1 = -\frac{4\pi}{c^2}\frac{\partial \mathbf{J}_b}{\partial t} - 4\pi\nabla(\rho_1 + \rho_b). \tag{94}$$

Analogously the expansion of the term $\nabla \times \mathbf{J}_1$ in the equation for the magnetic field provides:

$$\frac{1}{c^2}\frac{\partial^2 \mathbf{B}_1}{\partial t^2} - \nabla^2 \mathbf{B}_1 + \frac{\omega_p^2}{c^2}\mathbf{B}_1 = \frac{4\pi}{c}\nabla \times \mathbf{J}_b. \tag{95}$$

It is worth to be noted that the source term for the magnetic field depends only by the beam current, meaning that the response of the plasma is purely electrostatic.

The system described so far is valid under the approximations mentioned initially. It is further assumed from now on the validity of the quasi-static approximation described in Section 4.1.1. The change of variable provides the transformation for the derivatives:

$$\begin{cases} \frac{\partial}{\partial t} = v_b \frac{\partial}{\partial \xi} \rightarrow \frac{\partial^2}{\partial t^2} = v_b^2 \frac{\partial^2}{\partial \xi^2} \\ \frac{\partial}{\partial z} = -\frac{\partial}{\partial \xi} \rightarrow \frac{\partial^2}{\partial z^2} = \frac{\partial^2}{\partial \xi^2}. \end{cases} \tag{96}$$

Substituting the derivative in Eq.(94,95):

$$(\beta^2 - 1)\frac{\partial^2 \mathbf{E}_1}{\partial \xi^2} - \Delta \mathbf{E}_1 + k_0^2 \mathbf{E}_1 = -\frac{4\pi v_b}{c^2}\frac{\partial \mathbf{J}_b}{\partial \xi} - 4\pi\nabla(\rho_1 + \rho_b) \tag{97}$$

$$(\beta^2 - 1)\frac{\partial^2 \mathbf{B}_1}{\partial \xi^2} - \Delta \mathbf{B}_1 + k_0^2 \mathbf{B}_1 = \frac{4\pi}{c}\nabla \times \mathbf{J}_b \tag{98}$$

where $\beta = v_b/c$, $\Delta = \nabla^2 - \partial^2/\partial z^2$ and $k_0 = \omega_p/c$. Describing the system in cylindrical coordinates, further assuming that the beam is propagating along the $\hat{z}$ direction, the field equations can turn into:

$$-\frac{1}{\gamma^2}\frac{\partial^2 \mathbf{E}_1}{\partial \xi^2} - \Delta \mathbf{E}_1 + k_0^2 \mathbf{E}_1 = 4\pi \left(\frac{1}{\gamma^2}\frac{\partial \rho_b}{\partial \xi} + \frac{\partial \rho_1}{\partial \xi} \right) \hat{z} - 4\pi \frac{\partial}{\partial r}(\rho_b + \rho_1)\hat{r} \quad (99)$$

$$-\frac{1}{\gamma^2}\frac{\partial^2 \mathbf{B}_1}{\partial \xi^2} - \Delta \mathbf{B}_1 + k_0^2 \mathbf{B}_1 = -4\pi\beta \frac{\partial \rho_b}{\partial r}\hat{\theta} \quad (100)$$

where $\gamma^2 = (1-\beta^2)^{-1}$ is the Lorentz factor.

Since the only external perturbation is provided by the injected particle beam, it is helpful to express the wakefields in term of just the beam parameters, namely the beam density and current, using the fluid equations Eq.(89,90).

By taking the time derivative of the continuity equation and using the Euler equations one obtains the same equation for a driven harmonic oscillator as Eq.(30):

$$\frac{\partial^2 n_1}{\partial \xi^2} + k_p^2 n_1 = -k_p^2 n_b \quad (101)$$

with $k_p = \omega_p/v_b$ and having assumed an electron beam.

It is possible to solve the system by performing a Fourier-Hankel transform, defined by:

$$\hat{\Psi}(k, r) = \int_{-\infty}^{\infty} \Psi(\xi, r) e^{-ik\xi} d\xi \quad (102)$$

$$H_\nu(\tilde{\Psi}(r,k), k_r) = \tilde{\Psi}(k, k_r, \nu) = \int_0^\infty r \hat{\Psi}(r,k) J_\nu(k_r r) dr. \quad (103)$$

First applying the Fourier transform to Eq.(101) gives:

$$\hat{n}_1 = \frac{k_p^2}{k^2 - k_p^2}\hat{n}_b. \quad (104)$$

and substituting the result in the Fourier transformed Eq.(99,100) provides:

$$\frac{k^2}{\gamma^2}\hat{\mathbf{E}}_1 - \Delta \hat{\mathbf{E}}_1 + k_0^2 \hat{\mathbf{E}}_1 = -4\pi i k \frac{\frac{k^2}{\gamma^2} - k_0^2}{k^2 - k_p^2}\hat{\rho}_b \hat{z} - 4\pi \frac{k^2}{k^2 - k_p^2}\frac{\partial \hat{\rho}_b}{\partial r}\hat{r} \quad (105)$$

$$\frac{k^2}{\gamma^2}\hat{\mathbf{B}}_1 - \Delta \hat{\mathbf{B}}_1 + k_0^2 \hat{\mathbf{B}}_1 = -4\pi\beta \frac{\partial \hat{\rho}_b}{\partial r}\hat{\theta}. \quad (106)$$

The next step consists in applying the Hankel transform defined by Eq.(103). It is worth mention the Hankel transform of the cylindrical Laplace operator:

$$H_\nu \left[\left(\frac{\partial^2}{\partial r^2} + \frac{1}{r}\frac{\partial}{\partial r} - \frac{\nu}{r^2} \right) \Psi(r), k_r \right] = -k_r^2 \tilde{\Psi}_\nu(k_r). \tag{107}$$

Applying the Hankel transform to the Eq.(105,106) gives:

$$\left(k_r^2 + k_0^2 + \frac{k^2}{\gamma^2} \right) \tilde{E}_r(k, k_r, 1) = -4\pi \frac{k^2}{k^2 - k_p^2} H_1 \left(\frac{\partial \hat{\rho}_b}{\partial r}, k_r \right) \tag{108}$$

$$\left(k_r^2 + k_0^2 + \frac{k^2}{\gamma^2} \right) \tilde{B}_\theta(k, k_r, 1) = -4\pi\beta H_1 \left(\frac{\partial \hat{\rho}_b}{\partial r}, k_r \right) \tag{109}$$

$$\left(k_r^2 + k_0^2 + \frac{k^2}{\gamma^2} \right) \tilde{E}_z(k, k_r, 0) = -4\pi i k \frac{\frac{k^2}{\gamma^2} + k_0^2}{k^2 - k_p^2} H_0 \left(\hat{\rho}_b, k_r \right) \tag{110}$$

where only the components of the fields depending by the external perturbation has been evaluated, the others providing the equations for a cylindrical ordinary wave propagating in plasma. The explicit expression for the electromagnetic fields is therefore:

$$\tilde{E}_r(k, k_r, 1) = -4\pi \frac{k^2}{\left(k_r^2 + k_0^2 + \frac{k^2}{\gamma^2} \right)(k^2 - k_p^2)} H_1 \left(\frac{\partial \hat{\rho}_b}{\partial r}, k_r \right) \tag{111}$$

$$\tilde{B}_\theta(k, k_r, 1) = -4\pi\beta \frac{1}{\left(k_r^2 + k_0^2 + \frac{k^2}{\gamma^2} \right)} H_1 \left(\frac{\partial \hat{\rho}_b}{\partial r}, k_r \right) \tag{112}$$

$$\tilde{E}_z(k, k_r, 0) = -4\pi i k \frac{\frac{k^2}{\gamma^2} + k_0^2}{\left(k_r^2 + k_0^2 + \frac{k^2}{\gamma^2} \right)(k^2 - k_p^2)} H_0 \left(\hat{\rho}_b, k_r \right). \tag{113}$$

In order to obtain the expression in the co-moving frame for a generic extended source can be applied the convolution theorem, providing the equations:

$$E_z(r, \xi) = \int_{-\infty}^{\infty} \int_0^{\infty} \xi \, \mathrm{J}_0(k_r r) H_0 \left(\hat{\rho}_b, k_r \right) G_z(k_r, \xi - \xi') d\xi' dk_r \tag{114}$$

$$E_r(r, \xi) = \int_{-\infty}^{\infty} \int_0^{\infty} \xi \, \mathrm{J}_1(k_r r) H_1 \left(\frac{\partial \hat{\rho}_b}{\partial r}, k_r \right) G_r(k_r, \xi - \xi') d\xi' dk_r \tag{115}$$

$$B_\theta(r, \xi) = \int_{-\infty}^{\infty} \int_0^{\infty} \xi \, \mathrm{J}_1(k_r r) H_1 \left(\frac{\partial \hat{\rho}_b}{\partial r}, k_r \right) G_\theta(k_r, \xi - \xi') d\xi' dk_r \tag{116}$$

where

$$G_z(k_r, \xi - \xi') = -2i \int_{-\infty}^{\infty} k \frac{\frac{k^2}{\gamma^2} + k_0^2}{\left(k_r^2 + k_0^2 + \frac{k^2}{\gamma^2}\right)(k^2 - k_p^2)} e^{-ik(\xi - \xi')} dk \tag{117}$$

$$G_r(k_r, \xi - \xi') = -2 \int_{-\infty}^{\infty} \frac{k^2}{\left(k_r^2 + k_0^2 + \frac{k^2}{\gamma^2}\right)(k^2 - k_p^2)} e^{-ik(\xi - \xi')} dk \tag{118}$$

$$G_\theta(k_r, \xi - \xi') = -2\beta \int_{-\infty}^{\infty} \frac{1}{\left(k_r^2 + k_0^2 + \frac{k^2}{\gamma^2}\right)} e^{-ik(\xi - \xi')} dk. \tag{119}$$

are the Green functions.

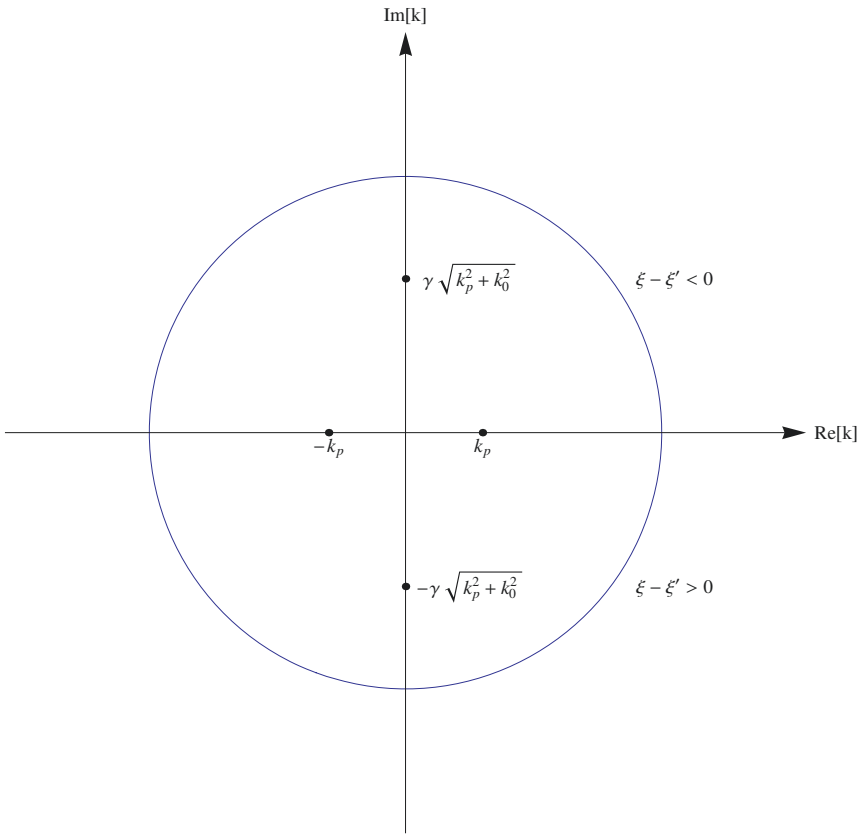

Figure 42: Contour of integration and poles for the Green functions of the wakefields.

The integral involving the Green functions can be solved by using the residue theorem by properly choosing the closing contour integral according

to the sign of $\xi - \xi'$: if $\xi - \xi' > 0$ then the closure is on the lower half plane(LHP), vice versa for $\xi' - \xi > 0$ the closure has to be chosen in the upper half plane (UHP). The poles arising in the integrals are:

$$k = \pm k_p \tag{120}$$

$$k = \pm i\gamma\sqrt{k_0^2 + k_r^2}. \tag{121}$$

The scheme of the contour integral is represented in Fig.42. The poles on the $Re[k]$ axis can be displaced in the LHP according to the Landau prescription. This way the integral on the UHP provides for the Green function for the z component:

$$G_z^{UHP}(k_r, \xi - \xi') = 4\pi\gamma^2 \frac{k e^{-ik(\xi-\xi')}\left(\frac{k^2}{\gamma^2} + k_0^2\right)}{(k-k_p)(k+k_p)(k+i\gamma\sqrt{k_0^2+k_r^2})}\Big|_{k=i\gamma\sqrt{k_0^2+k_r^2}} = -2\pi \frac{e^{\gamma\sqrt{k_0^2+k_r^2}(\xi-\xi')}k_r^2}{k_r^2+k_p^2}. \tag{122}$$

Analogously for the LHP:

$$\begin{aligned} G_z^{LHP}(k_r, \xi - \xi') = &- 4\pi\gamma^2 \frac{k e^{-ik(\xi-\xi')}\left(\frac{k^2}{\gamma^2} + k_0^2\right)}{(k^2-k_p^2)(k-i\gamma\sqrt{k_0^2+k_r^2}))}\Big|_{k=-i\gamma\sqrt{k_0^2+k_r^2}} + \\ &- 4\pi\gamma^2 \frac{k e^{-ik(\xi-\xi')}\left(\frac{k^2}{\gamma^2} + k_0^2\right)}{(k-k_p)(k^2+\gamma^2(k_0^2+k_r^2))}\Big|_{k=-k_p} + \\ &- 4\pi\gamma^2 \frac{k e^{-ik(\xi-\xi')}\left(\frac{k^2}{\gamma^2} + k_0^2\right)}{(k+k_p)(k^2+\gamma^2(k_0^2+k_r^2))}\Big|_{k=k_p} \end{aligned} \tag{123}$$

providing so:

$$G_z^{LHP}(k_r, \xi - \xi') = 2\pi \frac{e^{-\gamma\sqrt{k_0^2+k_r^2}(\xi-\xi')}k_r^2}{k_r^2+k_p^2} + 2\pi \frac{e^{ik_p(\xi-\xi')}k_p^2}{k_r^2+k_p^2} + 2\pi \frac{e^{-ik_p(\xi-\xi')}k_p^2}{k_r^2+k_p^2}. \tag{124}$$

So the complete solution for the longitudinal Green function is:

$$\begin{aligned} G_z(k_r, \xi - \xi') = &2\pi \left(2\frac{k_p^2}{k_r^2+k_p^2}\cos[k_p(\xi-\xi')] + \frac{k_r^2}{k_r^2+k_p^2}e^{-\gamma\sqrt{k_0^2+k_r^2}(\xi-\xi')}\right)\Theta(\xi-\xi') + \\ &- 2\pi\frac{k_r^2}{k_r^2+k_p^2}e^{\gamma\sqrt{k_0^2+k_r^2}(\xi-\xi')}\Theta(\xi'-\xi). \end{aligned} \tag{125}$$

By following the same procedure is possible to evaluate as well the radial and

poloidal components of the Green function:

$$G_r(k_r,\xi-\xi') = \pi\frac{k_p^2}{k_r^2+k_p^2}\sin[k_p(\xi-\xi')]\Theta(\xi-\xi') - 2\pi\gamma\frac{e^{-\gamma\sqrt{k_0^2+k_r^2}|\xi-\xi'|}\sqrt{k_0^2+k_r^2}}{k_r^2+k_p^2} \tag{126}$$

$$G_\theta(k_r,\xi-\xi') = 2\pi\gamma\beta\frac{e^{-\gamma\sqrt{k_0^2+k_r^2}|\xi-\xi'|}}{\sqrt{k_0^2+k_r^2}}. \tag{127}$$

The full expression for the fields is so, by replacing the Green functions in the integrals:

$$\begin{aligned} E_z(r,\xi) = 2\pi\int_0^\infty \frac{k_r}{k_r^2+k_p^2}\,\mathrm{J}_0(k_r r)\left(\int_0^\xi 2k_p^2 H_0(\rho_b(r,\xi'),k_r)\cos[k_p(\xi-\xi')]d\xi' + \right. \\ \left. +k_r^2\left(\int_{-\infty}^\xi H_0(\rho_b(r,\xi'),k_r)e^{-\gamma\sqrt{k_0^2+k_r^2}(\xi-\xi')}d\xi' - \int_\xi^\infty H_0(\rho_b(r,\xi'),k_r)e^{\gamma\sqrt{k_0^2+k_r^2}(\xi-\xi')}d\xi'\right)\right) dk \end{aligned} \tag{128}$$

$$\begin{aligned} E_r(r,\xi) = \pi\int_0^\infty \frac{k_r}{k_r^2+k_p^2}\,\mathrm{J}_1(k_r r)\left(\int_0^\xi k_p^2 H_1\left(\frac{\partial\rho_b(r,\xi')}{\partial r},k_r\right)\sin[k_p(\xi-\xi')]d\xi' + \right. \\ \left. -2\gamma\int_{-\infty}^\infty H_1\left(\frac{\partial\rho_b(r,\xi')}{\partial r},k_r\right)e^{-\gamma\sqrt{k_0^2+k_r^2}|\xi-\xi'|}\sqrt{k_0^2+k_r^2}d\xi'\right)dk_r \end{aligned} \tag{129}$$

$$B_\theta(r,\xi) = 2\pi\gamma\beta\int_{-\infty}^\infty\int_0^\infty k_r\,\mathrm{J}_1(k_r r)H_1\left(\frac{\partial\rho_b(r,\xi')}{\partial r},k_r\right)\frac{e^{-\gamma\sqrt{k_0^2+k_r^2}|\xi-\xi'|}}{\sqrt{k_0^2+k_r^2}}d\xi' dk_r. \tag{130}$$

To finally obtain the expression of the field in the co-moving frame for a generic beam profile, it is necessary to explicitly express the Hankel transform of the beam density. This provides integrals in r' that can be solved using the relation:

$$\int_0^\infty \frac{k_r}{k_r^2+k_p^2}\,\mathrm{J}_0(k_r r)\,\mathrm{J}_0(k_r r')dk_r = \begin{cases} \frac{\pi}{2}i\,\mathrm{J}_0(ik_p r')\,\mathrm{H}_0^{(1)}(ik_p r) = \mathrm{I}_0(k_p r')\,\mathrm{K}_0(k_p r) & \text{for } r>r' \\ \frac{\pi}{2}i\,\mathrm{J}_0(ik_p r)\,\mathrm{H}_0^{(1)}(ik_p r') = \mathrm{I}_0(k_p r)\,\mathrm{K}_0(k_p r') & \text{for } r'>r \end{cases} \tag{131}$$

and

$$\int_0^\infty \frac{k_r}{k_r^2+k_p^2}\,\mathrm{J}_1(k_r r)\,\mathrm{J}_1(k_r r')dk_r = \begin{cases} \frac{\pi}{2}i\,\mathrm{J}_1(ik_p r')\,\mathrm{H}_1^{(1)}(ik_p r) = \mathrm{I}_1(k_p r')\,\mathrm{K}_1(k_p r) & \text{for } r>r' \\ \frac{\pi}{2}i\,\mathrm{J}_1(ik_p r)\,\mathrm{H}_1^{(1)}(ik_p r') = \mathrm{I}_1(k_p r)\,\mathrm{K}_1(k_p r') & \text{for } r'>r \end{cases} . \tag{132}$$

The two expressions can be summarized as:

$$\int_0^\infty \frac{k_r}{k_r^2+k_p^2}\,\mathrm{J}_\nu(k_r r_>)\,\mathrm{J}_\nu(k_r r_<)dk_r = \mathrm{I}_\nu(k_p r_<)\,\mathrm{K}_\nu(k_p r_>). \tag{133}$$

The wakefields can be therefore expressed as:

$$\begin{aligned} E_z(r,\xi) = {} & 4k_p^2\pi \int_0^\infty \int_0^\xi \rho_b(r',\xi') r'\,\mathrm{I}_0(k_p r_<)\,\mathrm{K}_0(k_p r_>)\cos[k_p(\xi-\xi')]d\xi' dr' + \\ & + 2\pi \int_0^\infty \frac{k_r^3}{k_r^2+k_p^2}\,\mathrm{J}_0(k_r r)\left(\int_{-\infty}^\xi H_0(\rho_b(r,\xi'),k_r)e^{-\gamma\sqrt{k_0^2+k_r^2}(\xi-\xi')}d\xi' + \right. \\ & \left. - \int_\xi^\infty H_0(\rho_b(r,\xi'),k_r)e^{\gamma\sqrt{k_0^2+k_r^2}(\xi-\xi')}d\xi'\right)dk_r \end{aligned} \tag{134}$$

$$\begin{aligned} E_r(r,\xi) = {} & k_p^2\pi \int_0^\infty \int_0^\xi \frac{\partial\rho_b(r',\xi')}{\partial r'}\,\mathrm{I}_1(k_p r_<)\,\mathrm{K}_1(k_p r_>)\sin[k_p(\xi-\xi')]d\xi' dr' + \\ & - 2\gamma\pi \int_{-\infty}^\infty \int_0^\infty \frac{k_r}{k_r^2+k_p^2}\,\mathrm{J}_1(k_r r)H_1\left(\frac{\partial\rho_b(r,\xi')}{\partial r},k_r\right)e^{-\gamma\sqrt{k_0^2+k_r^2}|\xi-\xi'|}\sqrt{k_0^2+k_r^2}d\xi' dk_r \end{aligned} \tag{135}$$

$$B_\theta(r,\xi) = 2\pi\gamma\beta \int_{-\infty}^\infty \int_0^\infty \frac{k_r}{\sqrt{k_0^2+k_r^2}}\,\mathrm{J}_1(k_r r)H_1\left(\frac{\partial\rho_b(r,\xi')}{\partial r},k_r\right)e^{-\gamma\sqrt{k_0^2+k_r^2}|\xi-\xi'|}d\xi' dk_r. \tag{136}$$

Considering ultra relativistic driver, $k_0 \simeq k_p$, and discarding terms of order higher than γ^{-1} and exponential decaying factors the fields reduce to:

$$E_z(r,\xi) = -4k_p^2\pi \int_0^\infty \int_0^\xi \rho_b(r',\xi') r'\,\mathrm{I}_0(k_p r_<)\,\mathrm{K}_0(k_p r_>)\cos[k_p(\xi-\xi')]d\xi' dr' \tag{137}$$

$$W(r,\xi) = 4\pi k_p \int_0^\infty \int_0^\xi \frac{\partial\rho_b(r',\xi')}{\partial r'}\,\mathrm{I}_1(k_p r_<)\,\mathrm{K}_1(k_p r_>)\sin[k_p(\xi-\xi')]d\xi' dr'. \tag{138}$$

B Particle in Cell and Quasi-static VLPL

In this section is provided a short description of the Particle in Cell (PIC) approach for the numerical analysis of the plasma dynamics.

PIC codes are widely used for the study of the plasma dynamics [89–94]. The main advantage of this approach is the lower computational time required respect to Vlasov codes. A Vlasov code tracks the evolution of

the distribution function for the plasma particles, therefore the analysis is performed in a 6-dimensional phase-space, no matter the shape and extent of the distribution function. In a PIC code instead, the phase-space volume is sampled properly considering the volume occupied by the plasma particles, reducing therefore the phase-space volume that has to be taken into account (Fig.43).

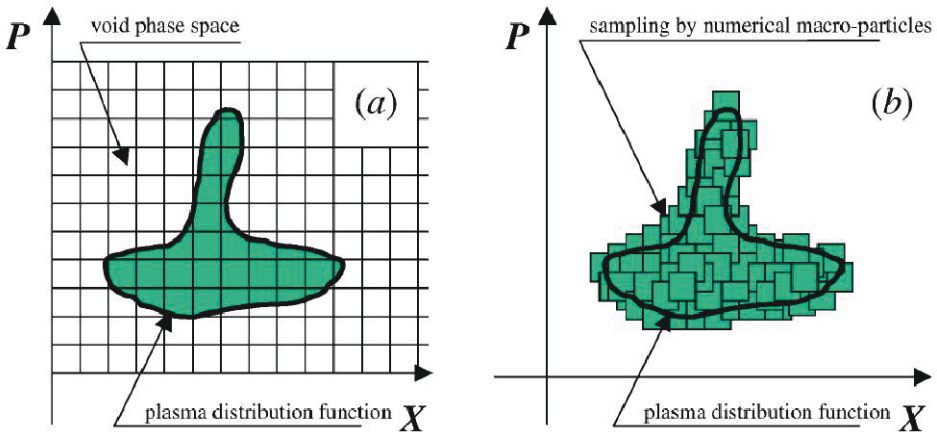

Figure 43: Sampling of the phase-space for a Vlasov code and for a PIC code (Picture taken from Ref. [88]).

A PIC code studies the dynamics of "numerical particles", defined as a phase-space sample of the plasma distribution function. These particles will evolves on the characteristics of the Vlasov equation, therefore the description is exactly analogous to that of a many-body analysis. Eventually, by reducing the size of the sampling, the PIC code can describe the dynamics of the real plasma particle.

The reason why PIC codes result more efficient is in the limited amount of phase-space that has to be taken into account for the description of the system, in contrast with Vlasov codes that has to track the evolution of the distribution function on the whole phase-space, no matter the portion occupied by the plasma.

The downside of the method is the numerical noise that goes as $N^{\frac{1}{2}}$ where N are the number of "numerical particles".

Without going too much in the details of the general approach for PIC codes, we focus the attention to the particular numerical scheme used in this work, namely the quasi-static approach.

As previously mentioned, one of the serious issues concerning the study of

the plasma is the different scales interacting each other. This is of course an issue as well when try to develop a numerical analysis for the plasma behavior. In the case of plasma based accelerators the relevant scales involved goes from the plasma wavelength (or the laser wavelength for laser-driven acceleration) to the acceleration length and several orders of magnitude can separates the two scales.

Among the approaches to ease this problem two are the most relevant ones: changing the reference frame in the co-moving one with the driver (the boosted frame) [95] or using the quasi-static approximation [96–98].

The last one, used in this work, is based on the assumptions of a slowly evolving driver respect to the time scale at which occurs the plasma dynamics. In order to separate the two scales a transformation in the co-moving frame is performed:

$$\tau = t \tag{139}$$

$$\xi = v_b t - z. \tag{140}$$

The scale τ is the slow time scale on which the driver evolves, while the co-moving variable ξ is the fastest one on which the plasma dynamics occurs.

The general scheme for the evolution of the system in such an approximation is to first evaluate the fields from the from of the beam up to the end, moving along the variable ξ, for a fixed time τ. Performing such evaluation the derivative respect to τ are discarded. Once evaluated the fields and the plasma distribution the driver is advanced on the next time step τ [88].

The general numerical scheme in quasi-static PIC codes involves first the deposition of the current and the charge on the grid according to the initial conditions of the driver. Then a layer of numerical macroparticles moves along the simulation box starting from the head of the driver up to the end, updating the plasma density and the fields on the grid while moving. Once finished, these fields are used to advance the driver on the next time step τ (Fig.44). Since in our analysis the driver is a particle beam its evolution is obtained by solving the motion of the particles under the newly updated fields. The number of operations that can perform the quasi-static PIC respect to a full PIC is provided by:

$$N_{QS} \simeq \frac{\lambda_0^2}{\lambda_\beta \lambda_p} N_{PIC} \tag{141}$$

where λ_0 is the laser wavelength, λ_p is the plasma wavelength and $\lambda_\beta = 2\pi c/\omega_\beta$ is the betatron wavelength. Such scale can easily improve the performances to six orders of magnitude respect to a full PIC. The downside of the quasi-static PIC on the other hand is the impossibility to include radiation emission.

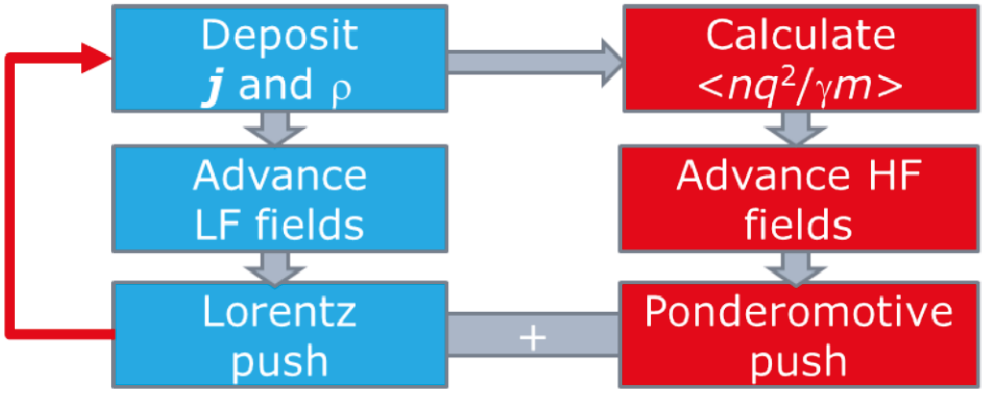

Figure 44: Steps in the numerical scheme for a quasi-static PIC code (Picture taken from Ref. [88]).

C Derivation of the beam envelope model

In Section5 we have introduced the envelope model for describing the transverse beam dynamics. As previously mentioned, the procedure presented is not accurate since it assume the possibility to describe the transverse beam dynamics by just considering the dynamics of the radius. Moreover the emittance force has been added "by hand" without a real reason provided by the model.

Here we present a rigorous derivation of the envelope model for the beam, describing the transverse dynamics by the behavior of the rms radius, so providing a statistical description for the beam. The contribute due to the emittance appear in this case in a natural way, without any need to add it.

The model here presented is derived in [64] and is based on the same assumptions presented in Section5 that we write here again for completeness:

- Paraxial approximation, i.e. the transverse particle velocity is smaller than the longitudinal velocity;
- Azimuthal symmetry for beam current density and fields;
- No mass spread whiting a transverse section of the beam;
- Uniform (external) soleinodal field across the beam;
- Small-angle multiple scattering allowed;
- No phase mixing, i.e. the beam slices do not overcome each other in the direction of propagation;

- No treatment of radiation losses.

We can start from the dynamics of a single beam charge particle, described by:

$$\dot{\mathbf{p}} = q(\mathbf{E} + \mathbf{v} \times \mathbf{B}) + \delta\mathbf{F} \tag{142}$$

where $\mathbf{p} = \gamma m\dot{\mathbf{r}}$ is the relativistic momentum, $\mathbf{E}$ and $\mathbf{B}$ are the electric and magnetic fields (both externally applied and self-generated by the beam) and $\delta\mathbf{F}$ is the rapidly fluctuating force arising from the scattering.

From the previous equation, by taking the scalar product with $\mathbf{v}$, is possible to derive the equation for the evolution of the relativistic energy $W = \gamma mc^2$ as:

$$\dot{W} = q\mathbf{v} \cdot \mathbf{E} + \mathbf{v} \cdot \delta\mathbf{F} = q(v_z E_z + \mathbf{v}_\perp \cdot \mathbf{E}_\perp) + \mathbf{v} \cdot \delta\mathbf{F} \simeq q v_z E_z + \frac{\delta W}{\delta t}. \tag{143}$$

We have used here the paraxial approximation for which the transverse term of the equation can be treated as an higher order correction. The term $\delta W/\delta t$ is again the rate of change of energy due to scattering with the medium.

Taking into account only of the transverse dynamics from Eq.(142) we obtain:

$$\frac{1}{\gamma}\dot{\gamma}\mathbf{v}_\perp + \dot{\mathbf{v}}_\perp = \frac{q}{m\gamma}(\mathbf{E}_\perp + v_z\hat{z} \times \mathbf{B}_\perp + \mathbf{v}_\perp \times B_z\hat{z}) + \frac{\delta\mathbf{F}_\perp}{\gamma m}. \tag{144}$$

The expression for the fields can be obtained by the Maxwell equations:

$$\nabla \cdot \mathbf{B} = 0 \longrightarrow B_r = -\frac{r}{2}\frac{\partial B_z}{\partial z} \text{ (since } \partial_\theta = 0) \tag{145}$$

$$E_\theta = -\frac{r}{2}\frac{\partial B_z}{\partial t}. \tag{146}$$

This leads to:

$$\frac{1}{\gamma}\dot{\gamma}\mathbf{v}_\perp + \dot{\mathbf{v}}_\perp = \frac{q}{m\gamma}(E_r\hat{r} - \frac{r}{2}\frac{\partial B_z}{\partial t}\hat{\theta} - v_z\frac{r}{2}\frac{\partial B_z}{\partial z}\hat{z}\times\hat{r} + v_z B_\theta\hat{z}\times\hat{\theta} + \mathbf{v}_\perp \times B_z\hat{z}) + \frac{\delta\mathbf{F}_\perp}{\gamma m}. \tag{147}$$

By noting that:

$$\frac{\partial B_z}{\partial t} + v_z\frac{\partial B_z}{\partial z} = \dot{B}_z \tag{148}$$

the equation can be recast as:

$$\frac{1}{\gamma}\dot{\gamma}\mathbf{v}_\perp + \dot{\mathbf{v}}_\perp = \frac{q}{m\gamma}((E_r - v_z B_\theta)\hat{r} - \frac{1}{2}\dot{B}_z\hat{z} \times \mathbf{r} + \mathbf{v}_\perp \times B_z\hat{z}) + \frac{\delta\mathbf{F}_\perp}{\gamma m}. \tag{149}$$

We can define the relativistic cyclotron and betatron frequencies:

$$\omega_c = \frac{qB_z}{\gamma m} \tag{150}$$

$$\omega_\beta^2 = \frac{q}{\gamma m}\frac{v_z B_\theta - E_r}{r} \tag{151}$$

so that the equation of motion of the charged particle can be rewritten as (dropping the $\perp$):

$$\frac{1}{\gamma}\dot{\gamma}\mathbf{v} + \dot{\mathbf{v}} + \omega_\beta^2\mathbf{r} + \omega_c\hat{z}\times\mathbf{v} + \frac{1}{2\gamma}\frac{d}{dt}(\gamma\omega_c)\,\hat{z}\times\mathbf{r} = \frac{1}{\gamma m}\delta\mathbf{F}. \tag{152}$$

So far we have addressed only the dynamics of a single charged particle. This is far from describing the behavior of the whole beam.

In order to extend the description to the beam dynamics we take the equations for the second moments of the variables characterizing the single particle dynamics, namely the velocity, the position and the angular momentum.

By taking the scalar product of Eq.(152) with the velocity we obtain an equation for the variation of the energy (as shown previously):

$$\frac{1}{\gamma}\dot{\gamma}v^2 + \frac{1}{2}\dot{v^2} + \frac{\omega_\beta^2}{2}\dot{r^2} + \frac{1}{2\gamma}\frac{d}{dt}(\gamma\omega_c)l = \frac{1}{\gamma m}\mathbf{v}\cdot\delta\mathbf{F} \tag{153}$$

with $l = \hat{z}\cdot(\mathbf{r}\times\mathbf{v}) = rv_\theta$ being the $\hat{z}$-component of the angular momentum.

Taking instead the scalar product of Eq.(152) with $\mathbf{r}$ we obtain the virial equation:

$$\frac{1}{2\gamma}\dot{\gamma}\dot{r^2} + \frac{\ddot{r^2}}{2} - v^2 + \omega_\beta^2 r^2 - \omega_c l = \frac{1}{\gamma m}\mathbf{r}\cdot\delta\mathbf{F}. \tag{154}$$

Finally by taking the cross product of $\mathbf{r}$ with Eq.(152) we obtain an equation for the angular momentum:

$$\frac{1}{\gamma}\dot{\gamma}l + \dot{l} + \omega_c\frac{\dot{r^2}}{2} + \frac{1}{2\gamma}\frac{d}{dt}(\gamma\omega_c)r^2 = \frac{1}{\gamma m}\hat{z}\cdot(\mathbf{r}\times\delta\mathbf{F}). \tag{155}$$

We have now the necessary equations for describing the beam dynamics. Taking the transverse average of the last three equations result in:

$$\frac{1}{\gamma}\dot{\gamma}V^2 + \frac{\dot{V^2}}{2} + \frac{1}{2}\overline{\omega_\beta\dot{r^2}} + \frac{1}{2\gamma}\frac{d}{dt}(\gamma\omega_c)L = \frac{W'}{\gamma m} \tag{156}$$

$$\frac{1}{2\gamma}\dot{\gamma}\dot{R^2} + \frac{\ddot{R^2}}{2} - V^2 + \overline{\omega_\beta^2 r^2} - \omega_c L = 0 \tag{157}$$

$$\frac{1}{\gamma}\dot{\gamma}L + \dot{L} + \omega_c\frac{\dot{R^2}}{2} + \frac{1}{2\gamma}\frac{d}{dt}(\gamma\omega_c)R^2 = 0 \tag{158}$$

where

$$R^2 = \frac{1}{N}\sum_{i=1}^{N} r_i^2 \tag{159}$$

$$V^2 = \frac{1}{N}\sum_{i=1}^{N} v_i^2 \tag{160}$$

$$L = \frac{1}{N}\sum_{i=1}^{N} l_i \tag{161}$$

$$W' = \frac{1}{\gamma N}\sum_{i=1}^{N} \gamma \mathbf{v}_i \cdot \delta\mathbf{F} \tag{162}$$

are the mean squared variables characterizing the particles and W' take into account the energy exchanged by scattering.

The terms involving the product of $\mathbf{r}$ with $\delta\mathbf{F}$ do not appear due to the isotropy of the scattering that so gives zero once taken the average.

The three equations derived can properly described the dynamics of the beam as a statistical average on the transverse profile of the dynamics of the single beam particles. It is anyway possible to obtain a single equation for the rms radius R that can alone describe the evolution of the beam radius for specific initial conditions and taking into account both the self-generated and externally applied fields.

In order to achieve this goal it is necessary on the other hand to impose an additional condition, this time on the shape of the current profile J_b. Specifically, we demand a self-similar expansion for the current profile that can be therefore defined as:

$$J_b = \frac{I_b}{2\pi R^2} F\left(\frac{r}{R}\right) \tag{163}$$

with F a generic function and I_b the beam current of the slice.

Such a profile for the beam current leads to:

$$\overline{\omega_\beta^2 r^2} = U = \int_0^\infty dr r F\left(\frac{r}{R}\right) \omega_\beta^2 r^2. \tag{164}$$

The actual value of the self-pinching field depends actually on the conditions of the system, specifically on the neutralization of the beam and it is left implicit for now.

Before evaluating the other average terms we can first rewrite the single particle velocity as:

$$\mathbf{v} = \frac{\mathbf{r}}{R}\dot{R} + \frac{Lr}{R^2}\hat{\theta} + \delta\mathbf{v}. \tag{165}$$

Therefore:

$$\overline{\omega_\beta^2 \dot{r^2}} = 2\overline{\omega_\beta^2 \mathbf{r}\cdot\mathbf{v}} = 2\overline{\omega_\beta^2 \mathbf{r}\cdot\frac{\mathbf{r}\dot{R}}{R}} = \frac{2}{R}\dot{R}\overline{\omega_\beta^2 r^2} = \frac{U}{R^2}\dot{R}^2. \tag{166}$$

We can now derive the envelope equation from the three equations for the energy, the virial equation and the angular momentum. Specifically the equation for the angular momentum leads to the conservation of the canonical angular momentum:

$$\frac{1}{\gamma}\dot{\gamma}L + \dot{L} + \omega_c\frac{\dot{R}^2}{2} + \frac{1}{2\gamma}\frac{d}{dt}(\gamma\omega_c)R^2 = \frac{1}{\gamma}\frac{d}{dt}\left(\gamma L + \gamma\omega_c R^2\right) = \frac{1}{\gamma}P_\theta = 0. \tag{167}$$

The conservation of the canonical momentum of the beam in obtained due to the isotropically distributed scattering.

From the virial equation we can obtain an expression for V^2:

$$V^2 = \frac{1}{2\gamma}\dot{\gamma}\dot{R}^2 + \frac{\ddot{R}^2}{2} + U - \omega_c L. \tag{168}$$

Substituting this expression in the equation for the energy:

$$\left(\frac{1}{\gamma}\dot{\gamma} + \frac{1}{2}\frac{d}{dt}\right)\left(\frac{1}{2\gamma}\dot{\gamma}\dot{R}^2 + \frac{\ddot{R}^2}{2} + U - \omega_c L\right) + \frac{U}{2}\frac{\dot{R}^2}{R^2} + \frac{1}{2\gamma}\frac{d}{dt}(\gamma\omega_c)L = \frac{W'}{\gamma m}. \tag{169}$$

All the terms involving L an be rearrange in order to fulfill the conservation of the canonical momentum, providing so:

$$\begin{aligned}&\left(\frac{1}{\gamma}\dot{\gamma} + \frac{1}{2}\frac{d}{dt}\right)(-\omega_c L) + \frac{1}{2\gamma}\frac{d}{dt}(\gamma\omega_c)L = -\frac{\omega_c}{2\gamma}\frac{d(\gamma L)}{dt} = \\ &= -\frac{\omega_c}{2\gamma}\frac{d}{dt}\left(P_\theta - \frac{\gamma\omega_c R^2}{2}\right) = \frac{\omega_c}{4\gamma}\frac{d}{dt}\left(\gamma\omega_c R^2\right).\end{aligned} \tag{170}$$

Replacing the expression in the previous equation gives:

$$\left(\frac{1}{\gamma}\dot{\gamma} + \frac{1}{2}\frac{d}{dt}\right)\left(\frac{1}{2\gamma}\dot{\gamma}\dot{R}^2 + \frac{\ddot{R}^2}{2} + U\right) + \frac{U}{2}\frac{\dot{R}^2}{R^2} + \frac{\omega_c}{4\gamma}\frac{d}{dt}\left(\gamma\omega_c R^2\right) = \frac{W'}{\gamma m}. \tag{171}$$

Rearranging the previous equation provides:

$$\frac{d}{dt}\left(\gamma^2 R^3\ddot{R} + \gamma\dot{\gamma}\dot{R}R^3 + \gamma^2 R^2 U + \frac{1}{4}\gamma^2\omega_c^2 R^4\right) = \frac{2\gamma R^2 W'}{m}. \tag{172}$$

Integrating both sides of the equation brings to envelope equation:

$$\ddot{R} + \frac{\dot{\gamma}}{\gamma}\dot{R} + \frac{U}{R} + \frac{\omega_c^2 R}{4} - \frac{C^2}{\gamma^2 R^3} = \frac{1}{\gamma^2 R^3}\int_{t_0}^{t} \frac{2\gamma R^2 W'}{m} dt' \tag{173}$$

with C being an integration constant related to the initial conditions set at the injection time t_0:

$$C^2 = \gamma^2 R^3 \left(\ddot{R} + \frac{\dot{\gamma}}{\gamma}\dot{R} + \frac{U}{R} + \frac{\omega_c^2 R}{4} \right) |_{t_0}. \tag{174}$$

A more useful expression for the constant C can be obtained by using the virial equation, providing:

$$\begin{aligned} &\gamma^2 R^3 \left(\ddot{R} + \frac{\dot{\gamma}}{\gamma}\dot{R} + \frac{U}{R} + \frac{\omega_c^2 R}{4} \right) = \\ &= \gamma^2 R^2 \left(V^2 - \dot{R}^2 + \omega_c L + \frac{\omega_c^2 R^2}{4} \right) = \\ &= \gamma^2 R^2 \left(V^2 - \dot{R}^2 - \frac{L^2}{R^2} \right) + P_\theta^2. \end{aligned} \tag{175}$$

We define the emittance squared as:

$$\epsilon^2 = \gamma^2 R^2 \left(V^2 - \dot{R}^2 - \frac{L^2}{R^2} \right). \tag{176}$$

The envelope equation can therefore be rewritten as:

$$\ddot{R} + \frac{\dot{\gamma}}{\gamma}\dot{R} + \frac{U}{R} + \frac{\omega_c^2 R}{4} - \frac{\epsilon^2(t_0) + P_\theta^2}{\gamma^2 R^3} = \frac{1}{\gamma^2 R^3}\int_{t_0}^{t} \frac{2\gamma R^2 W'}{m} dt'. \tag{177}$$

The envelope equation properly describes the transverse evolution of the rms radius of the beam. Such expression is more accurate of the one evaluated in Section5 since it takes into account of the statistical nature of the beam. Looking at the specific terms composing the equation we have:

- $\dot{\gamma}/\gamma\dot{R}$ is the term accounting for the reduction or increase of the beam energy;
- U/R is the term associated with the self-generated fields excited by the beam as well as those generated by the background. These fields are responsible for the focusing/defocussing of the beam;

- $\omega_c^2 R/4$ is the focusing force excited by the external magnetic field applied on the longitudinal direction $\hat{z}$. The azimuthal magnetic field of the beam can also be included, but according to the assumptions fixed in this model is a higher order term in the analysis, therefore does not play a role here;
- $P_\theta^2/\gamma^2 R^3$ is the centrifugal force generated my the poloidal motion of the beam;
- $\epsilon^2/\gamma^2 R^3$ is the expanding force exerted by the emittance. As we will see again the emittance force is associated to the thermal motion of the beam particles;
- $(\gamma^2 R^3)^{-1} \int_{t_0}^{t} (2\gamma R^2 W'/m)\, dt'$ is the energy exchange by the scattering with the background gas.

Assuming a constant beam energy $\gamma = const$, absence of an external azimuthal magnetic field and absence of scattering, the envelope equation turns into:

$$\ddot{R} + \frac{U}{R} - \frac{\epsilon^2(t_0) + P_\theta^2}{\gamma^2 R^3} = 0 \tag{178}$$

a similar expression to that obtained in Section5.

The main difference between the two is the nature of the self-generated force in the expression, being in this case the average over the transverse profile of the radial forces. The two expression are on the other hand exactly the same when considering homogeneous density profiles.

Lastly we want to describe few features of the emittance in the way represented in this model.

First of all we can see that the evolution of the emittance is related to the energy exchange in the scattering:

$$\ddot{\epsilon^2} = \frac{d^2(C^2 - P_\theta^2)}{dt^2} = \frac{2\gamma R^2 W'}{m} \tag{179}$$

since $P_\theta = const$. Therefore the emittance is conserved in absence of scattering.

A deeper insight on the nature of the emittance can be obtained by rewriting the V^2 term:

$$V^2 = \overline{v^2} = \dot{R}^2 + \frac{L^2}{R^2} + \overline{\delta v^2} \tag{180}$$

where δv is the small deviation of the velocity from the flow.

By replacing this term in the emittance expression we obtain:

$$\epsilon^2 = \gamma^2 R^2 \overline{\delta v^2}. \tag{181}$$

It appears clearly how the emittance is related to the effective transverse phase are occupied by the slice of beam and in particular how it is related to deviations of the velocity from the mean flow, taking into account a "temperature" of the beam.

The scattering increases the area occupied by increasing the velocity δv without a compensation in the rms radius.

In absence of scattering the emittance is conserved and therefore is conserved as well the area in the phase space occupied by the beam (the model can be cast in a Hamiltonian form).

References

[1] O. Chamberlain, E. Segrè, C. Wiegand, and T. Ypsilantis. *Phys. Rev.*, 100:947, 1955.

[2] J. E. Augustin et al. *Phys. Rev. Lett.*, 33:1406, 1974.

[3] J. J. Aubert, U. Becker, P. J. Biggs, J. Burger, M. Chen, G. Everhart, P. Goldhagen, J. Leong, T. McCorriston, T. G. Rhoades, M. Rohde, S. C. C. Ting, S. L. Wu, and Y. Y. Lee. *Phys. Rev. Lett.*, 33:1404, 1974.

[4] M. L. Perl et al. *Phys. Rev. Lett.*, 35:1489, 1975.

[5] D. P. Barber et al. *Phys. Rev. Lett.*, 43:830, 1979.

[6] UA1 Collaboration. *Phys. Lett. B*, 122:1, 1983.

[7] UA2 Collaboration. *Phys. Lett. B*, 122:5, 1983.

[8] CMS Collaboration. *Phys. Lett. B*, 716:30, 2012.

[9] CMS Collaboration. *High Energy Phys.*, 06:081, 2013.

[10] ATLAS Collaboration. *Phys. Lett B*, 716:1, 2012.

[11] T. Feder. *Physics Today*, 63:2, 2010.

[12] E. M. Rowe and F. E. Mills. *Particle Accelerators*, 4:211, 1973.

[13] http://www.synchrotron-soleil.fr/.

[14] U. Amaldi and G. Kraft. *Rep. Progr. Physics*, 68:8, 2005.

[15] D. Kramer. *Physics Today*, 68:6, 2015.

[16] http://theijpt.org/doi/pdf/10.14338/IJPT.14-editorial-2.1.

[17] E. S. Reich. *Nature*, 503:7475, 2013.

[18] F. Zimmermann, M. Benedikt, D. Schulte, and J. Wenninger, editors. *IPAC2014*, number 1, 2014.

[19] https://www.linearcollider.org/ILC/Publications/Technical-Design-Report.

[20] http://clic-study.web.cern.ch/content/conceptual-design-report.

[21] T. Tajima and J. M. Dawson. *Phys. Rev. Lett.*, 43:267–270, 1979.

[22] J. Faure, Y. Glinec, A. Pukhov, et al. *Nature*, 431:541–544, 2004.

[23] S. P. D. Mangles, C. D. Murphy, Z. Najmudin, et al. *Nature*, 431:535–538, 2004.

[24] R. Assmann, R. Bingham, T. Bohl, C. Bracco, B. Buttenschön, A. Butterworth, A. Caldwell, S. Chattopadhyay, S. Cipiccia, and E. Feldbaumer et al. *Plasma Phys. Control. Fusion*, 56:084013, 2014.

[25] A. Caldwell, E. Adli, L. Amorim, R. Apsimon, T. Argyropoulos, R. Assmann, A.M. Bachmann, F. Batsch, J. Bauche, and V.K. Berglyd Olsen et al. Path to awake: Evolution of the concept. *arXiv preprint*, arXiv:1510.01071, 2015. Nucl. Instr. Meth. A (submitted).

[26] N. Kumar, A. Pukhov, and K. Lotov. *Phys. Rev. Lett.*, 104:255003, 2010.

[27] H. Geiger and E. Marsden, editors. *Proceedings of the Royal Society, Series A*, volume 82, 1909.

[28] E. Rutherford. *Philosophical Magazine, Series 6*, 21:669, 1911.

[29] O. Jäkel, editor. *AIP Concerence Proceedings*, volume 958, 2007.

[30] O. Lawrence and M. Livingston. *Phys. Rev*, 40:19, 1932.

[31] http://pd.chem.ucl.ac.uk/pdnn/inst2/work.htm.

[32] http://rasmus-ischebeck.de/media/Accelerator Physics/Advanced Accelerator Concepts/Livingston 0Plot/slides/Livingston Plot 2.html.

[33] Francis F. Chen. *Introuction to Plasma Physics and Controlled Fusion. Volume 1: Plasma Physics*. Plenum Press, 1984.

[34] L. D. Landau and E. M. Lifshitz. *Physical Kinetics*. Pergamon Press, 1981.

[35] L. Tonks and I. Langmuir. *Phys. Rev.*, 33:195, 1929.

[36] S. Ichimaru. *Statistical Plasma Physics. Volume 1: Basic Principles*. Addison-Wesley Publishing Company, 1992.

[37] P. W. Debye and E. Huckel. *Phys. Z.*, 24:185, 1923.

[38] E. Esarey, P. Sprangle, J. Krall, and A. Ting. *IEEE transaction on plasma science*, 24:2, 1996.

[39] P. Chen, J. M. Dawson, R. W. Huff, and T. Katsouleas. *Phys. Rev. Lett.*, 55:1537, 1985.

[40] M. Litos, E. Adli, W. An, et al. *Nature*, 515:92–95, 2014.

[41] D. Gordon, K. C. Tzeng, C. E. Clayton, et al. *Phys. Rev. Lett*, 80:2133, 1998.

[42] S. Cipiccia, M. R. Islam, B. E. Ersfeld, et al. *Nature Physics*, 7:867–871, 2011.

[43] S. Wang, C. E. Clayton, B. E. Blue, et al. *Phys. Rev. Lett*, 88:13, 2002.

[44] W. P. Leemans, A. J. Gondalves, H.-S.Mao, et al. *Phys. Rev. Lett*, 113:245002, 2014.

[45] X. Wang, R. Zgadzaj, N. Fazel, et al. *Nature Communications*, 4:1988, 2012.

[46] M. Hogan. Facet. facility for accelerator science and experimental tests. Advanced Accelerator Concepts Workshop, Annapolis, MD, 2010.

[47] Y. Kitagawa, T. Matsumoto, T. Minamihata, K. Sawai, K. Matsuo, K. Mima, K. Nishihara, H. Azechi, K. A. Tanaka, H. Takabe, and S. Nakai. *Phys. Rev. Lett*, 68:48, 1992.

[48] C. E. Clayton, M. J. Everett, A. Lal, D. Gordon, K. A. Marsh, and C. Joshi. *Phys. Plasmas*, 1:1753, 1994.

[49] F. Amiranoff, J. Ardonceau, M. Bercher, D. Bernard, B. Cros, A. Debraine, J. M. Dieulot, J. Fusellier, F. Jacquet, J. M. Joly, M. Juillard, G. Matthieussent, P. Matricon, P. Mine, B. Montes, P. Mora, R. Morano, J. Morillo, F. Moulin, P. Poilleux, A. Specka, and C. Stenz, editors. *AIP Concerence Proceedings*, volume 335, 1995.

[50] A. K. Berezin, Ya. B. Fainberg, V. A. Kiselev, A. F. Linnik, V. V. Uskov, V. A. Balakirev, I. N. Onishchendo, G. L. Sidelnikov, and G. V. Sotnikov. *Plasma Phys. Rep.*, 20:596, 1994.

[51] Y. B. Fainberg, V. A. Balakirev, I. N. Onishchendo, G. L. Sidelnikov, and G. V. Sotnikov. *Plasma Phys. Rep.*, 20:606, 1994.

[52] K. Nakajima, D. Fisher, T. Kawakubo, H. Nakanishi, A. Ogata, Y. Kato, Y. Kitagawa, R. Kodama, K. Mima, H. Shiraga, K. Suzuki, K. Yamakawa, T. Zhang, Y. Sakawa, T. Shoji, Y. Nishida, N. Yugami, M. Downer, and T. Tajima. *Phys. Rev. Lett.*, 74:4428, 1995.

[53] J. Krall, A. Ting, E. Esarey, P. Sprangle, and G. Joyce. *Phys. Rev. E*, 48:2157, 1993.

[54] A. Pukhov and J. Meyer ter Vehn. *Appl. Phys. B*, 74:355, 2002.

[55] A. Ting, E. Esarey, and P. Sprangle. *Phys. Fluids B*, 2:1390–1394, 1990.

[56] P. Sprangle, E. Esarey, and A. Ting. *Phys. Rev. Lett.*, 64:2011–2014, 1990.

[57] R. Kenigs and M. Jones. *Phys. Fluids*, 30:252, 1987.

[58] B. N. Breizman et al., editors. *AIP Conf. Proc.*, volume 396, 1997.

[59] F. Massimo, A. Marocchino, and M. Ferrario. *Nucl. Instr. Meth. Phys. Res. A*, 740:242, 2014.

[60] E. Esarey, C. B. Schroeder, and W. P. Leemans. *Rev. Mod. Phys*, 81:1229, 2009.

[61] T. Katsouleas, S. Wilks, P. Chen, J. M. Dawson, and J. J. Su. *Particle Accelerators*, 22:81, 1987.

[62] Martin Reiser. *Theory and Design of Charged Particle Beams*. Wiley-VCH, 2008.

[63] Jr. Stanley Humphries. *Charged Particle Beams*. John Wiley and Sons, 2002.

[64] E. P. Lee and R. K. Cooper. *Particle Accelerators*, 7:83, 1976.

[65] J. B. Rosenzweig. *Phys. Rev. Lett.*, 58,6:555–558, 1987.

[66] P. Chen et al. *Phys. Rev. Lett.*, 56,12:1252, 1986.

[67] K. L. Bane et al. *IEEE Trans. Nucl. Sci.*, 32:3524–3526, 1985.

[68] *Proceedings of the Second All-Union Conference on New Methods of Charged Particle Acceleration*, volume 7. Springer, 1989.

[69] *Proccedings of the 9th Advaned Accelerator Concepts Workshop*, 2000.

[70] J. P. Farmer, R. Martorelli, and A. Pukhov. *Phys. Plasmas*, 22:123113, 2015.

[71] P. Muggli, V. Yakimenko, M. Babzien, E. Kallos, and K. P. Kusche. *Phys. Rev. Lett.*, 101:054801, 2008.

[72] I. Will and G. Klemz. *Opt. Express*, 16:14922, 2008.

[73] A. Pukhov, N. Kumar, T. Tueckmantel, A. Upadhyay, K. Lotov, P. Muggli, V. Khudik, C. Siemon, and G. Shvets. *Phys. Rev. Lett*, 107:145003, 2011.

[74] I. V. Pogorelsky and I. Ben-Zvi. *Plasma Physics and Controlled Fusion*, 56:8, 2014.

[75] M. Ferrario, D. Alesini, M. Anania, A. Bacci, M. Bellaveglia, O. Bogdanov, R. Boni, M. Castellano, E. Chiadroni, A. Cianchi, S.B. Dabagov, C. De Martinis, D. Di Giovenale, G. Di Pirro, U. Dosselli, A. Drago, A. Esposito, R. Faccini, A. Gallo, M. Gambaccini, C. Gatti, G. Gatti, A. Ghigo, D. Giulietti, A. Ligidov, P. Londrillo, S. Lupi, A. Mostacci, E. Pace, L. Palumbo, V. Petrillo, R. Pompili, A.R. Rossi, L. Serafini, B. Spataro, P. Tomassini, G. Turchetti, C. Vaccarezza, F. Villa, G. Dattoli, E. Di Palma, L. Giannessi, A. Petralia, C. Ronsivalle, I. Spassovsky, V. Surrenti, L. Gizzi, L. Labate, T. Levato, and J.V. Rau. *Nucl. Instr. Meth. Phys. Res. B*, 309:183, 2013.

[76] M. Gross, R. Brinkmann, J. D. Good, F. Grüner, M. Khojoyan, A. Martinez de la Ossa, J. Osterhoff, G. Pathak, C. Schroeder, and F. Stephan. *Nucl. Instr. Meth. Phys. Res. A*, 740:74, 2013.

[77] J. Krall and G. Joyce. *Phys. Plasmas*, 2:1326, 1995.

[78] J. J. Su, P. Chen, J. M. Dawson, M. Jones, T. C. Katsouleas, R. Kenigs, and S. Wilks, editors. *12th IEEE Particle Accelerator Conference*, number 127, 1987.

[79] K. V. Lotov. *Phys. Plasmas*, 22:103110, 2015.

[80] R. Martorelli and A.Pukhov. Characterization of the equilibrium configuration for modulated beams in a plasma wakefield accelerator. *arXiv preprint*, arXiv:1602.04039, 2016. Physics of Plasmas (submitted).

[81] R. Martorelli and A.Pukhov. Optmized stability of a modulated driver in a plasma wakefield accelerator. *arXiv preprint*, arXiv:1603.04326, 2016. Physics of Plasmas (submitted).

[82] J. Krall, K. Nguyen, and G. Joyce. Numerical simulations of axisymmetric erosion processes in ion-focused regime transported beams. *Phys. Fluids B*, 1:2099, 1989.

[83] H. Lee Buchanan. Electron beam propagation in the ion-focused regime. *Phys. Fluids*, 30:221, 1987.

[84] N. Barov and J. B. Rosenzweig. Propagation of short electron pulses in underdense plasmas. *Phys. Rev. E*, 49:4407–4416, 1994.

[85] W. An, M. Zhou, N. Vafei-Najafabadi, K. A. Marsh, C. E. Clayton, C. Joshi, W. B. Mori, W. Lu, E. Adli, and S. Corde et al. *Phys. Rev. ST Accel. Beams*, 16:101301, 2013.

[86] M. Zhou, C. E. Clayton, C. Huang, C. Joshi, et al., editors. *Proceedings of PAC07*, number 3064, 2007.

[87] K. V. Lotov. *Phys. Plasmas*, 5:785, 1998.

[88] A. Pukhov. *arXiv preprint*, arXiv:1510.01071, 2015. to appear in CERN reports.

[89] J. Villasenor and O. Buneman. *Comp. Phys. Comm.*, 69:306, 1992.

[90] J. Dawson. *Reviews Modern Phys.*, 55:403, 1983.

[91] R. W. Hockney and J. W. Eastwood. *Computer Simulation Using Particles*. McGraw Hill, 1981.

[92] C. Nieter and J. R. Cary. *J. Comp. Phys.*, 196:448–472, 2004.

[93] C. K. Huang et al. *J. Comp. Phys.*, 217:658–679, 2006.

[94] A. Pukhov. *Journal of Plasma Physics*, 61:425–433, 1999.

[95] J. L. Vay. *Phys. Rev. Lett.*, 98:130405, 2007.

[96] P. Mora and Jr. T. M. Antonsen. *Phys. Plasmas*, 4:217, 1997.

[97] C. Huang, V. K. Decyk, C. Ren, M. Zhou, W. Lu, W. B. Mori, J. H. Cooley, T. M. Antonsen Jr., and T. Katsouleas. *Journal of Computational Physics*, 217:658, 2006.

[98] K. V. Lotov. *Phys. Rev. ST Accel. Beams*, 6:061301, 2003.

Acknowledgments

If I managed to complete this work is also thanks to the support of several people, and their names have to be mentioned in this thesis.

The first mention is reserved to Prof. Pukhov who gave me the possibility to go through such an experience, providing support not only in the everyday work but also in my desire to broaden my knowledges.

I must thank as well Prof. Müller, always available to spend some of his time for dealing with my worries and concerns, advising me far beyond what is expected by his role as a mentor.

I know very well that this work would not be completed withouth the help of Frau Gröters, who was able to remove every single obstacle represented by a form to be submitted, and of Evgenij Bleile, whose patient to deal with my computer problems is lower only to his skills.

A special mention is deserved to John Farmer and Friedrich Schluck, the first assisting me in my first steps in this new project, the second in my first steps in my new life in Düsseldorf (this one might appear not work-related but actually it is).

When I was in the need of a little advise, or just of a coffe I know that I would have always find some of my collegues ready to help me. They have as well given their contribute to this work: Selym, Longquing, Zi-Yu, Martin, Matthias, Phuc, Vural, Johannes, Götz, Christoph, Mykyta, Debin, Anvar, Tobias, Liangliang and Oliver.

As in all the most important achievements in my life the biggest gratitude goes to my family, the one that is there since ever, my mother, my father and my brother, as well as the one built over the years, Andrea, Francesco, Alessandro, Michele, Mustafa, Marta, Giulia, Pouria. To that special member of my large family that is my girlfriend Karo. I will always be in debt with all of you for having the patience to listen me complaining about everything and never run away or disappear.